

DELINEATION OF STRUCTURAL FEATURES
FAVOURABLE FOR U-MINERALIZATION WITHIN
BASEMENT AND DERIVATION OF BASEMENT
CONFIGURATION BELOW THE KHAI RAGARH GROUP
OF ROCKS BY USING GRAVITY, MAGNETIC AND
TIME DOMAIN ELECTROMAGNETIC (TEM) SURVEYS
IN BETWEEN BIJEPAR - RAMATOLA TRACT, GONDIA
DISTRICT, MAHARASHTRA

by

DOMMATI JALANDER

ENGG1G201801017

Bhabha Atomic Research Centre, Mumbai

*A thesis submitted to the
Board of Studies in Engineering Sciences*

In partial fulfillment of requirements

for the Degree of

MASTER OF TECHNOLOGY

of

HOMI BHABHA NATIONAL INSTITUTE

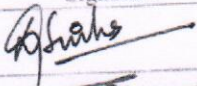
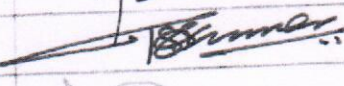
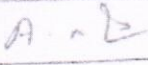
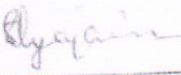
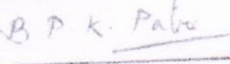
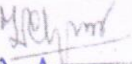
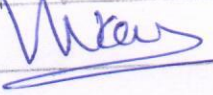


February, 2021

Homi Bhabha National Institute

Recommendations of the Thesis Examining Committee

As members of the Thesis examining Committee, we recommend that the thesis prepared by Dommati Jalandar entitled "Delineation of structural features favourable for U-mineralization within basement and derivation of basement configuration below the Khairagarh Group of rocks by using Gravity, Magnetic and Time Domain Electromagnetic (TEM) surveys in between Bijepar - Ramatola tract, Gondia district, Maharashtra" be accepted as fulfilling the thesis requirement for the Degree of Master of Technology.

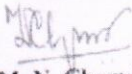
	Name	Signature
Member-1	Dr. D. K. Sinha	
Member-2	Dr. T. S. Sunil Kumar	
Member-3	Dr. V. Ramesh Babu	
Member-4	Dr. A. Rama Raju	
Technical advisor	M. V. Satyanarayana	
Examiner	Dr. B. P. K. Patro	
Guide & Convener	Dr. M. N. Chary	
Chairman	Prof. Vivekanand Kain	

Final approval and acceptance of this thesis is contingent upon the candidate's submission of the final copies of the thesis to HBNI.

I hereby certify that I have read this thesis prepared under my direction and recommend that it may be accepted as fulfilling the thesis requirement.

Date: 11-02-2021

Place Hyderabad


(Dr. M. N. Chary)
Guide

DECLARATION

I, hereby declare that the investigation presented in the thesis has been carried out by me. The work is original and has not been submitted earlier as a whole or in part for a degree / diploma at this or any other Institution / University.

A handwritten signature in blue ink, appearing to read 'Dommati Jalandar', with a horizontal line extending from the end of the signature.

(Dommati Jalandar)

ACKNOWLEDGEMENT

Immeasurable appreciation and deepest gratitude for the help and support are extended to the following persons who in one way or another have contributed in making my M. Tech study possible.

*Foremost, I would like to express my sincere gratitude to my project guide **Dr. M.N. Chary**, Adjunct Professor, HBNI for the continuous support of my M. Tech study, for his patience, motivation, enthusiasm, and immense knowledge. His guidance helped me in all the time of research and writing of this thesis. I could not have imagined having a better advisor and mentor for my M. Tech study.*

*I am very much indebted to my technical advisor **Shri M.V. Satyanarayana**, SO/D, EGPG, AMD-CR, Nagpur, for extended discussions, encouragement and valuable suggestions which have contributed greatly throughout this project.*

*I acknowledge my sincere gratitude to **Regional Director**, and **Deputy Regional Director**, of AMD, Central Region, Nagpur for their constant encouragement and support.*

*I would wish to express my thanks to, **Director, AMD, Hyderabad** for giving me permission to work on this project.*

*I also wish my thanks of gratitude to **Additional Director (Op.-I)**, AMD, **Hyderabad** for his support and encouragement in completing this research work.*

*I am thankful to all my senior colleagues and teachers, who taught me during my training period and extended their hands in every stage of my M. Tech work. My special thanks to **Shri A. Markandeyulu**, Incharge, EGPG Group, AMD-Hyderabad, **Shri P. Allipeera**, SO/G (retd), **Shri B.V. L Kumar**, SO/G, **Dr. V. Ramesh Babu**, SO/G, **Shri A. K Maurya**, SO/E, **Shri Y. Harsha**, SO/D, **Shri. S. Vijaya Kumar**, SO/D, and **Shri Srinivasulu**, SO/D.*

I am grateful to **M. Bandyopadhyay, SO/G, Incharge, EGPG, AMD-CR, Nagpur** who helped a lot and taken so much of care in teaching new things, queries solved related to modelling, data processing and provided many research papers related to my project work.

I would like to appreciate all my colleagues **B. Shanakraiah, SO/D, Viney Kumar, SO/D, A. Vamsi Krishna, SO/D, and Shri. T. Subhash, SO/D, Shri M. Anjaneyamurthy, SO/C, Shri M.H. Ansari SO/C, Shri K. Damodhar, SO/C, Shri T. Manoj kumar, SO/C, Shri K. Rajesh SO/C, Shri D. Ragavender, SO/C, and Shri Ch. Satish, SO/C of EGPG, AMD** for helping me throughout of this research work.

I would like to express my sincere appreciation and gratitude to, **Head & In-charge, BARC Training School, AMD Complex, Hyderabad** for their support and for ensuring the optimum academic environment that has helped me in completion of this project.

I also offer my thankful to **my colleagues OCES 2018-19** from Training school, all technical and non-technical staff who has supported me directly or indirectly in the completion of my project work.

My sincere thanks also goes to my M. Tech thesis examining committee: **Prof. Vivekanand Kain, Dr. D.K. Sinha, Dr. T. S. Sunil Kumar, Dr. A. Rama Raju, Dr. V Ramesh Babu and Dr. B. P. K. Patro** for their continued support, suggestions and encouragement.

Last but not the least, I offer my sincere thankful to the **competent authority of HBNI** for providing the opportunity to pursue the M. Tech degree.



(Dommati Jalander)

CONTENTS

<i>SYNOPSIS</i>	<i>V</i>
<i>LIST OF FIGURES</i>	<i>VII</i>
<i>LIST OF TABLES</i>	<i>X</i>
CHAPTER-1 INTRODUCTION	
1.1 Introduction	1
1.2 India's Atomic Energy Programme	2
1.3 Uranium and its occurrence	3
1.4 Classification of Uranium Deposits	5
1.5 Role of Geophysics in Uranium exploration	10
CHAPTER-2 GEOLOGY OF KHAIRAGARH BASIN	
2.1 Introduction	11
2.2 Geology	13
2.2.1 Regional geology	13
2.2.2 Local geology	16
2.3 Previous studies done in and around the study area	18
2.3.1 Geological studies	18
2.3.2 Geophysical surveys	20

CHAPTER-3 GRAVITY METHOD

3.1 Introduction	21
3.2 Rock densities in the geological environment of study area	23
3.3 Instruments	25
3.4 Gravity data acquisition	26
3.5 Reduction of gravity data	29
3.6 Data processing	31
3.6.1 Bouguer Gravity Anomaly(BGA)	31
3.6.2 Data processing techniques	33
3.6.2.1 Upward continuation of Bouguer Gravity Anomaly (BGA) map	33
3.6.2.2 Analytic signal (Total derivative or Total gradient) method	36
3.6.2.3 Euler Depth solutions	38
3.6.2.4 3D Modelling of Gravity	40
3.7 Data interpretation	42

CHAPTER-4 MAGNETIC METHOD

4.1 Introduction	45
4.2 Magnetic properties of rocks in geological environment of study area	46
4.2.1 Magnetic susceptibility measurement of rock samples	47
4.3 Data acquisition	49
4.3.1 Instruments	49
4.3.2 Magnetic survey planning	53
4.3.3. Data reduction	55
4.4 Data processing and enhancement	56

4.4.1 Profile analysis	56
4.4.2 Continuation filters	57
4.4.3 Reduction-to-pole (RTP)	59
4.4.4 Analytic signal	61
4.4.5 Euler depth solutions	63
4.5 UBC-MAG 3D Modelling	66
4.6 Data Interpretation	69
CHAPTER-5 TIME DOMAIN ELECTROMAGNETIC METHOD (TEM)	
5.1 Introduction	73
5.2 Electromagnetic theory	75
5.3 Subsurface conductivity and EM responses	78
5.3.1 Homogeneous subsurface	78
5.3.2 Confined conductor	81
5.3.3 Conductor quality	82
5.4 Acquisition of Time-Domain Electromagnetic data	83
5.4.1 System parameters	83
5.4.2 System geometry	86
5.5 Data Interpretation	87
5.5.1 Profile and pseudo-conductivity cross section analysis	87
5.5.2 Decay curve analysis over conducting zones	92
5.5.3 1D Inversion of In-loop soundings	95
5.5.4 Demarcation of conducting zones	98

CHAPTER-6 INTEGRATED INTERPRETATION, RESULTS AND DISCUSSIONS

6.1 Gravity method 101

6.2 Magnetic method 101

**6.2.1 Understanding of causative sources of magnetic anomalies from
petrology results 102**

6.3 Time-Domain Electromagnetic (TEM) method 106

CHAPTER-7 CONCLUSION 109

PUBLICATION 111

FUTURE SCOPE OF THE STUDY 112

REFERENCES 113

SYNOPSIS

Proterozoic sedimentary basins have been recognized as the prime target for unconformity type of U-mineralization. The Khairagarh Basin is one of the promising areas in Central India searching for U-mineralization. The present study area is located along Bijepar- Ramatola tract to the SW of the Khairagarh basin. Earlier geological and geophysical studies around the present study area proved an ideal geological setup for hosting Proterozoic unconformity/sandstone type U-mineralization and also few radioactive anomalies associated with Bijli rhyolites are reported by Atomic Minerals Directorate for Exploration and Research (AMD). Geophysical methods play a dominant role in identifying the subsurface features associated with U-mineralisation, alteration zones and structural features (shears/fractures). Geophysical surveys comprising Magnetic, Gravity and Time Domain Electromagnetic (TEM) methods are applied over an area of 35 sq. km, 20 sq. km and 2.2 sq. km respectively to delineate structural features (shears/fractures), basement configuration, the unconformity contact between basement Bijli rhyolites and Bortalao sediments, and thickness of Bortalao sandstone below the Khairagarh Group of rocks.

Unconformity contact between basement Bijli rhyolites and Bortalao sandstone, litho-contact between Bortalao sandstone and Sitagota basalt in the eastern part of the study area is deciphered by a sharp gradient of Bouguer anomaly. Structural features i.e. faults/fractures and lineaments trending in NW-SE, NE-SW and E-W are identified within basement Bijli rhyolites and few of these features are running below the sandstones. Out of all these inferred structural features, NW-SE trending features are dominating in the study area. Two parallel NW-SE faults/fractures intruded by quartz vein are demarcated towards the NE of *Bijepar* village, where surface radioactive anomalies are reported. Interpretation of magnetic data facilitated in identifying structural features trending in NW-SE & NE-SW in the study area. Among the

identified magnetic lineaments, NW-SE trending lineaments are dominated which are linked with a major fault zone. Basement faults/fractures showing their depth persistency and majority of which are confined to basement rocks and rest are running into deeper parts of basin. A few NW-SE structural features are coinciding with features inferred from gravity data and found good correlation. One major NW-SE trending fault cross cut by two (2) NE-SW trending fractures at north-east of *Bijepar* village, form a zone where surface radioactive anomalies are reported. Radioactive anomalies reported at *Ramatola* and *Patratola* villages are falling at the intersection zones of fault/fractures and unconformity contact. Magnetic anomaly maps depicted the lithological variations in basement rhyolites. Basement rhyolites are divided into two types i.e., grey and pink rhyolites based on magnetic susceptibility values and amplitude ranges of anomalies in the study area. Interpretation of magnetic data demarcated the zones dominantly associated with intrusive basic activity within the sediment as well as basement rocks apart from the identification of structural features. One E-W trending ultra-mafic rock at a depth of 70 to 100 m with vertical to sub-vertical nature towards NE of *Bijepar* village is clearly mapped and quantitatively interpreted using 2D and 3D modelling techniques. Zones of interest are demarcated from potential methods are covered by TEM survey and data have helped in identifying conducting zones at north-east of *Bijepar* village. These inferred conducting zones could be fractures filled with conducting minerals i.e. sulphides within the Bortalao sandstone and/or at unconformity contact important for mineralization. Near and around *Bijepar* village EM soundings data offered lithological succession.

Integrated map of inferred structural features from all geophysical methods along with geology has been generated. Integrated interpretation of Gravity, Magnetic and TEM data along with other exploration data sets i.e. Geology and borehole data successfully mapped potential target areas for further exploration program in the study area.

LIST OF FIGURES

Figure No.	DESCRIPTION	Page No.
1.1	Position of uranium deposit types with respect to the main fractionation processes. The types of uranium-rich magma are: PAK: peralkaline, HKCa: high K calc-alkaline, Pal: peraluminous (IAEA-TECDOC-1843, UDEPO, 2016 Edition, pp. 13-14).	5
.2.1	Regional geological map of the Khairagarh Basin and its surroundings (After GSI).	15
2.2	Proposed study area laid on the Toposheet.	16
2.3	Geological map of parts of Khairagarh basin showing study area.	17
3.1	Laboratory measurements of density(ρ).	23
3.2	Density values of the rock samples collected from the study area.	24
3.3	Schematic diagram of a gravimeter.	26
3.4	Gravity survey layout superimposed on geological map of the study area.	28
3.5	Sequence of data corrections applied over gravity data of the study area.	29
3.6	Bouguer Gravity Anomaly (BGA) of study area.	32
3.7	Residual gravity anomaly map produced by subtracting regional anomaly from bouguer gravity anomaly.	35
3.8	Analytical signal (AS) map of study area.	37
3.9	Euler depth solutions with their respective structural features.	39
3.10	UBC GRAV3D Modelling for Gravity data of Bijepar-Ramatola block.	41
3.11	Bouguer Gravity Anomaly with inferred structural features.	43
4.1	Kappa meter for magnetic susceptibility measurements in the field.	47

4.2	Susceptibility values of the rock samples collected from the study area.	48
4.3	Proton-Precession magnetometer.	50
4.4	Working principle of PPM magnetometer	51
	a. The elements of a proton-precession magnetometer.	
	b. Current in the magnetizing coil produces a strong field F that aligns the magnetic moments (“spins”) of the protons.	
	c. When the field F is switched off, the proton spins precess about the geomagnetic field B_t, inducing an alternating current in the coil with the Larmor precessional frequency f.	
4.5	Magnetic survey layout superimposed over geology map of study area.	54
4.6	Diurnal curve of the base magnetic field utilized for diurnal correction.	55
4.7	Magnetic anomaly profile and its filter outputs for line number 2345900N.	56
4.8	Upward continuation of TMI maps for different heights.	58
4.9	Reduction to Pole (RTP) map showing structural features.	60
4.10	Analytical signal map study area showing structural features.	62
4.11	Correlation of Euler’s depth solutions with inferred structural features from TMI map.	65
4.12	UBC-MAG3D model for E-W concealed basic body in the study area.	68
4.13	a). Total Magnetic Intensity (TMI) contour map.	71
	b). Total Magnetic Intensity (TMI) map showing structural features.	
5.1	Schematic illustration of an Electromagnetic induction phenomenon in the subsurface.	76
5.2	Schematic illustration of the diffusion of the eddy current system in a	78

conductive half-space at different delay times (Reid and Macnae. 1998).

(a) Early, (b) mid and (c) late delay times.

5.3	TDEM secondary decay for power-law response plotted on log–log axes with decay constant k.	81
5.4	Decay curve for different quality conductor.	82
5.5	TEM survey lay out over imposed on geology map of Bijepar village block.	85
5.6	Schematic diagram of In-loop configuration.	86
5.7	1D stitched 2D pseudo conductivity cross section along 2344300N line.	88
5.8	1D stitched 2D pseudo conductivity cross section along 2344700N line.	89
5.9	1D stitched 2D pseudo conductivity cross section along 2344900N line.	90
5.10	1D stitched 2D pseudo conductivity cross section along 2345100N line.	91
5.11	TEM profile response showing conducting zone on Line No-23443000N.	93
5.12	Decay curve and their respective time constant (τ) of stations for Line No-2344300N.	94
5.13	1D stitched 2D cross section of Line No-2344300N.	96
5.14	1D Inversion of loop size 400 m X 400 m at station number 445000E-2345200N.	97
5.15	Inferred EM conducting zones super imposed on geology map.	99
6.1	Thin sections under microscope for different type of rhyolites collected from study area.	104
6.2	Total magnetic Intensity (TMI) showing petrological results with their respective geophysical anomalous zones.	105
6.3	Inferred structural features superimposed over geology map.	107

LIST OF TABLES

Table No.	DESCRIPTION	Page No.
2.1	Chrono-stratigraphic succession of the study area (After Deshpande <i>et al.</i> , 1990).	14
3.1	Average density of rock samples	24
4.1	Average susceptibility of rock samples	49

CHAPTER 1

INTRODUCTION

1.1 Introduction

To maintain the life of the human community, and in order to facilitate the life, many important inventions were discovered. There is no doubt that the most important of these inventions is electricity, which we depend on in the current modern time. We better understand the importance of electricity in our life during a few minutes of power outages we encounter. The people's social life almost stops in power outages.

Global demand for energy is increasing rapidly, because of population and economic growth, especially in emerging market economies. While accompanied by greater prosperity, rising demand creates new challenges. Energy security concerns can emerge as more consumers require ever more energy resources, and higher consumption of fossil fuels leads to higher greenhouse gas emissions, particularly carbon dioxide (CO₂), which contributes to global warming. At the same time, the number of people without access to electricity remains unacceptably high. But such challenges can create opportunities. A sustainable energy future will require new thinking and new systems essentially a transformation in the way we produce, deliver and consume energy. If our goal is to raise living standards, provide access to modern energy services, use energy more efficiently, protect the global environment, ensure reliable energy supplies and green growth.

Growing concerns over climate change have highlighted the need to step up contribution of nuclear energy in the energy mix and to reduce the dependence on fossil fuels in the years to come. Nuclear energy has the ability to produce electricity without

greenhouse gas emissions. It produces electricity with less pollution. It is cleaner than many other forms of energy production. Essentially, nuclear power would be “carbon-zero” if the uranium were mined and transported in a more efficient way. Nuclear reaction releases more energy, as compared to hydro or wind energy and making nuclear fuel much more efficient than fossil fuels (A pellet of nuclear fuel weighs approximately 0.1 ounce (6 grams)). However, that single pellet yields the amount of energy equivalent to that generated by a ton of coal, 120 gallons of oil or 17,000 cubic feet of natural gas). Large quantity of energy is generated from a single nuclear power plant. Nuclear reactors make use of uranium as fuel and produces huge amounts of energy from small amounts of uranium metal. The Earth has the high reserves of uranium. Current estimates put the uranium supply as enough to last for 30 to 60 years. Moreover, other fuel like Thorium is available for power generation. Whereas, oil reserves and other fossil type fuels are likely to run out shortly. Nuclear power plants operate reliably and have a continuous output of power. The plants do not generally face operations and maintenance problems. This is a contrast to other alternative energies which depend on the activity of the weather. Although nuclear power reactors are expensive to build, they are relatively cheap to operate. Fuel is inexpensive and a plant can be operated by small group of people. A nuclear plant is not dependant on local sources like oil & coal and can be set up in any part of the globe. It also does not require a lot of space and so can be placed in already developed areas and the power does not have to be transferred over long distances.

1.2 India’s Atomic Energy Programme

India has consciously proceeded to explore the possibility of tapping nuclear energy for the purpose of power generation. Uranium and Thorium having good potential to be utilized as nuclear fuel in Indian Nuclear Power Reactors. Dr. Homi Jehangir Bhabha

(30th October 1909 – 24th January 1966) was an Indian nuclear physicist, colloquially known as "Father of the Indian nuclear programme" formulated India's three-stage nuclear power programme in the 1950s and the ultimate focus on the programme is on enabling the uranium and thorium reserves of India to be utilized in meeting the country's energy requirements. In the first stage of the programme, natural uranium fuelled pressurized heavy water reactors (PHWR) produce electricity while generating plutonium-239 as by-product. In the second stage, fast breeder reactors (FBRs) [moderators not required] would use plutonium-239, recovered by reprocessing spent fuel from the first stage, and natural uranium. A stage III reactor or an advanced nuclear power system involves a self-sustaining series of thorium-232 and uranium-233 fuelled reactors.

Atomic Minerals Directorate for Exploration and Research (AMD), a constituent unit of Department of Atomic Energy (DAE) is playing an important role in the frontend of Indian Nuclear Power Programme. The prime mandate of AMD is to identify and evaluate uranium resources required for the successful implementation of atomic energy program of the country. In India, uranium deposits are identified mainly in Singhbhum Shear Zone, Jharkhand; in parts of Chhattisgarh; Southern parts of Meghalaya; Cuddapah Basin, Andhra Pradesh; in parts of Karnataka; Aravalli- and Delhi Super groups, Rajasthan and Haryana.

1.3 Uranium and its occurrence

Uranium is a naturally occurring radioactive element that has the highest atomic weight (~238 g/mole). It can be found in minute quantities in most rocks, soils and waters (normally < 5 ppb), but the real challenge is to find geological setups having high enough concentrations to make it economically feasible to mine. Natural uranium is constituted primarily of U238 (99.3%) with 0.7% of U235 and a small amount of its isotope U234.

Three isotopes, U236, U233 and U232, are also produced by reactors from U235 and thorium. Uranium-238 which alone constitutes 99.3% of natural uranium has the longest lifetime, its half-life period is 4.5 billion years, about the age of Earth. Its very long period says it is still present in the Earth crust. This U238 is a fertile material, captures neutron and leads to the formation of fissile material Pu239 in a nuclear reactor. This impressive potential of fission energy in Pu239 remains still largely unexploited. The purpose of the fourth-generation breeder reactors is to recover this fantastic potential. Uranium-235, the only existing fissile nucleus found in natural uranium, is used as a nuclear fuel in reactors because of its fissile nature. This very rare isotope, present at the concentration of 0.7% in natural uranium, is thus a highly strategic and coveted material. Its very long half-life period, 700 million years, is however, 6.5 times shorter than its isotope U238. At the time of the formation of Earth, U235 was 85 times more abundant than the present. The 0.7% of U235 observed today is a pale residue of this past abundance. Uranium-234 is the first long-lived descendant of Uranium-238. In a natural sample of uranium, these nuclei are present in the unalterable proportions of the radioactive equilibrium of the Uranium-238 filiations at a ratio of one atom of Uranium-234 for 18,800 atoms of Uranium-238, so that the two isotopes contribute equally to the radiations emitted by uranium. The primary uranium ore mineral is uraninite (UO₂) also known as pitchblende. A range of other uranium minerals can be found in various deposits, these include carnotite, tyuyamunite, torbernite and autunite. A large variety of secondary uranium minerals are known, many of which brilliantly coloured and fluorescent. The most common are gummite, autunite (with calcium), saleeite (magnesium) and torbernite (with copper) and hydrated uranium silicates such as coffinite, uranophane (with calcium) and sklodowskite (magnesium).

1.4 Classification of Uranium Deposits

Fifteen types of deposits have been retained in the new International Atomic Energy Agency (IAEA) classification scheme. In contrast to the ordering of previous IAEA classifications, the economic parameter has not been taken into account. Instead, they are listed in a geologically meaningful order from deep, primary magmatic deposits to sedimentary and surficial deposits as shown in Figure 1.1.

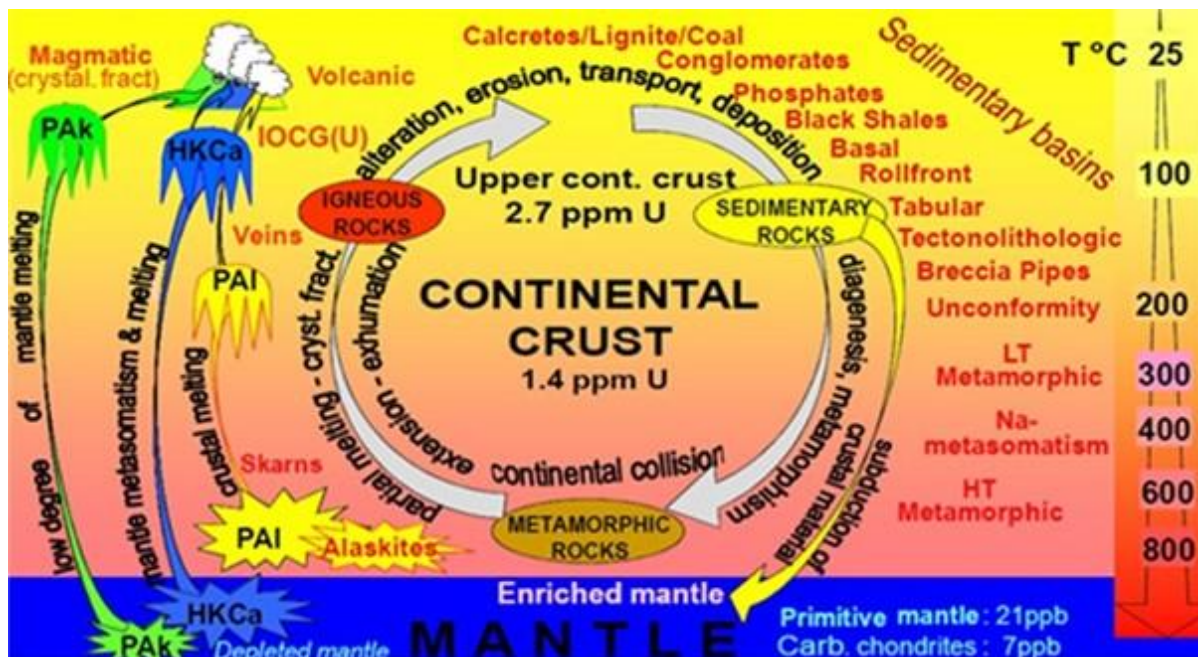


Figure 1.1 Position of uranium deposit types with respect to the main fractionation processes. The types of uranium-rich magma are: Pak: peralkaline, HKCa: high K calc-alkaline, Pal: peraluminous (IAEA-TECDOC-1843, UDEPO, 2016 Edition, pp. 13-14).

The 15 types are as follows:

1. Intrusive
2. Granite-related
3. Polymetallic iron oxide breccia complex
4. Volcanic-related
5. Metasomatite
6. Metamorphite
7. Proterozoic unconformity
8. Collapse breccia pipe
9. Sandstone
10. Palaeo quartz-pebble conglomerate
11. Surficial
12. Lignite–coal
13. Carbonate
14. Phosphate
15. Black shale

Within the 15 types of deposits defined, 36 subtypes and 14 classes have also been retained.

Most subtypes and classes are defined (Dahlkamp, 2010) with minor modifications and additions. For each type, subtype and class, typical deposit examples are listed.

1. Intrusive

1.1. Anatectic: pegmatite–alaskite (Rössing, Namibia; Bancroft District, Canada)

1.2. Plutonic

1.2.1. Quartz monzonite (Bingham Canyon, USA; Chuquicamata, Chile)

1.2.2. Peralkaline complex (Kvanefjeld, Greenland; Poços de Caldas, Brazil)

1.2.3. Carbonatite (Palabora, South Africa; Catalão, Brazil)

2. Granite-related

2.1. Endogranitic (La Crouzille District, France; Xiazhuang District, China)

2.2. Perigranitic (Příbram region, Czech Republic; Niederschlema–Alberoda, Germany)

3. Polymetallic iron oxide breccia complex (Olympic Dam, Australia)

4. Volcanic-related

4.1. Stratabound (Dornod No. 7 ore zone, Mongolia; Maureen, Australia)

4.2. Structure-bound (Streltsovskoye–Antei, Russian Federation; Kuriskova, Slovakia)

4.3. Volcano-sedimentary (Anderson, USA; Sierra Pintada District, Argentina)

5. Metasomatite

5.1. Na-metasomatite

5.1.1. Granite derived (Kirovograd District, Ukraine; Lagoa Real, Brazil; Coles Hill, USA)

5.1.2. Metasediment–metavolcanic derived (Krivoy Rog District, Ukraine; Michelin, Canada)

5.2. K-metasomatite (Elkon District, Russian Federation)

5.3. Skarn (Mary Kathleen, Australia; Tranomaro, Madagascar)

6. Metamorphite

6.1. Stratabound (Forstau, Austria; Nuottijarvi, Finland)

6.2. Structure-bound

6.2.1. Monometallic veins (Schwartzwalder, USA; Ace-Fay-Verna, Canada; Rozna, Czech Republic)

6.2.2. Polymetallic veins (Shinkolobwe, Democratic Republic of Congo; Port Radium, Canada; Jaduguda, India)

6.2.3. Marble-hosted phosphate (Itataia, Brazil; Zaozernoje, Kazhakstan)

7. Proterozoic unconformity

7.1. Unconformity-contact (Cigar Lake, Key Lake, McArthur River, Canada)

7.2. Basement-hosted (Jabiluka, Ranger, Australia; Eagle Point, Millennium, Canada)

7.3. Stratiform fracture-controlled (Lambapur, Chitrial, India)

8. Collapse breccia pipe (Arizona Strip, USA)

9. Sandstone

9.1. Basal channel (Dalmatovskoye, Russian Federation; Beverley, Australia)

9.2. Tabular (Arlit District, Niger; Ambrosia Lake District, USA)

9.2.1. Continental fluvial, U associated with intrinsic reductant (Arlit type, Niger)

9.2.2. Continental fluvial, U associated with extrinsic humate (Grants type, USA)

9.2.3. Continental fluvial vanadium–uranium (Salt Wash-type, USA)

9.3. Roll-front (Wyoming, USA; Chu-Sarysu Basin, Kazakhstan)

9.3.1. Continental basin, U associated with intrinsic reductant (Wyoming type, USA)

9.3.2. Continental to marginal marine, U associated with intrinsic reductant (Chu-Sarysu type, Kazakhstan)

9.3.3. Marginal marine, U associated with extrinsic reductant (South Texas type, USA)

9.4. Tectonic-lithologic (Lodève Basin, France; Franceville Basin, Gabon)

9.5. Mafic dykes/sills in Proterozoic sandstone (Westmoreland District, Australia)

10. Palaeo quartz-pebble conglomerate

10.1. U-dominant (Elliot Lake District, Canada)

10.2. Au-dominant (Witwatersrand Basin, South Africa)

11. Surficial

11.1. Peat-bog (Kamushanovskoye, Kyrgyzstan; Flodelle Creek, USA)

11.2. Fluvial valley (Yeelirrie, Australia; Langer Heinrich, Namibia)

11.3. Lacustrine–playa (Lake Maitland, Lake Way, Australia)

11.4. Pedogenic and fracture fill (Beslet, Bulgaria)

12. Lignite–coal

12.1. Stratiform (Koldzhat, Kazakhstan; Williston Basin, USA)

12.2. Fracture-controlled (Freital, Germany; Turakavak, Kyrgyzstan)

13. Carbonate

13.1. Stratabound (Tumalappalle, India)

13.2. Cataclastic (Mailuu-Suu, Kyrgyzstan; Todilto District, USA)

13.3. Karst (Sanbaqi, China; Tyuya-Muyun, Kyrgyzstan)

14. Phosphate

14.1. Organic phosphorite (Mangyshlak Peninsula, Kazakhstan; Ergeninsky region, Russian Federation)

14.2. Minerochemical phosphorite (Phosphoria Formation and Florida Land Pebble District, USA; Gantour, Morocco)

14.3. Continental phosphate (Bakouma District, Central African Republic)

15. Black shale

15.1. Stratiform (Ranstad and MMS Vicken, Sweden; Chattanooga Shale Formation, USA)

15.2. Fracture-controlled (Ronneburg District, Germany; Dzhantuar, Uzbekistan)

1.5 Role of Geophysics in Uranium exploration

Geophysics is a science engaged in the study of the Earth and its environment by physical methods. One advantage of geophysical methods is that, for measurements mostly made at the surface, deductions related to subsurface geological features can be readily made. Widely used geophysical methods include gravimetry, magnetometry and borehole logging as well as geoelectrical, radiometric and seismic techniques.

Despite a very high density, uranium mineralization, in all its forms, does not give rise to observable gravity anomalies. Low magnetic susceptibility does not enable the direct detection of uranium by means of magnetic contrast. While the electrical resistivity of uranium is extremely low, uranium mineralization does not manifest itself as a good conductor. In general, uranium minerals cannot be distinguished by electrical conductivity contrasts from neighbouring rocks directly.

Geophysical surveys are indirect methods in uranium exploration and deals with contrast of physical properties of different rock types in subsurface. The physical properties of rocks and their contrast with neighbouring geological environments in subsurface are a clue to identify favourable zones associated with uranium mineralization by utilizing suitable geophysical method for that environment. Uranium is radioactive, and radiometric methods are the primary detection techniques used during exploration. The application of gravity, magnetic, electrical, electromagnetic and seismic prospecting techniques can significantly enhance the understanding of an area's subsurface geological setting. Geophysical methods of prospecting are carried out from the air, ground and in boreholes. Some of these techniques overcome the logistical difficulty of exploration in remote and inaccessible areas.

CHAPTER 2

GEOLOGY OF KHAIRAGARH BASIN

2.1 Introduction

Proterozoic sedimentary basins have been recognized as the prime target for unconformity type of U-mineralisation. The Khairagarh Basin is one of the promising areas in Central India for U-mineralisation. The present study area falls in Khairagarh Basin comes under Dongargarh-Kotri Belt (DKB), trending roughly N-S over 250 km in Bastar Craton, covers parts of Bastar, Durg, Rajnandgaon districts of Chhattisgarh and Gadchiroli, Bhandara districts of Maharashtra and Balaghat district of Madhya Pradesh. It encompasses the rocks of Paleoproterozoic Nandgaon Group (Bijli Rhyolite, Pitepani Volcanics & Dongargarh Granite) in Central part and Mesoproterozoic volcano sedimentary sequence of Khairagarh Group in northern part and Abujhmar Group at southern fringe. Khairagarh Basin has been the thrust area for uranium mineralization owing to its favourable geological setting and environment for unconformity and sandstone type of Uranium mineralization. Exploration for Atomic Minerals in this geological domain commenced in late sixties in parts of Maharashtra and Chhattisgarh and has resulted in small scale uranium deposits along with various uranium anomalies/occurrences.

- Quartz-Pebble Conglomerate (QPC) type, associated with basal portion of the Bailadila Group, e.g. Goturmura, Dalli-Rajahara, etc.
- Iron Ore Breccia (IOB) type of uranium mineralization in the entire Dongargarh-Kotri Belt, e.g. Langi-Darekasa, etc.
- Vein type associated with the sheared meta-amphibolites and rhyolites of Nandgaon Group, e.g. Bodal-Bhandaritola, etc.

- Unconformity type at the unconformity contact between the basement complex comprising Nandgaon Group and Dongargarh Granites and the overlying Khairagarh Group of sediments, e.g. Nalpani, etc.
- Proterozoic sandstone type associated with basal conglomerates/sandstones of Khairagarh Group, e.g. Mogarra, Malharbordi, etc.

Established uranium deposits near Nalpani and Mogarra in Dongargarh-Kotri belt are hosted by sediments of Bortalao Formation.

The present study area falls along Bijepar-Ramatola tract has similar ideal set up thus, subjected to intensive exploration for atomic minerals. Earlier geological and geophysical studies done by Atomic Minerals Directorate for Exploration and Research (AMD) (Sinha, D.K., 1986, pp 1-23, Chaturvedi, A.K., 1986, pp. 1-23 and Shukla *et.al.*, 2018, pp. 21-29) in and around the study area indicated possibility of fractured/unconformity type and Sandstone type of uranium mineralisation near the basement. Geophysical surveys are indirect methods in uranium exploration play a dominant role in identifying the subsurface features associated with uranium mineralisation, alteration zones and structural features (shears/fractures).

The objective of present research work is to delineate structural features (shears/fractures) within basement and its configuration, the unconformity contact between basement Bijli rhyolites and Bortalao sediments, and thickness of Bortalao sandstone below the Khairagarh Group of rocks. To meet the objectives, study area covered an area of 35 sq. km, 20 sq. km and 2.2 sq. km by Magnetic, Gravity and Time Domain Electromagnetic (TEM) surveys of geophysical methods respectively.

2.2 Geology

2.2.1 Regional geology

The paleo-proterozoic sequence of volcano-sedimentary rocks in the Dongargarh belt, Central Indian Craton, known as Dongargarh Super group forms a belt, about 100 km wide, which extends in NNE-SSW direction for more than 150 km and it is sandwiched between the Sakoli belt on the west and the Chhattisgarh Basin on the east. This volcanic-sedimentary sequence is comprised predominantly of a bimodal volcanic suite and subordinate thinner sedimentary rocks of both mature and immature types. The Dongargarh-Kotri belt is one of the promising uranium provinces of central India owing to its ideal litho-structural setup for uranium mineralisation (Sarkar *et al.*, 1994, pp. 117-126).

Khairagarh basin falls in this Dongargarh-Kotri belt and it has been the thrust area for uranium mineralization owing to its favourable geological setting and environment for unconformity and sandstone type of uranium mineralization. Khairagarh Group comprises a volcano-sedimentary suite of rocks of middle proterozoic age laid in a basin that occupies approximately 2,250 sq.km area. The sandstone–basalt alterations of Khairagarh Group overlie the Nandagaon Group and Dongargarh granite. The major rock units that transgress the area are Bijli rhyolites of Nandagaon Group, Bortalao sandstones, Sitagota basalts, Karutola sandstones, Mangikuta volcanics, Ghogra sandstones and Kotima volcanics of Khairagarh Group. Bortalao sandstone is the basal formation consisting of conglomerates, arkosic arenite, siltstone, and shale. Sitagota basalt comprises massive, porphyritic and amygdular basalt containing xenoliths of Bortalao sandstone.

Table 2.1 Chrono-stratigraphic succession of the study area (After Deshpande *et al.*, 1990)



2.2.2 Local geology

The study area falls in the parts of Toposheet No. 64 C/7, 64 C/8, 64 C/11 & 64 C/12 is located to the SW margin of the Khairagarh basin (Figure 2.2).

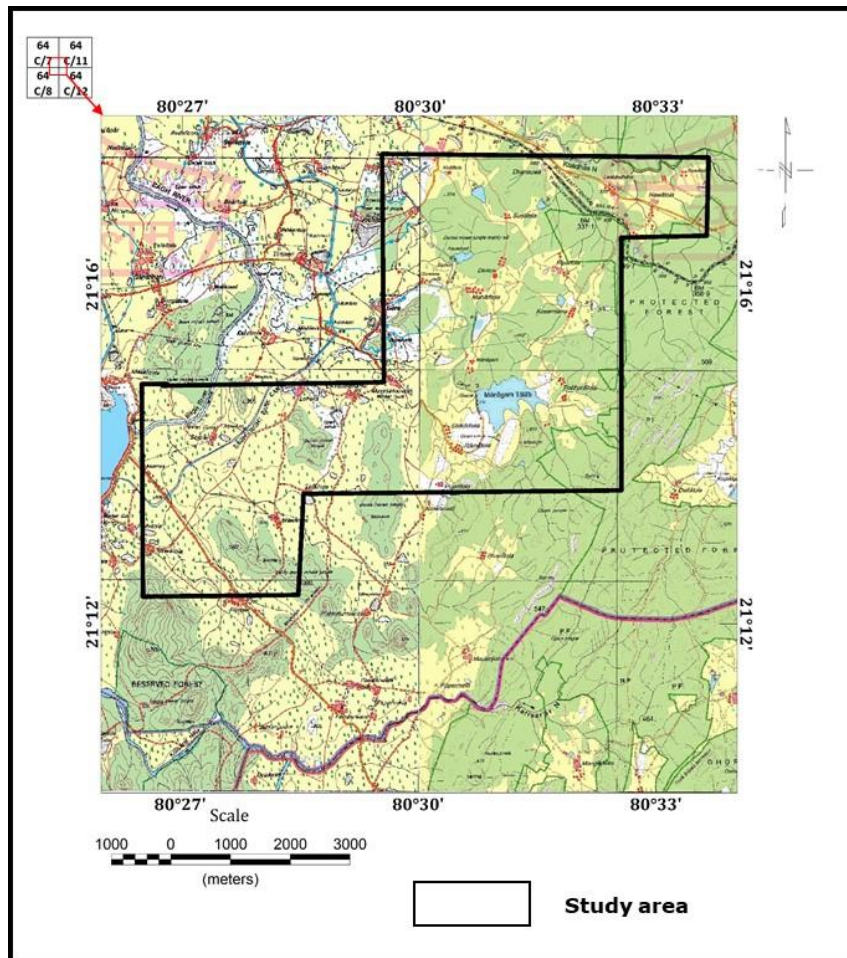


Figure 2.2 Location of study area laid on the Toposheet.

Major rock types that transgress the area are Bijli rhyolites of Nandagaon Group, Bortalao sandstones and Sitagota basalts of Khairagarh Group. Bortalao sandstone is the basal formation consisting of conglomerates, arkosic arenite, siltstone, and shale. The shale is locally ferruginous in nature. Sitagota basalts comprise massive, porphyritic and amygdular basalt containing xenoliths of Bortalao sandstone. The general strike of the rock units exposed in the area is N20°E-S20°W. Few ferruginised quartz reefs associated with structural features are also exposed in the study area.

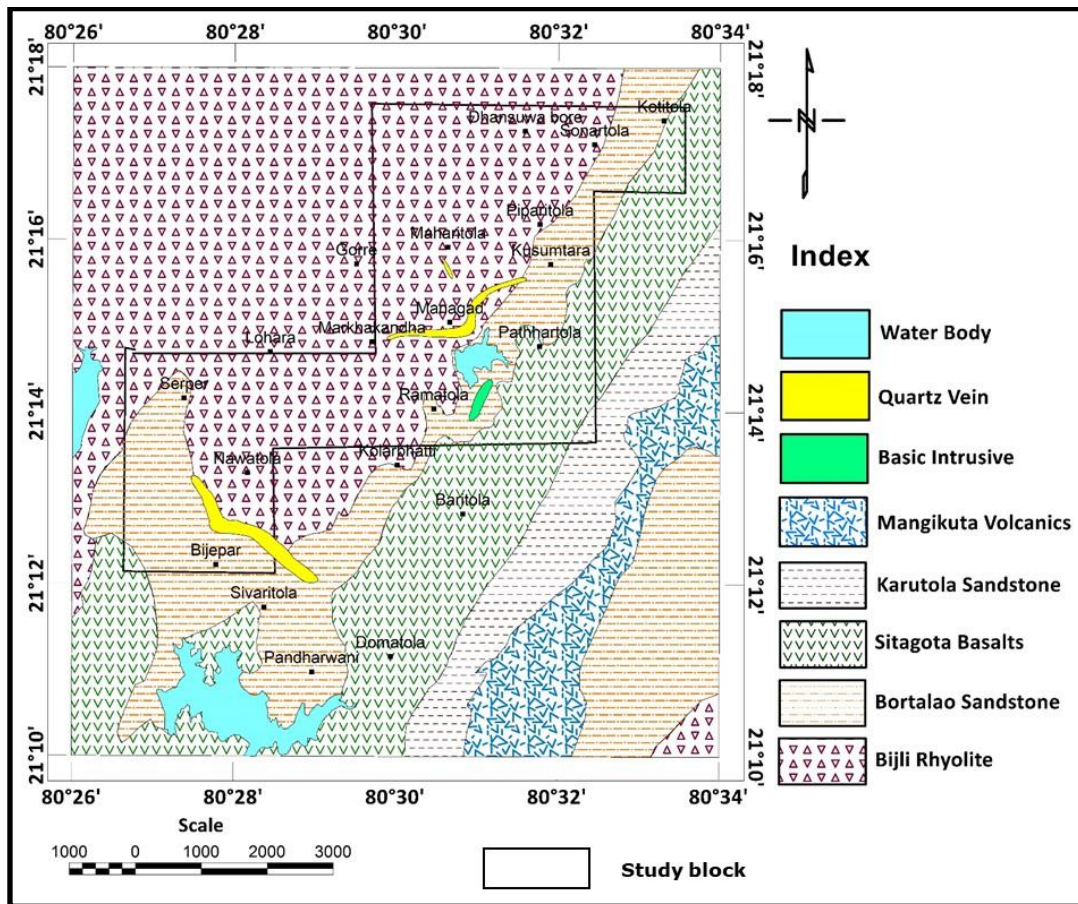


Figure 2.3 Geological map of parts of Khairagarh basin showing study area.

Bijli rhyolite forms the basement over which the sandstone and conglomerates of Bortalao formation rests unconformably. The unconformity contact is noticed between the Bortalao Formation and underlying Bijli rhyolite at the western side of study area. The rhyolitic agglomerates also noticed at places. Rhyolite has been affected by a number of fractures and joints. Bortalao Formation is represented by sandstone and basal conglomerates. The basal conglomerate consists angular to sub-angular clasts of red rhyolite, set up in arenaceous matrix. The sandstone is pink to buff coloured fine to medium grained, texturally and mineralogically immature, comprising of sub-angular to sub-rounded clasts of quartz, pink feldspar, plagioclase and lithic fragments comprising of chert and rhyolite. The sandstone near the unconformity contact has been identified as fine grained immature sandstone. The interformational conglomerate having coarse grained, well rounded clasts in sandstone at the

upper stratigraphic levels nearer to the Sitagota basalts is noticed. Sandstone has undergone ferruginization and brecciation at places. Dark green to dirty gray colored Sitagota basalts overlies Bortalao sandstone. Sitagota volcanics forms the core of Sitagota syncline and stands out as high conical hills rising above the Bortalao sandstone. It comprises of two variants, i.e. the porphyritic and non-porphyritic with amygdaloidal structures. The amygdules are filled with secondary silica. Bortalao sandstone fragments also noticed with in Sitagota basalts at places.

2.3 Previous studies done in and around the study area

2.3.1 Geological studies

Reconnaissance, regional, detailed radiometric, geological and geophysical surveys carried out in different phases in Dongargarh-Kotri belt and identified potential zones for uranium mineralisation. These previous studies done by Atomic Minerals Directorate for Exploration and Research (AMD) has brought out number of surface radioactive occurrences in to the light of exploration programme and these occurrences are associated with Basement Bijli rhyolites, Proterozoic Bortalao sandstone, Karutola sandstones and Dongargarh granites. Few radioactive occurrences are also associated with ferruginization, illitisation and other alterations that are associated with Bortalao sandstones (viz. Ramatola, Bijepar, Darekasa and Dongargarh) and basement rocks (Sinha, D.K., 1991, 20).

Bijepar area

Reconnaissance radiometric survey in parts of Gondia district (Bhandara district old name) led to the discovery of a surface uranium occurrence associated with shear zone near Bijepar village. Subsequent study of geology and structure resulted in identification of significant radioactivity, ranging from 2 to 10 x bg was recorded in sheared feldspathic quartzite with a dimension of 50m x 4m. Along the shear quartz vein is exposed over a

length of 2 km intermittently intruded. The quartz vein at places carries copper mineralisation consists of Chalcopyrite, Bornite, stains of Malachite and Azurite. Also contains Pyrite. In this area, quartzites are formed from Bortalao sandstones due to dynamo thermal metamorphism as it is evidenced that sandstone to quartzite transformation while approaching towards quartz vein. Shear zone is trending in NNW direction. Along this shear zone, silicification, brecciation, drusy cavities, conjugate set of joints in feldspathic quartzite are common. Samples from the area (200 m X 10 m) have assayed eU_3O_8 up to the order of 0.011% and 0.012% U_3O_8 (β/γ).

Ramatola area

Radioactivity associated with Bortalao sandstone of feldspathic composition coated with limonite stains are recorded at 300m ESE of Ramatola village. The samples had assayed from 0.017% to 0.019% U_3O_8 (β/γ). One more anomaly at 1.3 km ESE of Ramatola village over a patch of 20 m X 2 m, of polymetic conglomerate belonging to Bortalao sandstone is recorded.

Patratola area

Radioactive anomaly is identified along a brecciated quartz reef having infiltrated iron solution patches within the Bortalao sandstone. The radioactive sample analysed values are up to 0.012% eU_3O_8 and 0.015% U_3O_8 (β/γ).

Kolarbhatti area

Subsequently, detailed geological and radiometric investigations in between Bijepar and Ramatola villages were studied in recent years (2017-18) for unconformity and sandstone type mineralisation. These studies have resulted in locating few radioactive occurrences along the unconformity contact between Bijli Rhyolites and Bortalao sandstones and associated within ferruginous sandstones at Kolarbhatti village. In this area, the

basement Bijli rhyolite serves as a potential source due to its high intrinsic concentration of uranium. The overlying Bortalao Formation represented by immature sediments in the area having high ferruginous concentration have been proved as good host for mineralization in earlier exploration works. The presence of Sitagota volcanics plays a vital role by providing the necessary geothermal gradient to mobilize the uranium within the system. Small scale fractures and faults cross-cutting the basement and the overlying sediments act as conduits for the hydrothermal solutions. The radioactive sample values assaying up to 0.029% U_3O_8 with negligible thorium supports the above discussed points. Subsurface exploration in this area has identified lean mineralisation associated with basement Rhyolites and few patches in Bortalao sandstones (Shukla *et.al.*, 2018, pp. 21-29).

2.3.2 Geophysical surveys

As such most of the area is under soil cover, geophysical studies also done in recent years (2018-19). These surveys are resulted in identifying the unconformity contact between Bijli rhyolites and Bortalao sandstones. Magnetic studies have helped in identifying the zones of high thickness Bortalao sandstone based on low magnetic signature and structural features such as fractures/faults. Apart from the lithological variations and subsurface distribution of basic rocks, few structural features such as faults/fractures trending in NW-SE and NE-SW are identified. Gravity studies also helped in identifying litho-units, structural features and unconformity contact in the area. Time-Domain Electromagnetic (TEM) survey has brought out the conductor locations that could be fractures/shears within the basement Rhyolite rocks and found correlation with magnetic lows (Satyanarayana *et al.*, 2019, 41).

CHAPTER 3

GRAVITY METHOD

3.1 Introduction

It is well known that every object on the earth's surface is attracted towards the earth's center with a force equal to the weight of the object. The force experienced by a mass of one gram on the earth's surface is numerically equal to the acceleration due to gravity. This force also called the gravity field or gravity force of the earth. This force is the resultant of the forces of attraction due to the various shells of the earth minus or negative the component of the earth's centrifugal force along the resultant. A dominant part of this gravity force is due the mantle and core, and about only 0.3% of its magnitude is derived from the materials in the crust. Due to the regular shape of the mantle and the core, and due to the systematic variation in density, with depth, of the materials in them, the gravitational force due to them varies uniformly in a lateral direction. But the crustal rocks and those present at the Mohorovicic discontinuity are not laterally uniform in their density. Consequently, they produce a minor gravity field which varies from point to point on the earth's surface. Since gravity varies inversely as the square of the distance, the rocks very close to the earth's surface account for a substantial part of the variation in gravity on the earth's surface. Other factors responsible for the variation in gravity are the centrifugal force of the earth, departure of the earth's surface from that of a sphere and the topography of the earth's surface. Corrections can, however, be worked out and applied to the observed gravity for the effects of the topography. The gravity values, thus corrected, differ from the earth's 'normal' gravity which includes the effects of the other two sources also. These differences are known as the gravity anomalies, and are caused by lateral changes in density of the materials at different depths below the ground surface (Musset, A.E. et al., 2009, 107, Kearey, P. et al., 2002, pp. 125-182). Gravity surveying, or prospecting, is one primary geophysical method in mineral

exploration. In this gravity method, we measure acceleration due to gravity (g) in order to investigate subsurface geological bodies or structures that are associated with lateral density variation. These include ore bodies and intrusions whose density differs from that of the surrounding host rocks, basins occupied by less dense rocks, faults if they offset rocks so that there are lateral density differences, and cavities. By mapping these gravity anomalies on the ground surface, it is possible to predict the underlying density variations which can be related to the sources of geological interest.

The entire method of gravity prospecting can be divided into three stages. The first is the field work, where the gravity and elevation data are collected along with spatial localities on the earth's surface. The second step is the reduction of the observed gravity data, by making corrections for various extraneous disturbances and subtracted from the observed gravity to compute the gravity anomaly. The third step is the interpretation of these gravity anomalies in terms of geology. Obviously, for the successful application of the gravity method, the presence of a lateral density variation is necessary i.e., the target, which is being looked for, must differ substantially in its density from that of the surrounding host rocks. The difference in the densities of the target and the surrounding rocks is the density contrast. Thus, the presence of density contrast between the targets and the surrounding rocks is essential for the success of gravity prospecting. The absence of gravity anomalies may not necessarily mean the absence of ore deposits or geological structures because these, even when present, may not possess any density contrast. Such deposits and structures may provide other physical parameter contrast which may be useful in other geophysical method. Thus, the physical properties of the targets and the surrounding host rocks must be examined before planning and executing a geophysical survey.

3.2 Rock densities in the geological environment of study area

An understanding of the density of geological materials and geological causes for variations in density is crucial for making geologically realistic interpretations of gravity data. Density of rock specimens can be measured using Archimedes principle. The specimen's weight in air and when immersed in water are compared. This gives the specific gravity of the specimen, i.e. its density relative to water, but given that water attains its maximum density of 1 g/cc at 4 °C, and that it changes very little with temperature, specific gravity is taken as the density of the rock specimen (ρ_{specimen}) and is given by

$$\rho_{\text{specimen}} = \text{Weight in air} / (\text{Weight in air} - \text{Weight in water}) \quad (3.1)$$

In order to obtain accurate measurements, the specimen should be fully saturated, and should be as large as possible to increase the likelihood of using representative samples of what may be a heterogeneous lithotype.

Densities of collected rock samples from study area measured with the help of precision electronic balance. This instrument will give us bulk density of rock sample and its works on Archimedes principle. Porous rock samples which are sandstones were kept in water up to 24 hours to overcome porosity effect on density values and rest of samples are done on same day.



Figure 3.1 Laboratory measurements of density(ρ).

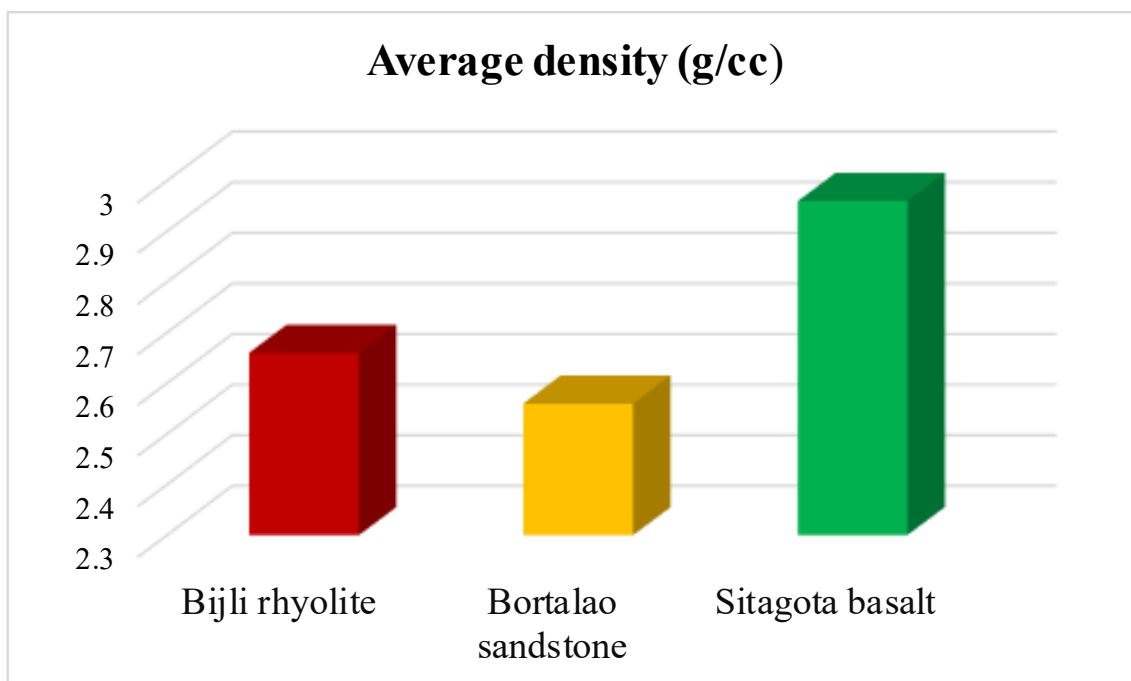


Figure 3.2 Density values of the rock samples collected from the study area.

Table 3.1 Average density of rock samples.

Lithounit	No.of samples (n)	Density range (g/cc)	Mean(μ)	S.D(σ)
Bijli Rhyolite	51	2.27-2.72	2.66	0.06
Bortalao sandstone	25	2.52-2.62	2.56	0.16
Sitagota basalt	15	2.75-3.10	2.96	0.08

Average density values of rock samples of the study area are showing (Figure. 3.2) high density values over basement Rhyolite rocks (ranging from 2.27-2.72 g/cc) and Sitagota basalt (ranging from 2.75-3.10 g/cc). Medium density values are observed over Bortalao sandstone (ranging from 2.52-2.62 g/cc), quartz reef (2.64 g/cc) and low density values obtained over weathered Rhyolites i.e. 2.27 g/cc. These density values were used in the qualitative and quantitative interpretations (modelling of the profile data) of the gravity data.

3.3 Instruments

The instrument for measuring gravitational acceleration is known as a gravity meter. Gravity surveys for exploration measure differences in gravity between the survey stations and a survey base station, i.e. relative measurements (Chapin, 1998, pp. 100-112). Modern gravimeters or gravimeters can detect changes in g as small as a hundredth of a mGal or about $10^{-8} g$.

Nearly all gravimeters used for geophysical surveying rely on a mass, supported by some kind of spring, responding to the pull of the Earth's gravity as shown in Figure 3.3. Because the changes to be measured are so small, the spring is arranged to amplify the effect. Initially, the beam is at rest in position (i), with the pull of the spring balancing the pull of gravity on the mass. When the gravimeter is moved to where g is larger, the beam rotates to a new balance (ii), where the extra pull of the extended spring balances the extra pull of gravity. The spring pulls obliquely to the beam so that, as the beam rotates clockwise, the spring's pull becomes more oblique to the beam (θ decreases to θ'), which partly cancels the effect of the extra tension of the spring resulting from its extension. As a result, the beam rotates far more than it would have had the spring pulled vertically upwards. By careful choice of spring and its angle to the beam the two effects can be made almost to cancel, greatly increasing the sensitivity of the instrument to changes of g . The deflection is not measured; instead, the beam is returned to its initial (zero) position – this makes it a 'null instrument' – by moving the top end of the spring up a little, by a screw turned from outside the case. The turns of the screw are calibrated in mGal or g.u. In practice, springs are not identical so a conversion table is given for each instrument to correct the readings. The beam needs to be strong and light, and the elastic properties of the spring should change as little as possible with time. As changes of temperature affect the readings, the mechanism may be placed in a vacuum flask to reduce temperature fluctuations; alternatively, it is kept at a

constant temperature by a thermostatically controlled heater, though this needs batteries that are heavy and require recharging. Changes do still occur, due to slow extension of the spring due to creep and other causes, and constitute the instrumental drift.

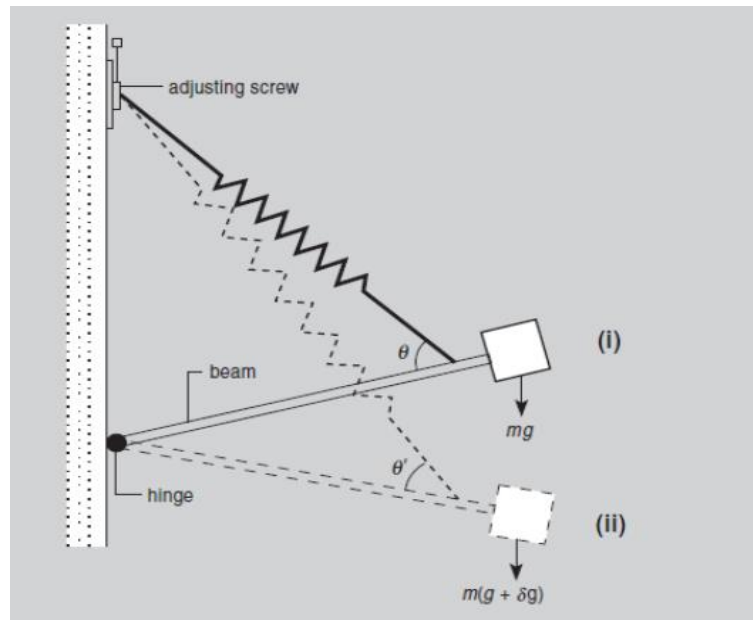


Figure 3.3 Schematic diagram of a gravimeter.

3.4 Gravity data acquisition

Gravity survey has been conducted in the study area with the prime target of delineating basin configuration, litho and unconformity contacts, fault/fracture zones etc., associated with basement and sediments of Khairagarh basin. Gravity survey lines are planned in the direction of East-West, which are more or less perpendicular to the general strike (NNE-SSW) of geological formations in the study area of Bijepar-Ramatola tract. To meet the objectives, survey was planned on semi-detailed scale with traverse interval of 200 m and readings are made at every 50 m station interval as shown in Figure 3.4.

To map out the variations in the gravity field of this area, a set of data acquisition parameters has been estimated based on the variations in the density property, and the

minimum required dimensions of the anomalies to be recorded. The base is established nearby Kolarbhatti village towards east of the study area. To get the combine map for this area along with previous acquired data, base station has fixed at the same location which is previously established at Kolarbhatti village.

Station elevations need to be measured with an accuracy of about 5 cm (vertical and horizontal) in order to calculate the free-air correction to an accuracy of 0.001 mGal, this requirement has fulfilled by making help of Differential Global Positioning System (DGPS; Spectra Geospatial made).

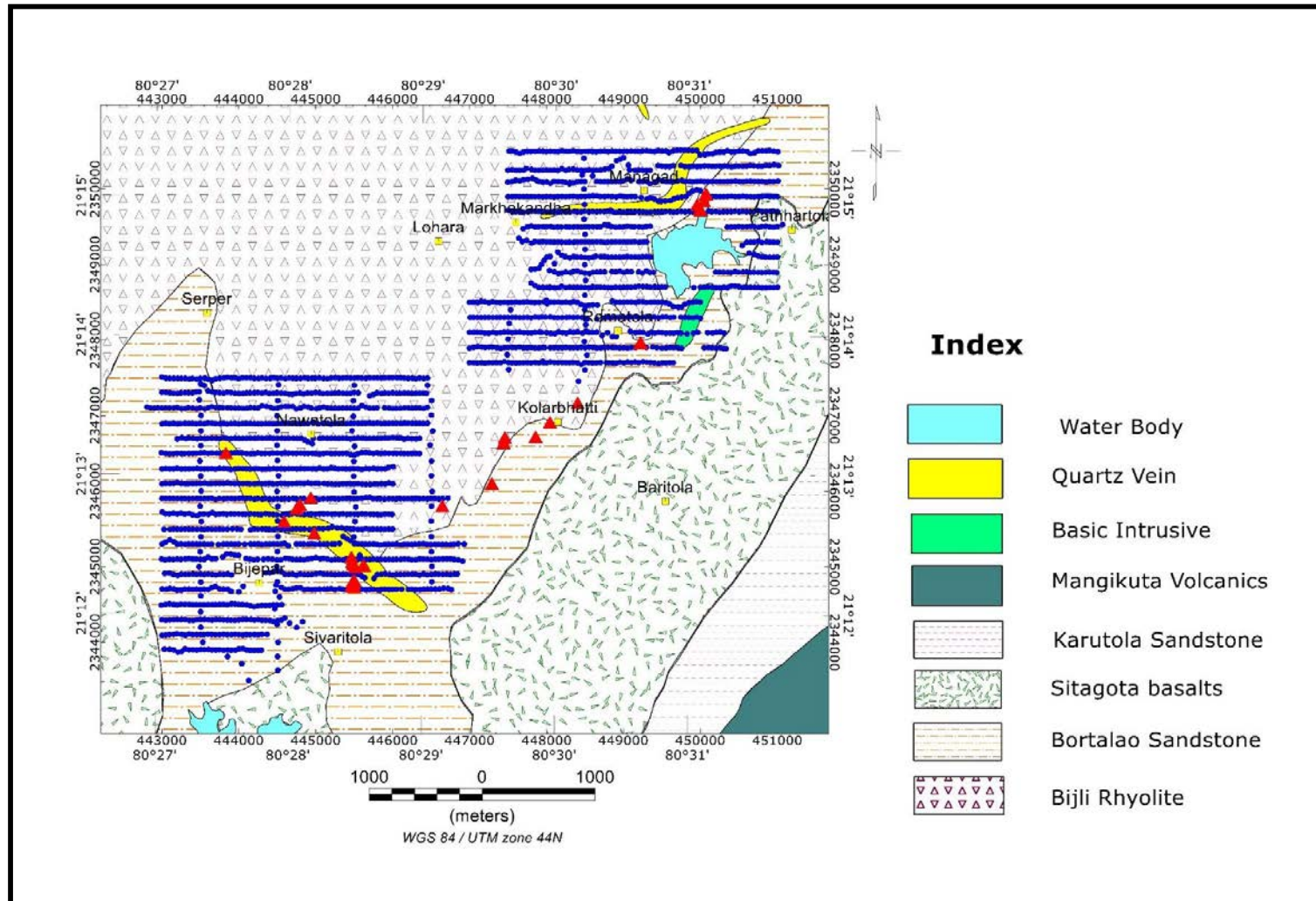


Figure 3.4 Gravity survey layout superimposed on geological map of the study area.

3.5 Reduction of gravity data

The corrections applied to remove unwanted variations in gravity are known as reduction of data. They correct or compensate, and we consider them in the order that they are applied to the observed data. The data reduction sequence is summarised as shown in figure 3.5.

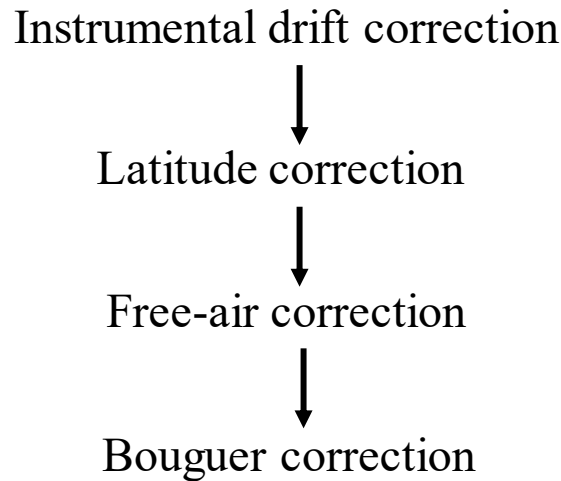


Figure 3.5: Sequence of data corrections applied over gravity data of the study area.

Instrument drift

The drift correction compensates for drift in the instrument's reading over time. The drift correction can be carried out based on repeat readings at the base station. By recording the time of each reading, the drift rate can be determined and the effect removed from each gravity measurement. The assumption is made that the drift is linear during the time between base station readings.

Latitude correction

The variation in gravity due to the difference in latitude between the survey station and the survey base station is compensated with the latitude correction. At the scale of most mineral exploration activities, the change in normal gravity is sufficiently smooth and gradual that it appears as a very small linear increase in the direction of the nearest

geographic pole. The latitude gradient represents the change in gravity with north–south distance from a base station and is given by

$$\mathbf{g}_\phi = 0.812 \sin 2\phi \text{ mGal/km} \quad (3.2)$$

where, ϕ is the latitude (negative for southern hemisphere) of the base station. This formula is accurate enough for most exploration applications for distances up to about 20 km north and south of the base station (preferably located central to the survey area).

Free-air correction

The change in gravity with height is compensated with the free-air correction given by

$$\mathbf{g}_{\text{FA}} = 0.3086h \text{ mGal/m} \quad (3.3)$$

where, h = height (m) of the gravity station above the datum (usually the geoid)

Station height needs to be measured with an accuracy of about 3 cm in order to calculate the free-air correction to an accuracy of 0.001 mGal. The free-air correction compensates for height variations of the gravity meter above or below the datum level. The free-air correction is added to the gravity reading if station is above the datum and will be deduct for the station below the datum.

Bouguer correction

The free-air correction only accounts for the difference in height between the instrument and the datum level. When the gravity station is located on topography above the survey datum, it is located on a layer of rock that contributes mass between the gravity meter and the datum. The rock layer increases the measured value of gravity. It's effect is compensated by the Bouguer correction, which assumes that the Earth is flat, i.e. not curved, and that the rock layer is a horizontal slab of uniform density extending to infinity in all directions. It is given by

$$\mathbf{g}_{\text{BC}} = 0.04192\rho h \text{ mGal/m} \quad (3.4)$$

where, ρ = Bouguer density (g/cc) (average density of the slab between the gravity station and the datum level). The Bouguer correction is deducted from the gravity reading if station is above the datum and will be add to the station below the datum. Bouguer correction was done by considering the density of 2.67 g/cc which is average density of the Bijli rhyolites in the study area.

After all necessary corrections mentioned in data redustion process have been attempted on acquired gravity data of study area and derived Bouguer Gravity Anomaly (BGA). Gravity data of the study area have not been corrected for the terrain correction, which accounts negligible effect as the terrain is relatively flat in 5 km radius from base station. Terrain corrections are generally necessary if a topographic difference within a sector is more than about 5% of its distance from the station (Lowrie, 2007, 79).

3.6 Data processing

3.6.1 Bouguer Gravity Anomaly(BGA)

Bouguer gravity anomaly map is prepared with a cell size of 50m by choosing minimum curvature gridding method. The anomalies ranging from -1.49 to 7.7 mGal with a total relief of 9 mGal are recorded. Lower order of gravity anomalies (-1.49 to 0.5 mGal) associated with Bijli rhyolite and quartz reefs in the western and central part of the map is observed. Moderate gravity anomalies ranging from 0.5 to 2.0 mGal associated with Bortalao sandstone in the eastern part of Ramatola and western, NW part of Bijepar villages are observed. Anomalies more than 2.0 mGal associated with Sitagota basalt in the east of *Ramatola* village are observed (Figure. 3.6).

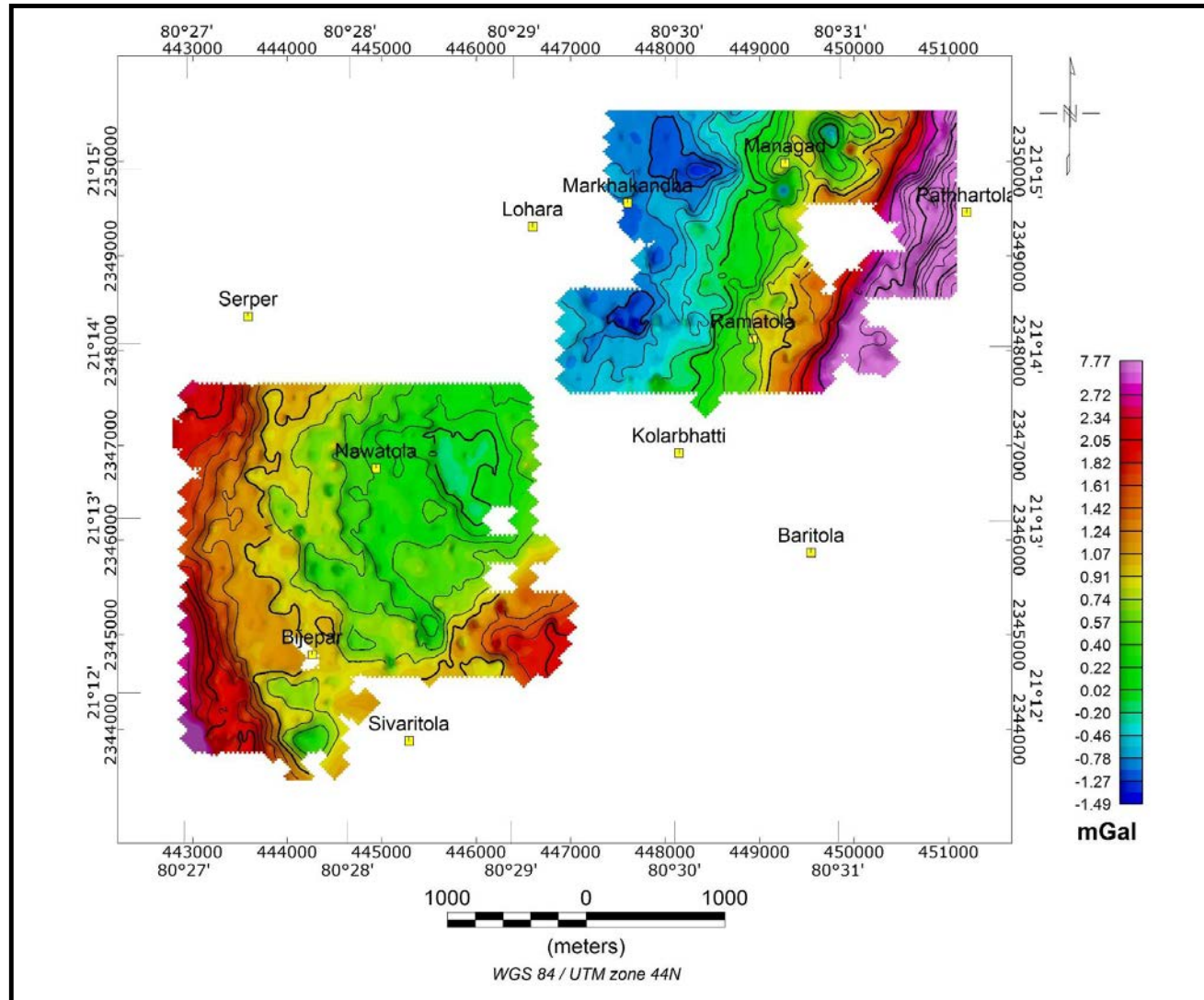


Figure 3.6 Bouguer Gravity Anomaly (BGA) of study area.

3.6.2 Data processing techniques

In order to present gravity potential field data in a comprehensible form, data processing and structural features enhancement techniques such as upward continuation, total derivative and Euler's depth solutions are performed on the bouguer gravity data.

3.6.2.1 Upward continuation of Bouguer Gravity Anomaly (BGA) map

Upward continuation methods are employed in gravity interpretation to determine the form of regional gravity variation over a survey area, since the regional field is assumed to originate from relatively deep-seated structures. The equation of the wave number domain filter to produce upward continuation is

$$\mathbf{F}(\omega) = e^{-h\omega} \quad (3.5)$$

Where, h = continuation height.

This function decays steadily with increasing wave number, attenuating the higher wave numbers (signal belongs to shallower depth) more severely, thus producing a map in which the more regional features predominate (Dean, 1957, pp. 97-127, Pawlowski, 1995, pp. 390-398). Continuation filters are important isolation and enhancement methods that project the observed gravity anomaly to other surfaces either above (upward continuation) or below (downward continuation) the original observation surface.

Here we attempted upward continuation technique over gravity data and it is a smooth, low-wave number pass filter which emphasizes the anomalies from the broader, deeper sources at the expense of the shallow-sourced anomalies. Because it is a smoothly varying filter, which preserves the character of the broader anomalies making it possible to quantitatively analyse the upward-continued anomalies. The smoothing effect of upward continuation is evident in figure 3.7. The result of upward continuation of a data set has been used as an approximation to the regional field which is subtracted from the observed

anomaly field to determine the residual anomalies. The height of the upward continuation to achieve an appropriate regional map will vary depending on the nature of the anomalies. The decision on the appropriate height is arbitrary and can best be determined by comparing results from a range of heights. Here we chosen upward continuation map for the height of 300 m as a regional anomaly and produced residual gravity anomaly map to get shallow structural features clearly.

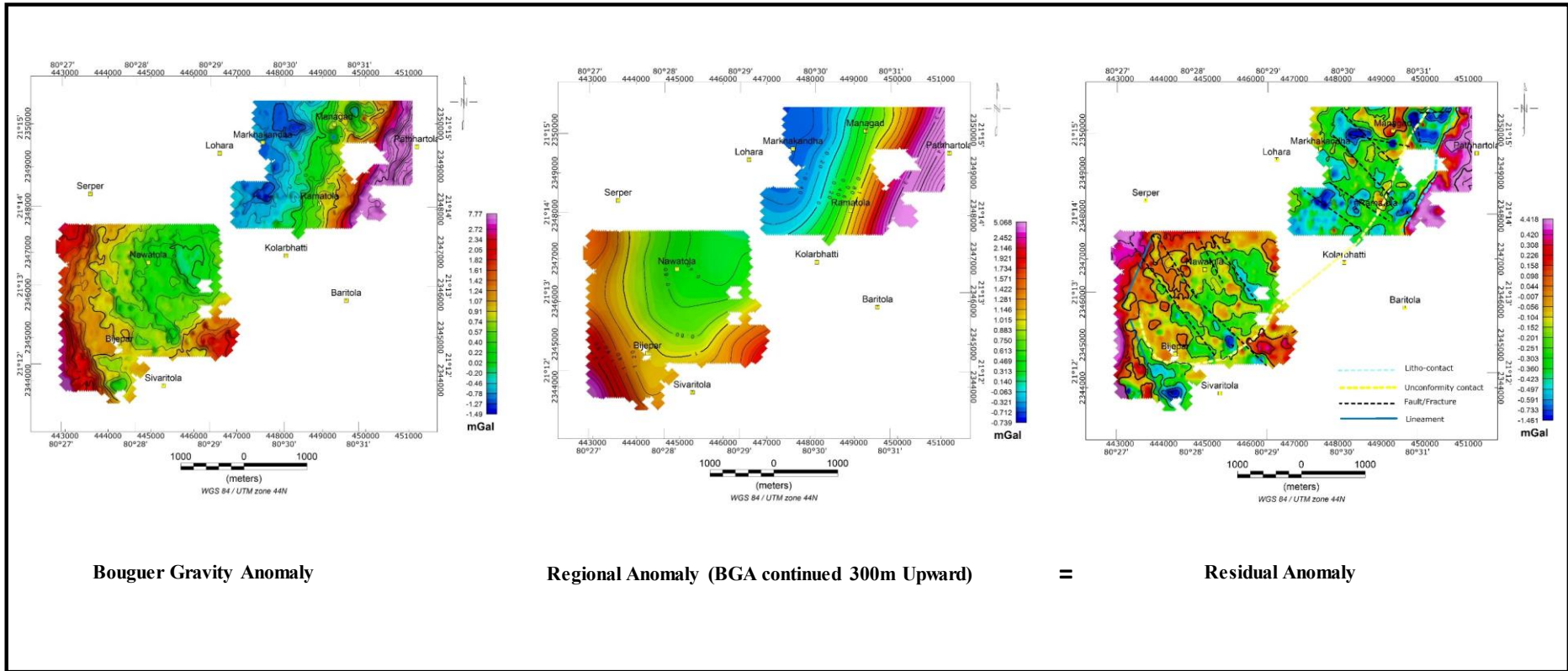


Figure 3.7 Residual gravity anomaly map produced by subtracting regional anomaly from bouguer gravity anomaly.

3.6.2.2 Analytic signal (Total derivative or Total gradient) method

The analytic signal method has been the subject of continuing investigation and improvements since it was first applied. The analytic signal concept can be applied to the gravity data by using horizontal and vertical derivatives of gravity vector components (Nabighian, 1974, pp. 85-92, and Pilkington, 2004, pp. 306-311). The absolute amplitude of the 3D analytic signal of the total magnetic anomaly field \mathbf{G} observed at a station A (x, y) can be defined as

$$|A(x, y)| = \sqrt{\left(\frac{\partial G}{\partial x}\right)^2 + \left(\frac{\partial G}{\partial y}\right)^2 + \left(\frac{\partial G}{\partial z}\right)^2} \quad (3.6)$$

where G is the gravity field.

The individual gradients can be determined with spatial domain techniques, but are generally calculated in the wave number domain.

To highlight the structural feature contact and its trend, analytical signal technique has been attempted over bouguer gravity data. From the analytical signal map, it is observed that there is a good agreement between analytical signal peaks and structural features inferred from Bouguer gravity anomaly map (Figure 3.8). Major litho-contact between Bortalao Sandstone and Sitagota basalt in the eastern part of *Ramatola* village has been marked accurately, but unconformity contact between basement Bijli rhyolites and Bortalao sandstone has not highlighted much by this technique.

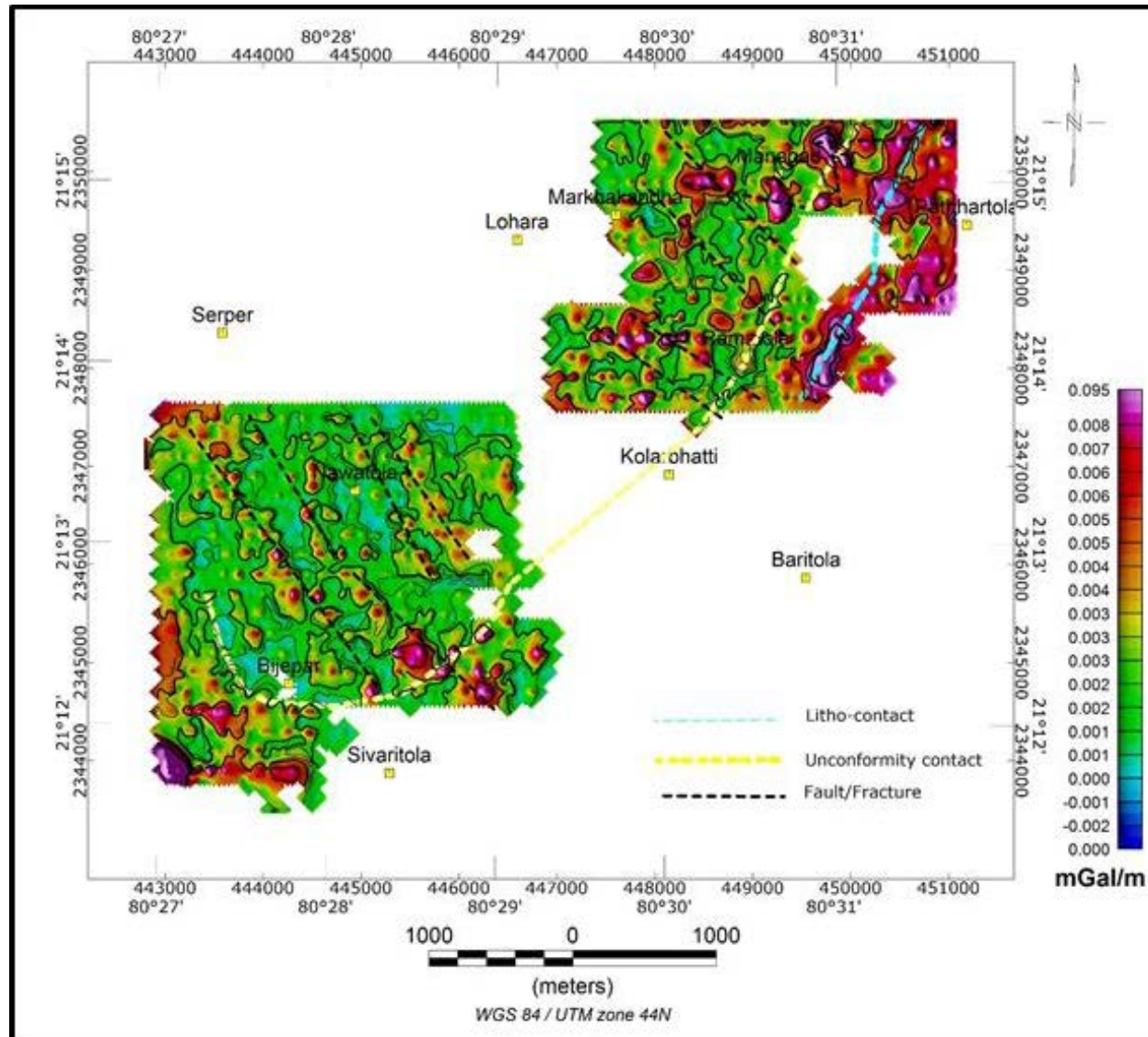


Figure 3.8 Analytical signal (AS) map of study area.

3.6.2.3 Euler Depth solutions

Euler deconvolution is used for rapid interpretation of gravity data. It is particularly good at delineating contacts and rapid depth estimations. To discriminate anomaly sources, the decay rate n , which is also called the structural index can be investigated using Euler's homogeneity Equation.

$$\Delta x \frac{\partial g(x, y, z)}{\partial x} + \Delta y \frac{\partial g(x, y, z)}{\partial y} + \Delta z \frac{\partial g(x, y, z)}{\partial z} = -N \times g(x, y, z) \quad (3.7)$$

Where $\Delta x = (x-x')$, $\Delta y = (y-y')$ and $\Delta z = (z-z')$, Structural Index (N) = Measure of the rate of change (fall-off rate) with distance of a field and it is a function of the geometry of the causative bodies (Thompson, 1982, pp. 31-37, Durrheim, R. J., pp. 545-550 and Cooper, G. R. J., 1998, 51-56).

After attempting Euler depth solution technique for Bouguer gravity anomaly with different window sizes and structural index, for structural index of 1 and window size of 9 is resulted reliable solutions and which are falling along the inferred structural features (Figure 3.9).

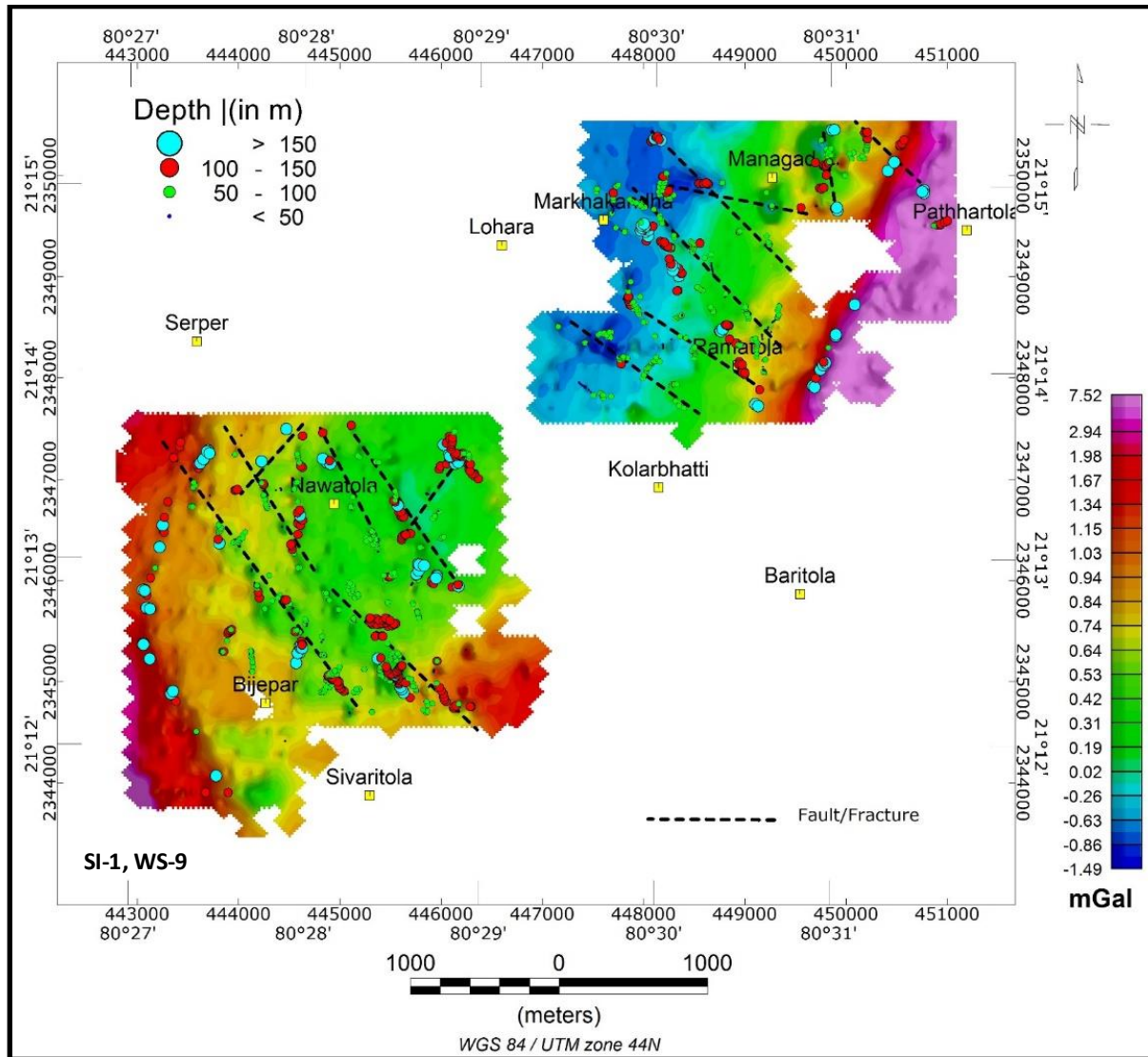


Figure 3.9 Euler depth solutions with their respective structural features.

3.6.2.4 3D Modelling of Gravity

GRAV3D is a program library for carrying out forward modelling and inversion of surface, airborne, and/or borehole gravity data to generate 3D models of density contrast (Li, X., 2008, pp. 990-1002). GRAV3D involves gravimetric data gathered anywhere at or above the surface of the Earth. These data are the vertical component of the gravity field caused by a three dimensional distribution of density contrast within the volume of ground directly beneath the survey area. This subsurface volume (with optional topography) is modelled as a set of rectangular cells each with constant density contrast. The inverse problem involves estimating the density contrasts of all the cells based upon measurements gathered during a field survey. GRAV3D modelling has been attempted and density values of collected rock samples are used effectively while preparing model from gravity data. Four (4) iso-surfaces of different density contrast as causative sources of gravity anomalies and lithological boundaries have marked tentatively for model due to lack of data at some places in the study area. The model more or less represents the reliable plausible geological model in the study area (Figure 3.10).

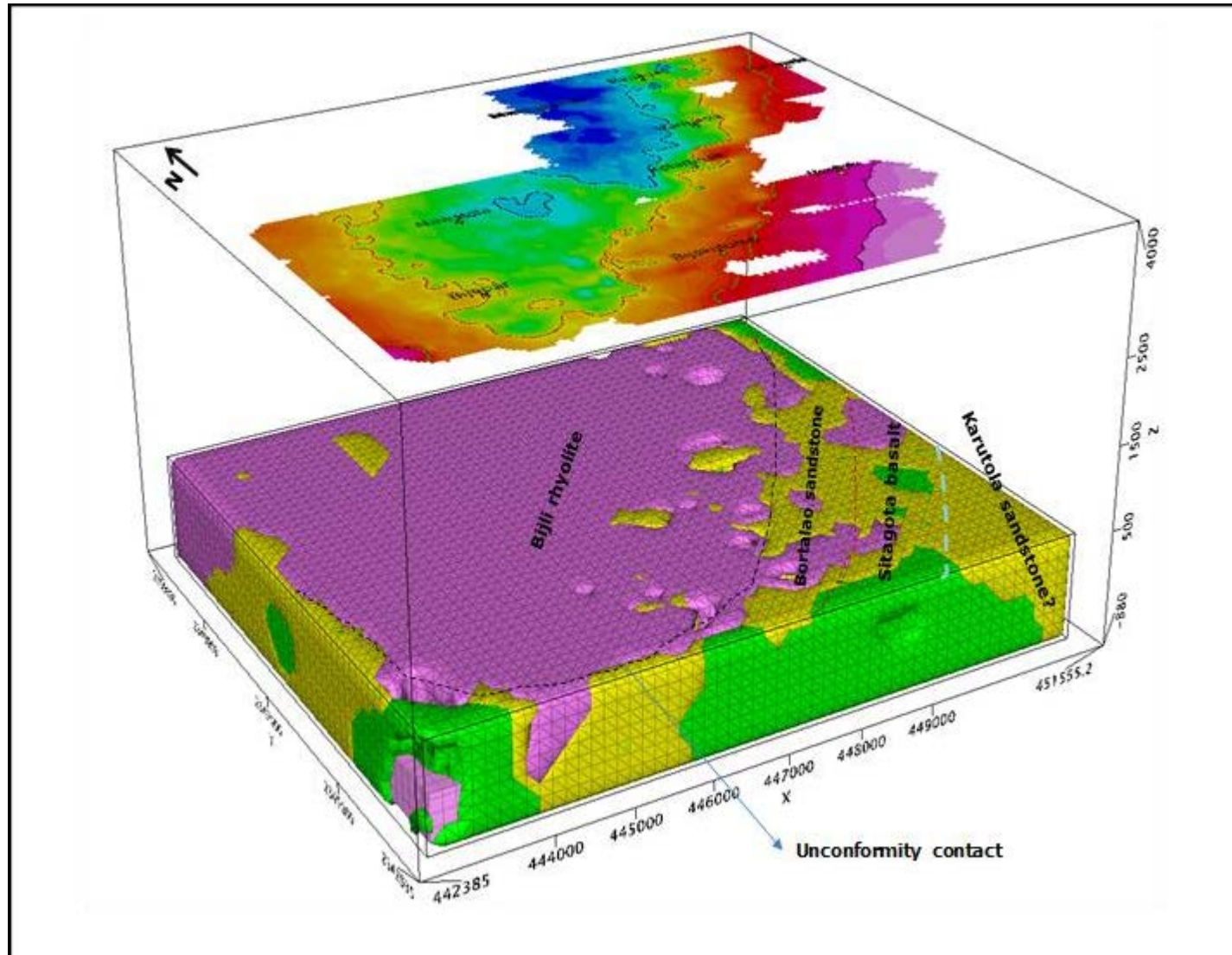


Figure 3.10 UBC GRAV3D Modelling for Gravity data of Bijepar-Ramatola block.

3.7 Data interpretation

The unconformity contact between Bijli Rhyolites and Bortalao sandstones, litho contact between Bortalao sandstones and Sitagota basalt cover are demarcated, which are more or less coinciding with a 1 mGal and 3 mGal contours of Bouguer gravity anomaly respectively with respect to gravity base station at *Kolarbhatti* village. These are well substantiated by magnetic data and discussed in the following chapter. Faults/fractures trending in NW-SE, WNW-ESE directions are demarcated towards north of *Ramatola* and *Markhakhanda* villages. It is noticed that most of these fractures are associated with quartz veins/reefs. Few lineaments (based on the alignment of gravity contours) trending in NW-SE and NE-SW directions in and around Bijepar village are identified. Out of these, NW-SE trending lineaments and zone of intersection of NW-SE & NE-SW towards north of Bijepar village which are well corroborated with Magnetic lineaments seem to be important in searching for mineralisation from the structural point of view. The major fault zone located at the immediate NE of *Bijepar* village showing its depth persistence and solutions ranging from 100 to 150 m are dominant in this zone. number of identified depth solutions ranging from 50 to 150 m is observed in the study area. Processed maps of gravity field proved to be immense help in interpreting/delineating boundaries of major geological units in the area and also in identifying major and minor structural features like faults/fractures associated with basement and sediments of Khairagarh Basin (Figure.3.11).

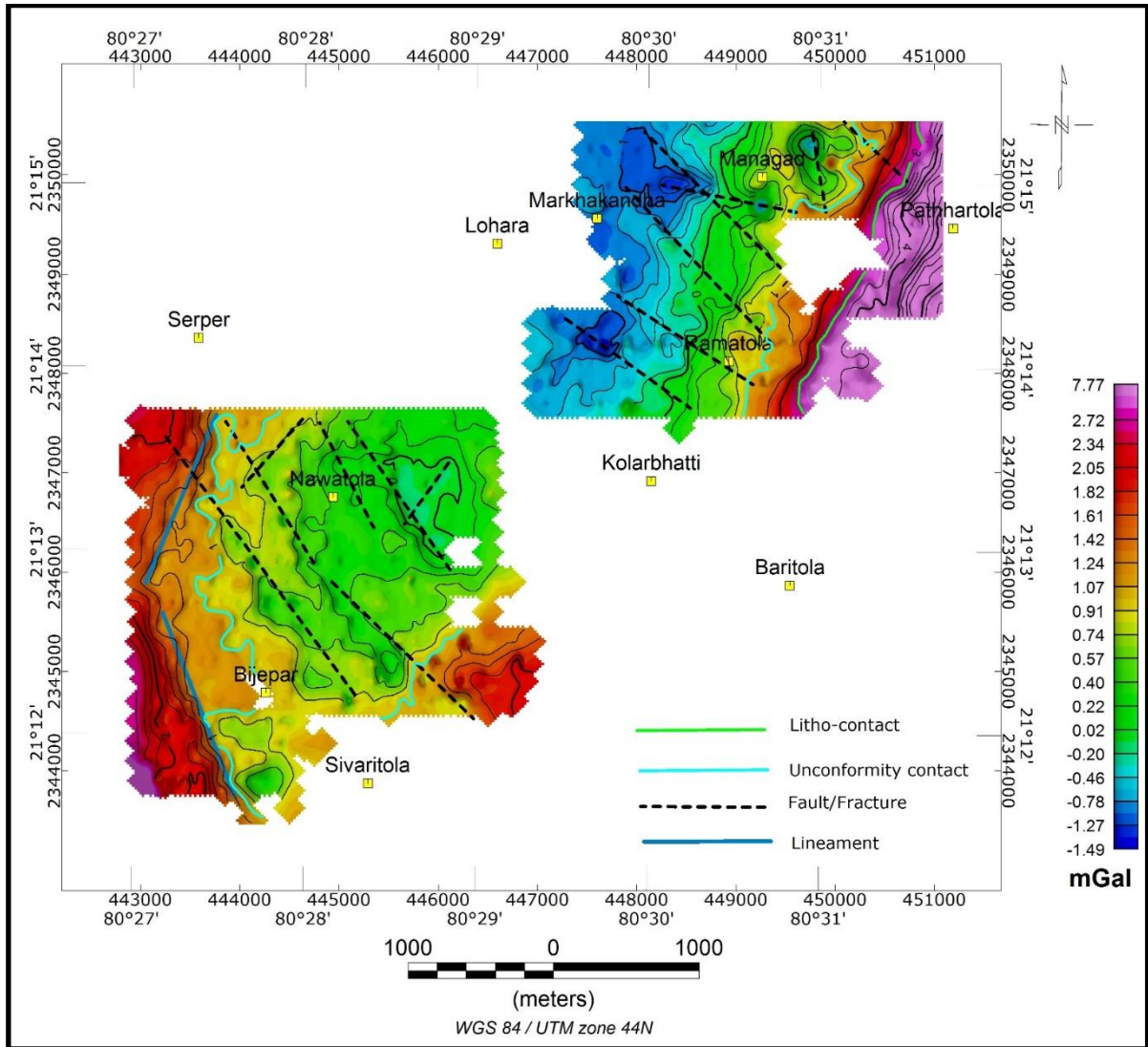


Figure 3.11 Bouguer Gravity Anomaly with inferred structural features.

CHAPTER 4

MAGNETIC METHOD

4.1 Introduction

The magnetic method is the oldest and one of the most widely used geophysical techniques for exploring the Earth's subsurface. It is a relatively easy and inexpensive tool to apply to a wide variety of subsurface exploration problems involving horizontal magnetic property variations from near the base of the Earth's crust to within the uppermost meter of soil. These variations cause anomalies in the Earth's normal magnetic field that are mapped by the magnetic method. The geomagnetic field is caused by electrical currents associated with convective movements in the electrically conducting outer core of the Earth. Additional significant components of the field are derived from variations in the magnetic properties of the lithosphere and electrical currents in the ionosphere as well as in the Earth. The main field roughly coincides with the Earth's axis of rotation and is dipolar in nature. The force of attraction between opposite magnetic poles, or repulsion between like poles, is proportional to the product of the strength of the poles and inversely proportional to the square of the distance between the poles in a manner analogous to the gravitational attraction between masses. For most exploration purposes the magnetic force per unit pole, or magnetic field strength, is measured either in a directional mode where the sensor is spatially oriented or in a non-directional mode where the sensor obtains total field measurements that are presumed to be collinear with the Earth's magnetic field. Modern magnetic measurements are obtained electronically by measuring the precession of atomic particles which is proportional to the ambient magnetic field. Typically, measurements to map variations in the magnetic properties of the lithosphere are made to a precision of roughly one part per 5,00,000 of the terrestrial field. The magnetic method is a passive exploration method in that it is based on mapping the natural or normal magnetic force field of the Earth. The geomagnetic field is

ever-present, but it varies both spatially and temporally. These variations distort the anomalous changes in the field (i.e. anomalies) caused by local subsurface conditions of interest in magnetic surveying, and thus must be removed from the observed data to produce interpretable measurements. Successful applications of the magnetic method require an in-depth understanding of its basic principles, and careful data collection, reduction, and interpretation. Interpretations may be limited to qualitative approaches which simply map the spatial location of anomalous subsurface conditions, but under favourable circumstances the technological status of the method will permit more quantitative interpretations involving specification of the nature of the anomalous sources (Telford, W.M, 2004, pp. 62-100).

The relative ease and simplicity of applying magnetic technique makes it a desirable first-choice methodology wherever it can solve or contribute to the solution of subsurface studies. The magnetic method is employed in study area by keeping its effectiveness of rapidity in acquisition and delineating structural features along with other geophysical methods (Gravity and TEM) to extract subsurface information.

4.2 Magnetic properties of rocks in geological environment of study area

An understanding of the magnetism of the geological environment and geological causes for variations in magnetism is crucial for making geologically realistic interpretations of magnetic data. The magnetism of rocks depends on the magnetic properties of their constituent minerals and their state. Rock magnetism varies far more than density with susceptibility varying by approximately five orders of magnitude in the common rock types. The most fundamental control on rock magnetism is iron content. Put simply, without iron magnetic minerals cannot form, but not all iron-minerals are strongly magnetic. Magnetic minerals may be formed in the primary igneous environment; others may be created by secondary processes such as metamorphism. They all may be destroyed by secondary processes, notably weathering. Unlike density, rock magnetism is not a bulk rock property.

Instead it depends on mineral species that usually comprise only a few per cent by volume of a rock's mineralogy. Magnetic mineralogy is often strongly affected by subtle changes in geochemistry and secondary processes, all of which can produce very different magnetic properties in similar lithotypes. An additional complication arises because magnetism is a vector property. One or both of the strength and direction of the rock's magnetism may be affected, and the affects may pertain to either, or both, of the remanent and induced magnetisms. Also, it is common for rocks to contain distinct populations of magnetic minerals with different characteristics, and these may be affected differently by geological events. The sensitivity of rock and mineral magnetism to the rock's geological history means that it can be a useful tool for studying that history (Dunlop, D.J., *et al.*, 1997, pp. 95-123 and Harrison, R.J., *et al.*, 2009, pp. 209-215).

4.2.1 Magnetic susceptibility measurement of rock samples

Magnetic susceptibility of rock units (collected along the traverses) is measured using Kappa meter instrument (KT-10). Susceptibility logging has also been done at available boreholes to get the idea about the subsurface susceptibility distribution/variations with respect to depth, which is useful to draw reliable conclusions getting from the later stages of magnetic data modelling.



Figure 4.1 Kappa meter for magnetic susceptibility measurements in the field.

Kappa meter used for the data collection is a most recent and advanced instrument with a sensitivity (1×10^{-6} SI units). Measurement can be made in normal mode (outcrop/lab samples), core mode (depends on size of cores) and scanner mode. Kappa meter can be used with a pin for rough surface measurements or without a pin when you can establish direct contact with the sample. In present study, data have been collected by using Kappa meter on the outcrop grab samples. Each measurement has been taken over a fresh rock surface made by breaking rock units and susceptibility value of a rock is considered as average of three measurements.

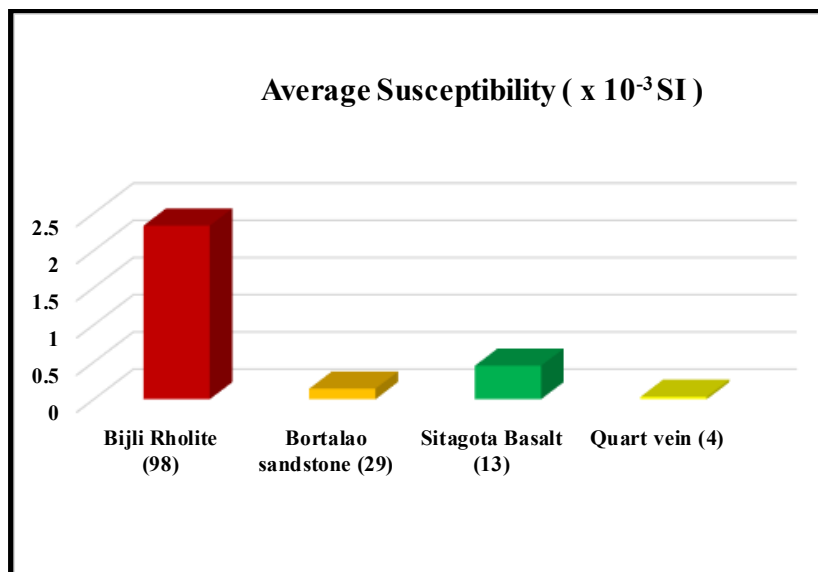


Figure 4.2 Susceptibility values of the rock samples collected from the study area.

Six measurements over different surfaces of samples have been taken and it was averaged. Data collected on the outcrop and rock samples is summarized in table-4.1. Average susceptibility values of the rock samples are showing higher values over rhyolites rocks.

Table 4.1: Average susceptibility of rock samples

S.No	Lithology & no. of samples	Susceptibility range ($\times 10^{-3}$ SI)	Mean sus./S.D
1	Bijli Rhyolite (98)	0.07-23.125	2.334/0.2
2	Bortalao sandstone (29)	0.0039-0.582	0.142/0.164
3	Sitagota Basalt (13)	0.237-0.805	0.451/0.174
4	Quartz vein (4)	0.014-0.045	0.033/0.011

Susceptibility values ranging from $0.07-23.125 \times 10^{-3}$ SI units are associated with Bijli Rhyolite rocks. Medium susceptibility values ranging from $0.237-0.805 \times 10^{-3}$ SI units are noticed with Sitagota basalts. Lower order values ranging from $0.0039-0.582 \times 10^{-3}$ SI units and $0.014-0.045 \times 10^{-3}$ SI units observed over sandstones and quartz veins respectively. At some places these sandstones are showing higher values (0.652×10^{-3} SI units) due to alterations like ferruginisation. Susceptibility values of surface rock samples of the study area are helped in qualitative and quantitative interpretations of magnetic data (Figure 4.2).

4.3 Data acquisition

4.3.1 Instruments

The present magnetic survey carried out with help of GSM-19T proton-precession magnetometer (PPM) made by GEM systems. The GSM-19T is a microprocessor based instrument with storing capabilities of large memory storage 32Mb (up to 5 million readings) and having integrated navigation. Synchronization of time between rover and the base station magnetometers for corrections of diurnal variations of magnetic field are done. The results of measurements are made available using a RS-232 for collection by data acquisition systems, terminals or computers. Both on-line Real Time Transmission (RTT) and post-operation transfers are possible.



Figure 4.3 Proton-Precession magnetometer.

Theory and operation

The proton precession magnetometer depends on the measurement of the free-precession frequency of protons of Hydrogen (H) nuclei, which have been polarized in a direction approximately normal to the direction of earth's magnetic field. When the polarizing field is suddenly removed, the protons precess like a spinning top, the earth's magnetic field supplying the precessing force corresponding to that of gravity in the case of spinning top. The protons precess at an angular velocity known as Larmor precession frequency, which is proportional to magnetic field strength F , so that

$$\omega = \gamma_p F \quad (4.1)$$

The constant γ_p is known as gyromagnetic ratio of proton, that is the ratio of magnetic moment to spin angular momentum. The detection is possible by means of a coil surrounding the sample, as voltage is induced is by moving proton at precession frequency. The essential

components of magnetometer include a source of protons (a small bottle of water or some organic fluid rich in hydrogen such as methanol, ethyl alcohol or benzene), a polarizing field considerably stronger than earth's field and directed normal to Earth's field, a pick up coil, an amplifier to boost the minute voltages and a frequency measuring device.

For the earth's magnetic field in the range of 30,000 to 60,000 nT, the corresponding precessional frequency is 1250 to 2500 Hz. For 1 nT sensitivity, 0.04 Hz frequency differences, and voltages of around 10 μ V (micro volt range).

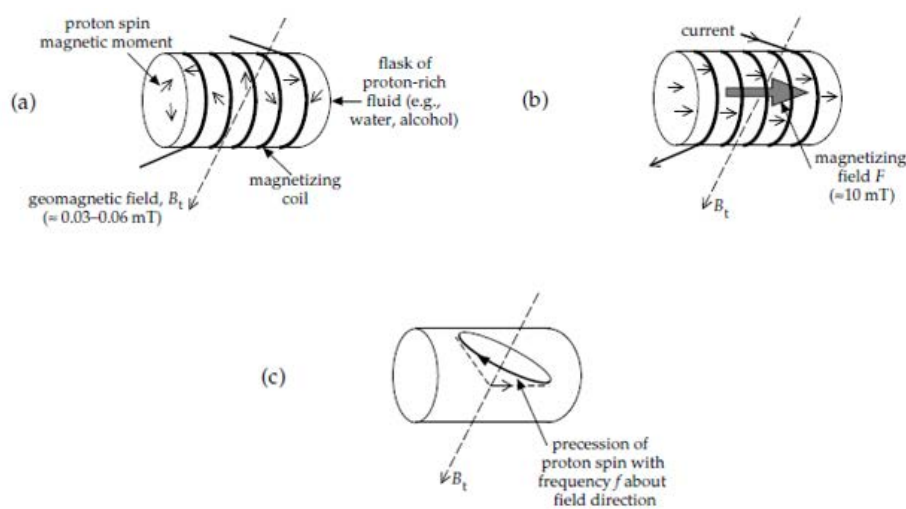


Figure 4.4 Working principle of PPM magnetometer

- a. The elements of a proton-precession magnetometer.
- b. Current in the magnetizing coil produces a strong field F that aligns the magnetic moments ("spins") of the protons.
- c. When the field F is switched off, the proton spins precess about the geomagnetic field B_t , inducing an alternating current in the coil with the Larmor precessional frequency f .

The proton free-precession magnetometer exploits - the tendency of a free proton (H^+) to align its magnetic moment with an ambient magnetic field and precess about that field direction when disturbed. A quantity (usually about half a litre) of some liquid rich in protons

such as water or alcohol in a sensor bottle is subjected to a strong applied magnetic field by way of passing a current through a coil wound around the bottle. Turning off that current causes the protons to search for the direction of the only remaining magnetic field - that of the earth - and to precess around it. The frequency of precession is given by

$$\boldsymbol{\omega} = \gamma_p \mathbf{F} \quad (4.2)$$

$$\mathbf{F} = \boldsymbol{\omega} / \gamma_p \quad (4.3)$$

Where, $\omega = 2\pi f$, f is precession frequency of proton over an ambient Earth's magnetic field

$$\text{Gyromagnetic ratio of proton } (\gamma_p) = 2.67513 \times 10^8 \text{ s}^{-1} \text{ T}^{-1}.$$

$$2\pi/\gamma_p = 23.4874 \pm 0.0018 \text{ nT/Hz}.$$

$$\mathbf{F} = \mathbf{23.4874 \pm 0.0018} f \text{ nT} \quad (f \text{ in Hertz}) \quad (4.4)$$

Proton precession instruments have been used widely and are still the preferred instrument for ground magnetic surveys where they are relatively inexpensive and offer more than adequate accuracy and sampling speed. Readings can, however, only be made discretely (rather than continuously) since it takes a finite time to polarise the protons and then observe the precession. The additional accuracy desirable in an airborne installation can only be achieved at the expense of longer sampling times. Nevertheless, instruments with 1 nT sensitivity and half-second sampling were still in use in airborne surveys into the 1990s, particularly perhaps in helicopter installations where slow speed and low ground clearance tend to give large anomalies and adequate time for an individual measurement.

4.3.2 Magnetic survey planning

Magnetic surveys usually comprise a series of parallel traverses and tie lines as appropriate. The line spacing and line direction are the main parameters to consider in survey design. In magnetic survey, measures total magnetic field of earth and readings are taken at specified locations based on survey design. Usually a station interval of 25 m, or even 15 m, is suitable for most purpose.

In present magnetic study, based on the objective of survey was designed with a station spacing of 25 m and traverse spacing of 200 m in E-W direction. The traverse direction of survey lines is basically perpendicular to general strike of the geological formations in the survey area. To increase the data density in between the E-W traverses, set of lines planned in N-S direction with station interval of 50 m and line spacing of 500 m (Figure. 4.5). It is important to establish a local base station in an area away from suspected magnetic targets or magnetic noise and where the local field gradient is relatively low. Ideally the base station is placed at least 100 m away from any large metal objects or travelled roads and at least 500 m away from any power lines i.e. ideally free from the magnetic noise to record the diurnal variations of magnetic field. Both the base and field magnetometers are synchronized for time and ambient magnetic field before recording the data in the survey area.

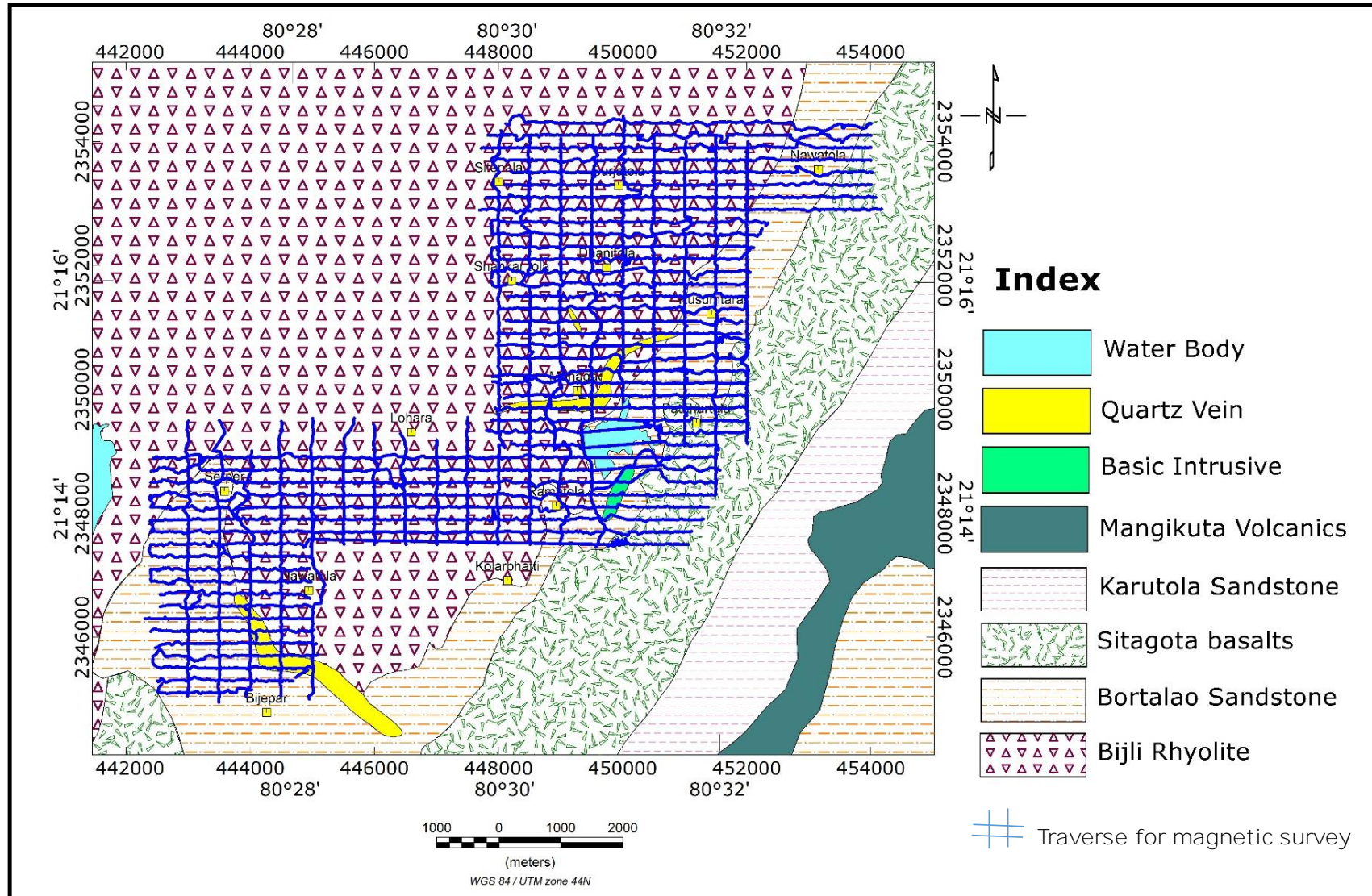


Figure 4.5 Magnetic survey layout superimposed over geology map of study area.

4.3.3. Data reduction

The reduction of magnetic survey data is principally aimed at removing the effects of temporal variations in the Earth's magnetic field that occur during the course of the survey. Continuous recording of magnetic field at base station is usually quite effective for removing diurnal variations in surveys. Magnetic base station is selected at *Kolarbhatti village*, and diurnal variations are recorded and corrected every day of Magnetic survey.

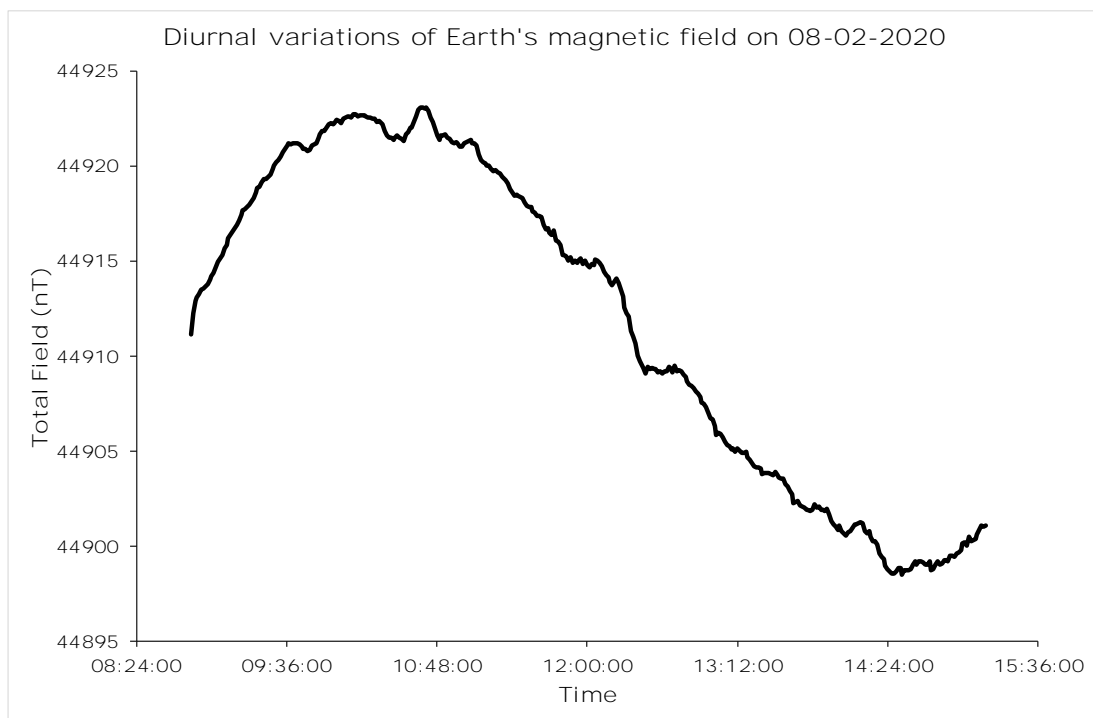


Figure 4.6 Diurnal curve of the base magnetic field utilized for diurnal correction.

4.4 Data processing and enhancement

4.4.1 Profile analysis

A common filtering operation applied to potential field data involves directly modifying the frequency content of the data. There are some filters which removes the spikes in magnetic profiles due to surface effects and smoothens the data. The prepared grids for this data after applying smoothing techniques over the profiles will produce clean maps to understand and analyze geophysical signatures. Here we attempted non-linear and low pass filters (only for appropriate bandwidth) over the magnetic line data and observed how unnecessary peaks are suppressed in their outputs (Figure. 4.7).

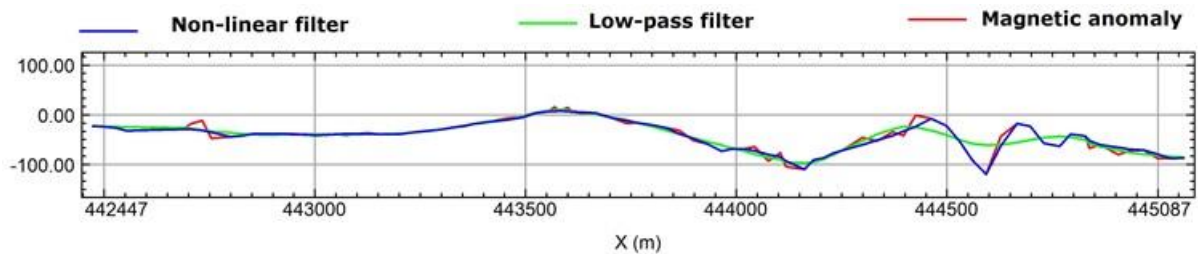


Figure 4.7 Magnetic anomaly profile and its filter outputs for line number 2345900N.

4.4.2 Continuation filters

Upward and downward continuation filters known as continuous filters applicable to potential field data. Upward continuation is equivalent to increasing the survey height, downward continuation to decreasing it. Upward continuation technique gives us deeper geological information, whereas downward continuation provides shallow geological information.

Here we applied upward continuation technique for magnetic data to know the depth persistency of structural features and basic bodies presence in deeper level. Upward continuation maps for 50 m, 100 m, 150 m, 200 m, 250 m and 300 m were prepared and analysed. Interestingly, north to the *Bijepar village*, E-W basic body still showing its presence even in 300 m upward continued map and inferred as deep seated body, whereas immediate north of *Managad village*, the spherical basic body vanishing after 250 m upward continued map. From structural point view, north of *Nawatola and Dhanitola villages* NW-SE trending fractures/faults showing its signatures in 300 m continued maps (Figure. 4.8).

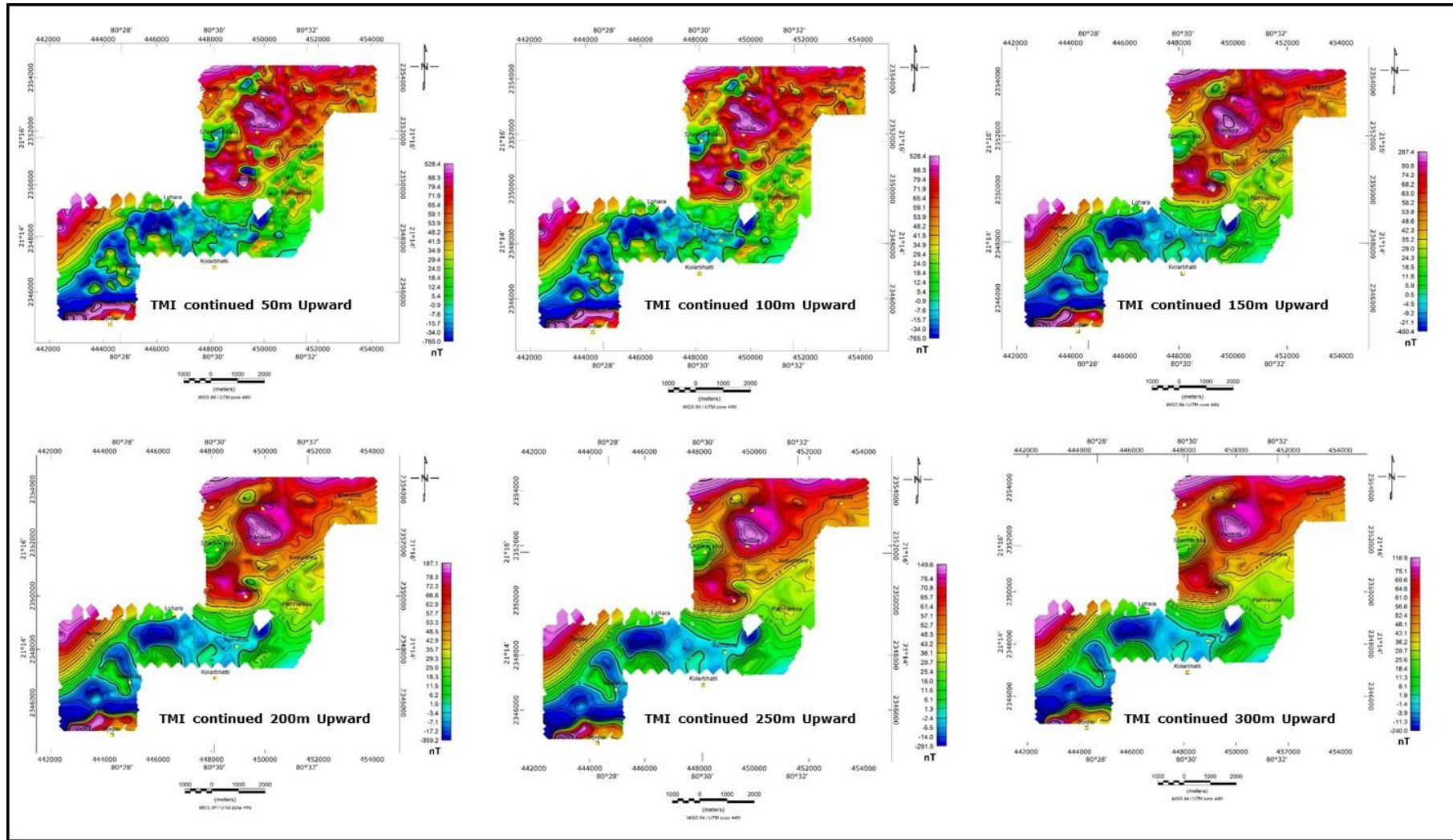


Figure 4.8 Upward continuation of TMI maps for different heights.

4.4.3 Reduction-to-pole (RTP)

The reduction-to-pole operator transforms magnetic anomalies resulting from the inclined magnetism of nonpolar regions into their equivalent polar response where a body's magnetism is vertical (Cooper, G. and Cowan, D., 2003, pp. 51-56). The magnetic inclination and declination of the inducing field are required for the transformation, and it is normally assumed that the magnetism of all the rocks in the area is parallel to the geomagnetic field and by implication is entirely induced.

Pole reduction can be calculated in the frequency domain using the following operator.

$$L(\theta) = \frac{1}{[\sin(I) + \cos(I) \cos(D - \theta)]^2} \quad (4.5)$$

Where

θ is the wave number direction.

I is the magnetic inclination.

D is the magnetic declination.

RTP is applied over a raw magnetic data set of the study area and it is located at the inclination of 32.1254° , declination of -0.1857° (*IGRF, 2020 March 01*) and the value of total magnetic field strength in the area is 44,992.8 nT. From the structural point of view, RTP map enhances trends of geophysical signatures and their position as compare TMI map alone (Figure 4.9).

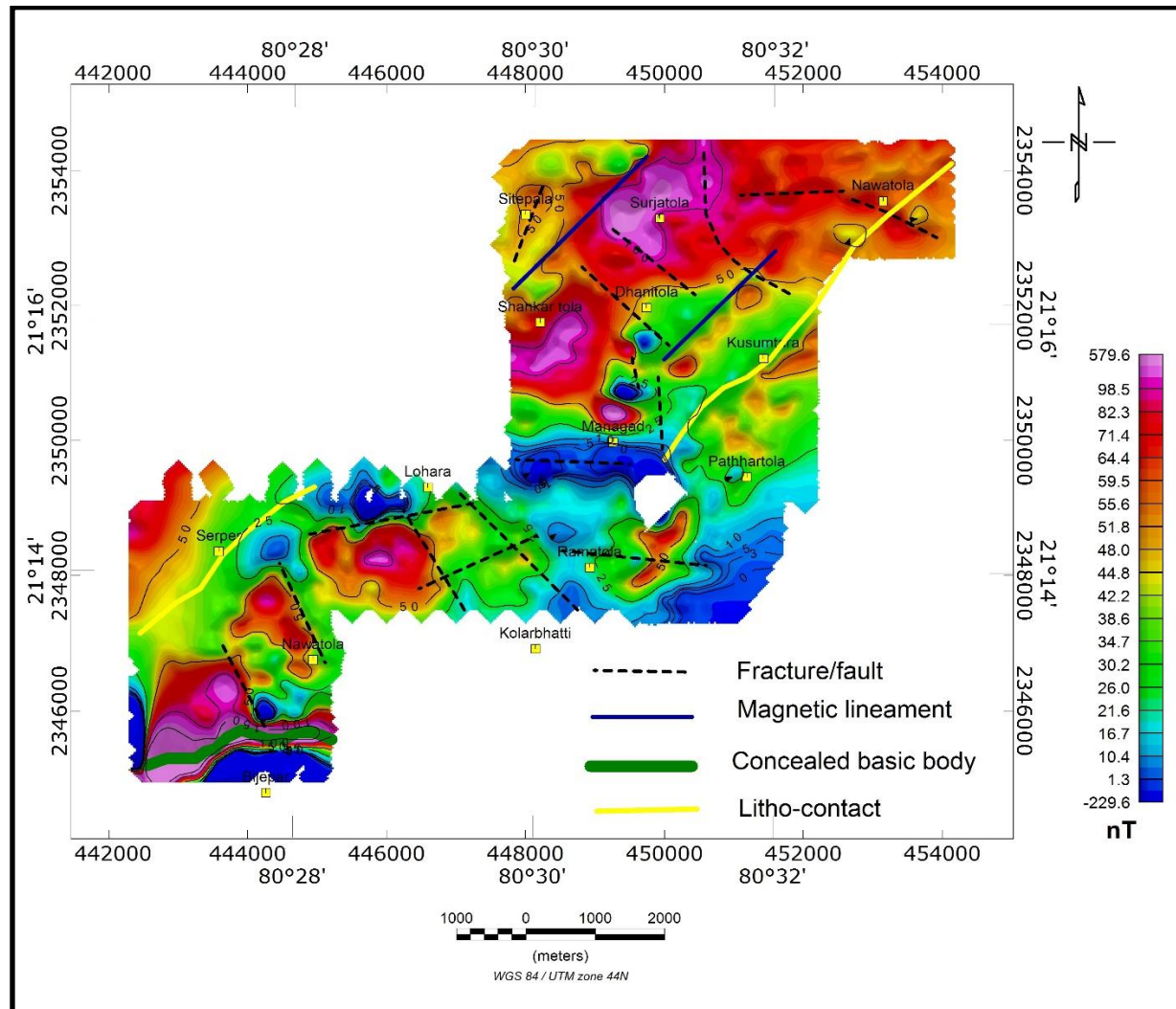


Figure 4.9 Reduction to Pole (RTP) map showing structural features.

4.4.4 Analytic signal

Combining the three directional gradients (X, Y and Z) of the magnetic field to obtain the total gradient, removes the complexities of derivative responses. When applied to potential field data, the total gradient at a location (x, y) is known as the analytic signal (AS) and given by:

$$AS(x, y) = \sqrt{\left(\frac{\partial f}{\partial x}\right)^2 + \left(\frac{\partial f}{\partial y}\right)^2 + \left(\frac{\partial f}{\partial z}\right)^2} \quad (4.6)$$

where f is the magnetic field.

magnetic analytic signal depends upon the strength and not the direction of a body's magnetism, it is particularly useful for analyzing data from equatorial regions, where the TMI response provides limited spatial resolution, and when the source carries strong remanent magnetization (MacLeod, *et al.*, 1993, pp. 679-688). The analytic signal has the form of a ridge located above the vertical contact, and is slightly displaced laterally when the contact is dipping. The analytic signal is effective for delineating geological boundaries and resolving close-spaced bodies.

Here we intended analytical signal technique to delineate geological boundary between Bijli rhyolite and Bortalao sandstone at west of *Serper village* where Bortalao sandstone taking sudden turn and this attempt clearly demarcated geological contact at west of *Serper village* (Figure. 4.10).

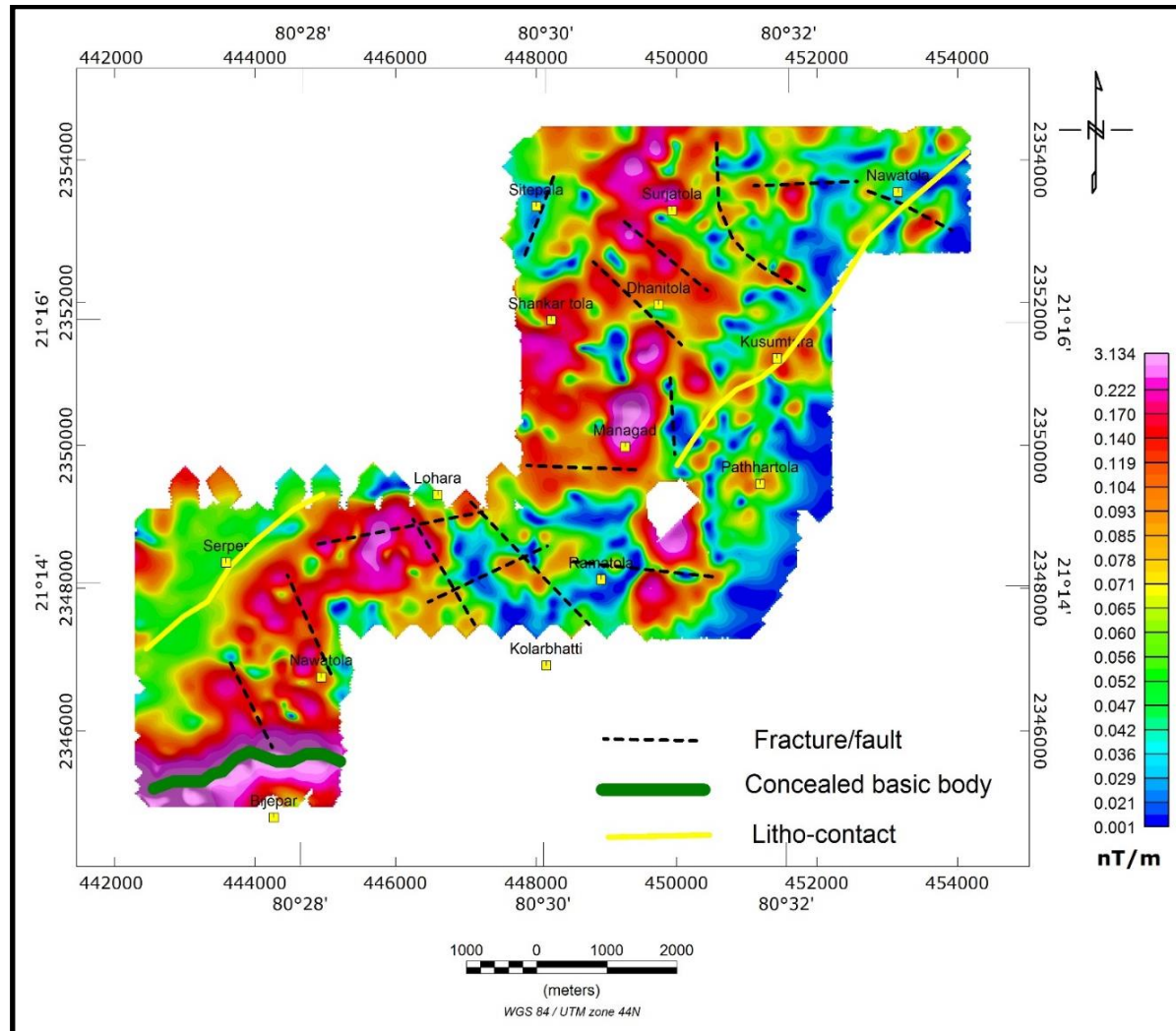


Figure 4.10 Analytical signal map study area showing structural features.

4.4.5 Euler depth solutions

Magnetic data in grid form may be interpreted rapidly for source positions and depths by deconvolution using Euler's homogeneity relation (Reid, J.E., *et al* 1990, pp. 1908-1913). Euler deconvolution is used for rapid interpretation of magnetic data. It is particularly good at rapid depth estimation of sources. An advantage of this method in the interpretation of magnetic data is that it is insensitive to magnetic inclination, declination and remanence. Euler's Equation for Potential Field T (magnetic field) measured at (x_i, y_i, z_i) can be defines as

$$(x_i - x_0) \frac{\partial T_i}{\partial x} + (y_i - y_0) \frac{\partial T_i}{\partial y} + (z_i - z_0) \frac{\partial T_i}{\partial z} = -n(T_i - B) \quad (4.7)$$

where (x_0, y_0, z_0) is the position of the magnetic source,

B = regional field (usually a constant) and n = structural index (SI).

To run Euler depth solution technique, we need a gridded data points at different location (x, y, z) e.g T (x_1, y_1, z_1) , T (x_2, y_2, z_2) , T (x_3, y_3, z_3) , etc, The 1st vertical derivative grids of T, i.e. dT/dx , dT/dy , and dT/dz , Structural Index (SI), and window size. As a result, we will get location of the causative source (x_0, y_0, z_0) and B. The quality of the depth estimation mostly depends on the choice of the proper structural index. The structural index (SI) is a measure of the rate of change (fall-off rate) with distance of a field. The window size should be chosen with the criteria of it should be large enough to incorporate substantial variation of the field and field gradient and small enough not to include significant effects from multiple sources. A solution is recorded if the depth uncertainty of the calculated depth is less than a specified tolerance (typically 15% of the depth) and the solution is within a limiting distance of the centre of the data window. When the solutions are plotted as circles on a map for a given SI and window size, a clustering of circles will be produced over

anomalies and tight clustering of Euler depth solutions is represent good estimates (Figure 4.11).

Euler depth solutions technique applied for magnetic data and observed the depth persistency of inferred structural features. Depth to the top of E-W basic body at north *Bijeper village* falling in the range of 50-100 m. NW-SE trending structural features nearby *Nawatola village* falling in the range of 100-150 m. NW-SE trending fracture/fault north of *Dhanitola village* and E-W trending fracture/fault south of *Managad village* falling in the range of >150 m.

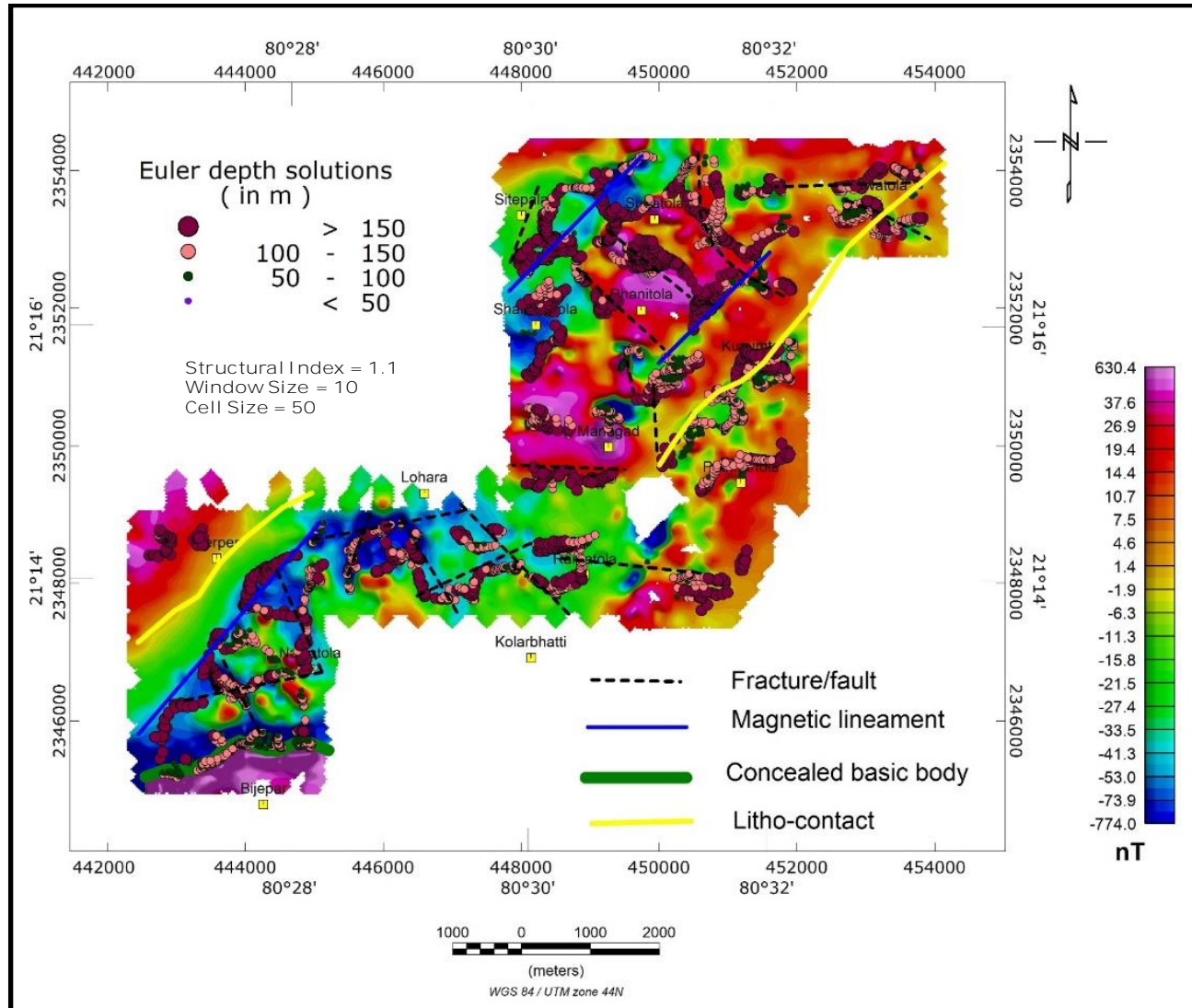


Figure 4.11 Correlation of Euler's depth solutions with inferred structural features from TMI map.

4.5 UBC-MAG 3D Modelling

Three-dimensional magnetic inversion allows the distribution of magnetic parameters to be obtained, and it is an important tool for geological exploration and interpretation. Three-dimensional magnetic inversion refers to the computation of the spatial distribution and properties of underground sources from magnetic anomalies of an observation surface (Dandan Jiang, *et al.*, 2020, pp. 1-5).

The material with susceptibility $k(x, y, z)$ is magnetized when the earth's main field with flux intensity \mathbf{B} impinges upon the subsurface formation. The magnetized material gives rise to a magnetic field, \mathbf{B}_i , which is superimposed on the inducing field to produce a total, or resultant, field. By measuring the resultant field and removing the inducing field from the measurements through numerical processing, one obtains the distribution of the anomalous field due to the susceptible material. The data from a typical magnetic survey is a set of magnetic field measurements acquired over a 2D grid above the surface. These data are first going through the different processing techniques to yield an estimate of the anomalous field due to the susceptible material within the subsurface over interested area. The goal of the magnetic inversion is to obtain, from the extracted anomaly data, quantitative information about the distribution of the magnetic susceptibility in the ground.

There are few important files which are used in UBC-MAG3D software, all are in ASCII text format, from which three files are very important as we discussed in further paragraphs such as namely mesh, topography and magnetic observation files.

Mesh file: The mesh can be designed in accordance with the area of interest and the spacing of the data available in the area. In general, the mesh consists of a core region which is directly beneath the area of available data, and a padding zone surrounding this core mesh.

Topography file: This file is used to define the surface topography of a mesh/model by the elevation at different locations.

Magnetic observations file: This file is used to specify the inducing field parameters, anomaly type, observation locations, and the observed magnetic anomalies with estimated standard deviation. The values of parameters specifying the inducing field anomaly type and observation locations are identical to those in file. The output of the forward modelling program has the same structure except that the column of standard deviations for the error is omitted.

Here, UBC-MAG3D programme is targeted to reveal subsurface basic body and its displacement due to NW-SE fault to the North of *Bijepar village*, which is not at all exposed in the study area. Small portions of body is falling in the present study area, so to get clear picture of basic body, previous survey data sets available in adjacent area are also taken up for plotting (Satyanarayana, et al., 2018, 30).

Processing procedure: To create magnetic observation file, 50m cell size has taken for a grid file and data were extracted to that grid file. The total data points were 6890, with magnetic elements such as Inclination (I), Declination (D) and Total magnetic field, magnetic observation file has been prepared. For mesh file, 25m mesh cell size has been taken; suitable padding blanks and depth were fixed for preparation of mesh file. Topography file has not taken and considered as flat topography due less undulations throughout the study area. After preparation of all required files, UBC-MAG3D program has been run with multiple iterations and got a file having coordinates, susceptibility and depth. This data set is used in Geosoft voxel to make subsurface susceptibility model.

4.6 Data Interpretation

Total magnetic intensity anomaly map of the survey area is prepared by using minimum curvature technique as a gridding method with a cell size 25. Qualitative and quantitative interpretation is done and all inferred features are posted on Total magnetic intensity (TMI) anomaly map of the study area (Figure 4.13). Magnetic anomalies range from -1118nT to 917nT are noticed and they are indicating good susceptibility contrast between the different rock types as well as intrusive/flow of basic rocks. The general trends of the magnetic contours in the northern portion are in NE-SW that indicates the general strike of the rock units, trend of the unconformity contact and/or litho contacts. In the central and SW portions in the vicinity of west of *Ramatola*, east of *Nawatola* and *Bijepar* villages, magnetic anomalies are due to the influence of grey rhyolites. In the NW of *Serpar* village high magnetic zone trending in NW-SE is due to the influence of basement Bijli rhyolite. Low magnetic anomalies associated with Bortalao sandstones and or grey rhyolites, moderate magnetic anomalies associated with Sitagota basalt and very high magnetic anomalies associated with Pink Rhyolites are demarcated. Unconformity contact between Bijli rhyolite and Bortalao sandstone at northern portion (yellow line shown as litho contact in map) is trending in NNE-SSW. At NE of *Ramatola* village influence of an intrusive basic body trending in NE-SW within Bortalao sandstone is observed, it is also exposed in limited area at NE of *Ramatola* village. One more intrusive E-W basic rock is identified along a fracture zone at immediate north of *Bijepar* village.

Data enhancement techniques such as upward continuation, RTP, Analytical Signal (AS) and Euler's depth solutions has brought out signatures of structural features in the study area and few of the inferred structural features are showing their depth persistency in basement Bijli rhyolites. From the Euler's depth solutions, cluster of solutions are falling along the inferred features from qualitative interpretation of magnetic data. From the

structural point of view, faults/fractures trending in NW-SE and NE-SW towards north of *Managad* and *Piparitola* are identified. These are dominantly associated with quartz veins. An intruded basic rock is observed within the Bortalao sandstone towards east of *Ramatola* to *Kusumtara* which might be a fracture zone in NE-SW along which the basic rock might be intruded. North of Bijepar, magnetic lineaments (faults and fractures) dominantly trending in NW-SE is delineated and is linked with major fault zone trending in NW-SE where the surface manifestation of quartz reef is noticed and also observed few NE-SW trending fractures/lineaments that cross cutting the major NW-SE structural feature. Intersection zones of these lineaments are falling in the area where surface radioactive occurrences are reported and these zones are important for further exploration activities in the area. Magnetic lineament trending in NE-SW direction near *Serper* village is identified and attributed to a contact of basement Bijli Rhyolites and Sandstones.

High magnetic signature associated with Intrusive basic rock (shown with continuous green line) trending in E-W direction is identified. This concealed body is important due to structurally disturbed by NW-SE fracture/fault zone at immediate north of Bijepar village where surface radioactive anomalies are located. From Euler's depth solutions, depth to top of the body is inferred as 50m to 80m and sub vertically dipping towards north. These quantitative depth parameters are useful in avoiding of encounter in bore hole drilling activity in further exploration programme in this area. UBC-MAG3D modelling also revealed the clear picture in terms of iso-surface of susceptibility ranging from 0.007 to 0.04 SI units.

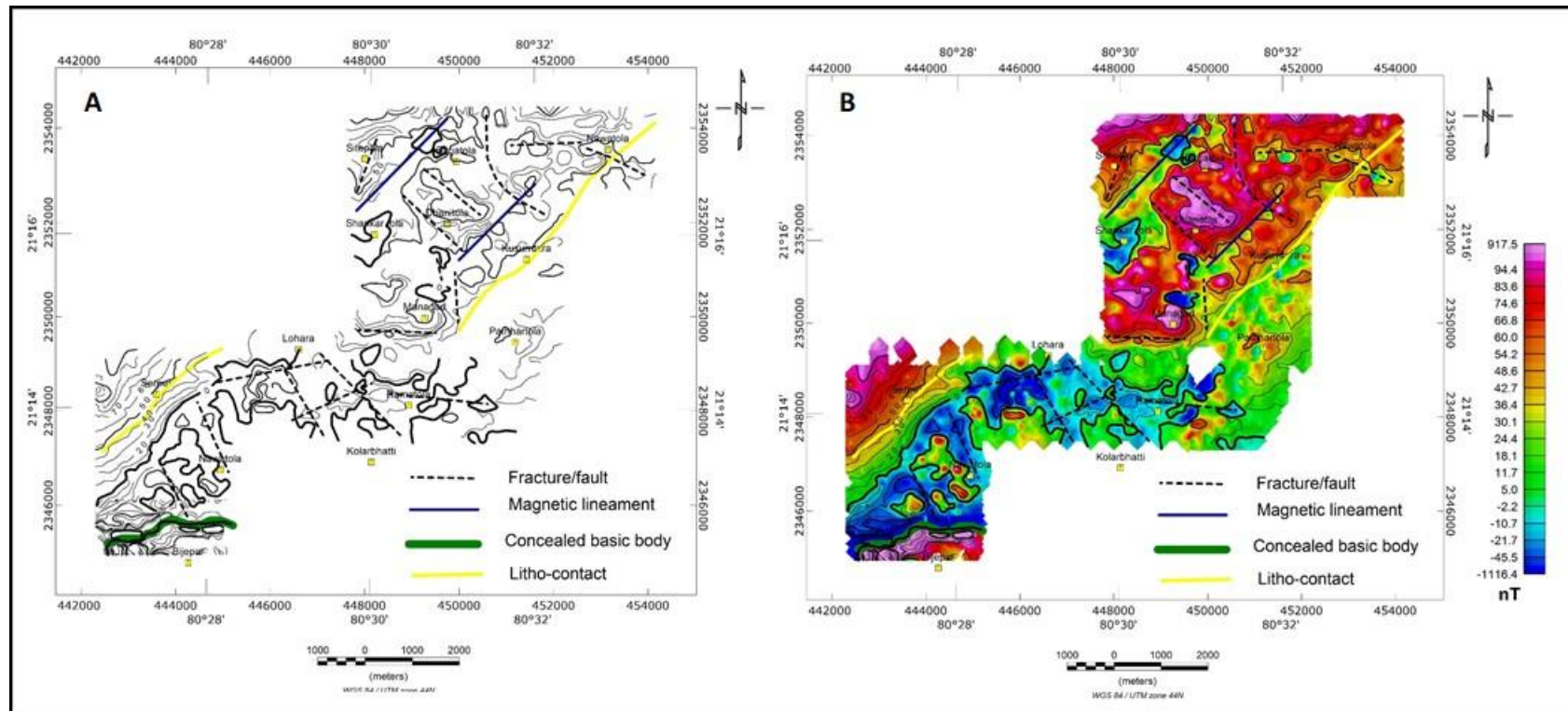


Figure 4.13 a). Total Magnetic Intensity (TMI) contour map.

b). Total Magnetic Intensity (TMI) map showing structural features.

CHAPTER 5

TIME-DOMAIN ELECTROMAGNETIC METHOD

5.1 Introduction

Electromagnetic (EM) surveying methods make use of the response of the ground to the propagation of electromagnetic fields, which are composed of an alternating electric intensity and magnetizing force. Primary electromagnetic fields may be generated by passing alternating current and/or direct current through a small coil made up of many turns of wire or through a large loop of wire. The response of the ground is the generation of secondary electromagnetic fields and the resultant fields may be detected by the alternating currents that they induce to flow in a receiver coil by the process of electromagnetic induction. The primary electromagnetic field travels from the transmitter coil to the receiver coil via paths both above and below the surface. Where the subsurface is homogeneous there is no difference between the fields propagated above the surface and through the ground other than a slight reduction in amplitude of the latter with respect to the former. However, in the presence of a conducting body the magnetic component of the electromagnetic field penetrating the ground induces alternating currents, or eddy currents, to flow in the conductor. The eddy currents generate their own secondary electromagnetic field which travels to the receiver. The receiver then responds to the resultant of the arriving primary and secondary fields so that the response differs in both phase and amplitude from the response to the primary field alone. These differences between the transmitted and received electromagnetic fields reveal the presence of the conductor and provide information on its geometry and electrical properties. The induction of current flow results from the magnetic component of the electromagnetic field. Consequently, there is no need for physical contact of either transmitter or receiver with the ground. Surface EM surveys can thus proceed much more rapidly than electrical surveys, where ground contact is required. EM methods are

widely used in prospecting for conductive ore bodies. All anomalous bodies with high electrical conductivity produce strong secondary electromagnetic fields. Some ore bodies containing minerals that are themselves insulators may produce secondary fields if sufficient quantities of an accessory mineral with a high conductivity are present. For example, electromagnetic anomalies observed over certain sulphide ore are due to the presence of the conducting mineral pyrrhotite distributed throughout the ore body.

Electromagnetic systems divided into two ways based their primary magnetic field generation with time, which leads to two classes of EM systems. Time-domain (TDEM) and Frequency- Domain (FDEM) systems. In the time domain the change in the primary magnetic field is produced by either abruptly turning off or turning on a steady current (DC). A pulse of current is induced in a conductor. The eddy currents circulate in the conductor for a short period and quickly decay as they lose energy. Their strength and duration depends on the electrical properties and geometry of the conductor, so monitoring their decay provides information about the subsurface conductivity. New survey and interpretation systems are continually evolving, and EM theory related to geophysical surveying is continually being developed. The result is a complex and diverse science. Making and understanding EM measurements in areas of conductive overburden is especially challenging. Future developments are aimed at improving signal detection and resolution of subtler conductivity contrasts, better depth penetration, especially beneath conductive overburden, and reducing the cost of EM surveying. Considerable work is ongoing in the mathematically complex area of improving data interpretation tools, which includes the development of associated software for building more accurate and complex 3D conductivity models of the ground from ever-increasing data volumes.

5.2 Electromagnetic theory

Electromagnetism is the phenomenon which deals with the interaction between an electric field and a magnetic field. Stationary charges in a system lead to an electric field and moving charges in a system lead to a magnetic field. The direction of electric field and magnetic field is always perpendicular to each other, and the wave travels at the speed of light. The Scottish scientist and mathematician James Clerk Maxwell, brought the correlation between electricity and magnetism for the first time using Maxwell's equations. Maxwell's four differential equations unified existing laws of electricity and magnetism such as Newton's

Law, Faraday's Law, Kelvin's law and Ampere Law.

The four basic Maxwell's Equations are as follows

1. *Gauss Law* : $\nabla \cdot E = \frac{\rho}{\epsilon_0}$
2. *Gauss Magnetism Law* : $\nabla \cdot B = 0$
3. *Maxwell – Faraday Equation* : $\nabla \times E = -\frac{\partial B}{\partial t}$
4. *Ampere Circuital Law* : $\nabla \times B = \mu_0 \left(J + \epsilon_0 \frac{\partial E}{\partial t} \right)$

Here, ρ represents net charge inside the surface, ϵ_0 represents permittivity of vacuum, B represents the magnetic field, E represents electric field and J represents current density. The first law states that the electric flux which forms across a closed surface is proportional to the charge enclosed. The second law states that the magnetic flux induced across a closed surface is zero. The third law states that the magnetic fields which vary with time lead to an electric field. The fourth law states that that time-varying electric fields or steady currents lead to a magnetic field.

The EM method utilize Maxwell's equations of electromagnetic theory. In the time domain electromagnetic method, the change in the primary magnetic field is produced by either abruptly turning off or turning on a steady current (DC). A pulse of current is induced in a conductor. The eddy currents circulate in the conductor for a short period and quickly decay as they lose energy. Their strength and duration depends on the electrical properties and geometry of the conductor, so monitoring their decay provides information about the subsurface conductivity.

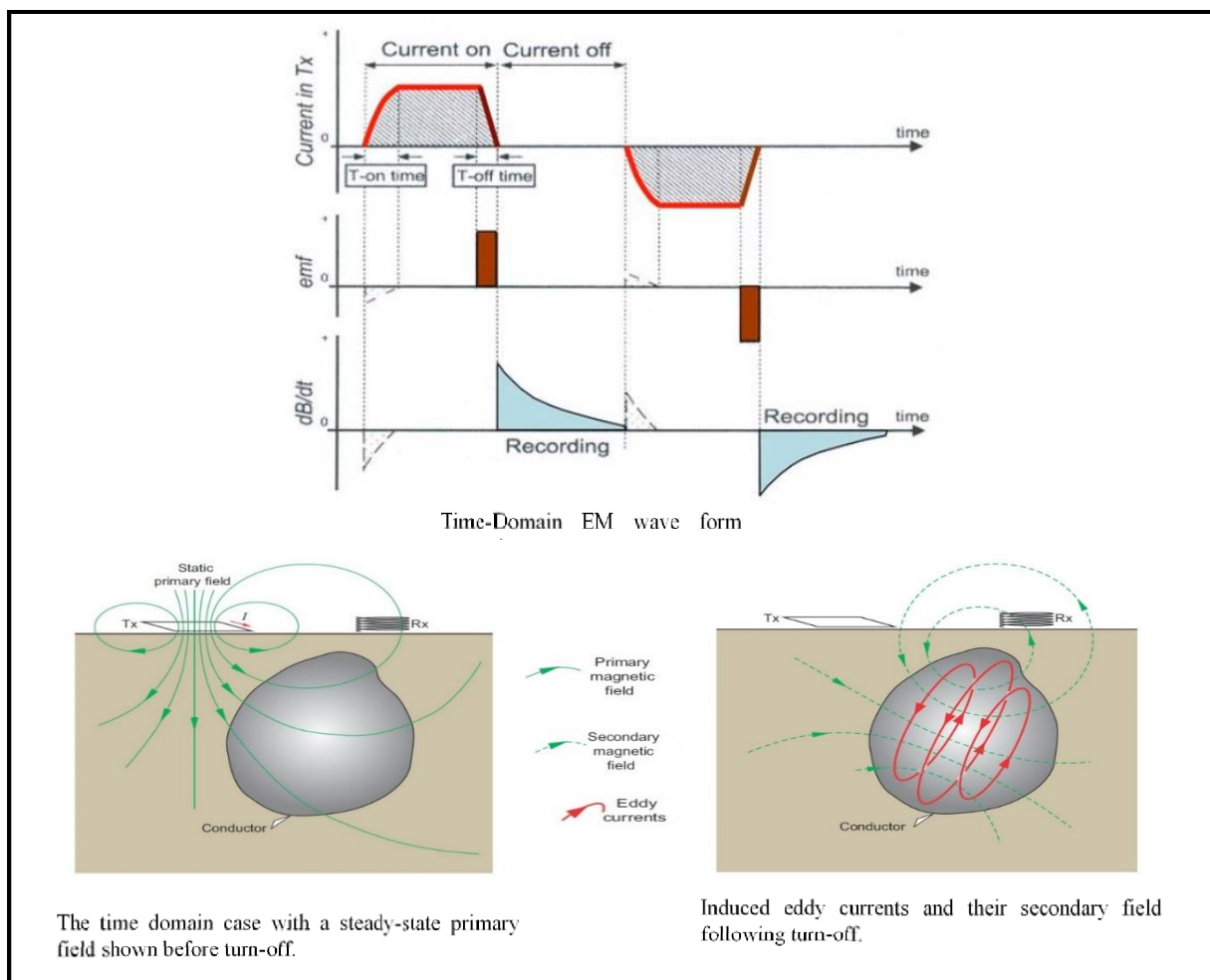


Figure 5.1 Schematic illustration of an Electromagnetic induction phenomenon in the subsurface.

The primary magnetic field in EM methods is usually created by using a large loop of wire and The strength of the magnetic field is quantified by the magnetic dipole moment (m) given by

$$\mathbf{m} = n\mathbf{IA} \quad (5.1)$$

where I = Current in amperes.

n = Number of turns in the coil or loop.

A = Area of the coil/loop in square meters.

The dipole moment has units of A m². Increasing the number of turns, and/or increasing the current in a loop, increases its dipole moment. The larger the transmitter's dipole moment the stronger is the primary field and the stronger the eddy currents it induces. This improves the signal-to-noise ratio of the secondary field measurement. There are several advantages in using

large loops as transmitters. A large loop has a larger dipole moment than a smaller loop, and increasing the size of the loop spreads the field over a larger volume of the ground. The strength of the field of small coils and loops decreases as 1/distance³ from the loop, but as approximately 1/distance² for a large loop, so deeper targets can be detected. Transmitter currents of up to several hundred amps are used and are limited by the level of the back emf produced at the instant of turn-off. The back emf is determined by the rate of turn-off of the current and the inductance of the loop, which is proportional to the square of its dimensions (L²) and the number of turns. A large multi-turn loop produces a large back emf, preventing the instantaneous step turn-off of the magnetic field. The current must be turned on, or off, at a slower rate over a period known as the ramp time. The magnetic field changes at a less desirable rate and has a detrimental effect on the EM response.

5.3 Subsurface conductivity and EM responses

Time domain EM responses of the subsurface can be complex, but they can be understood in terms of the responses of an electrically homogeneous background, a conductive overburden (if present) and localised ‘target’ regions of contrasting conductivity. Key to understanding TDEM responses is that at the instant of current turn-off, eddy currents are created at all interfaces across which there are contrasts in electrical conductivity, and the observed decay is due to a combination of their individual decays.

5.3.1 Homogeneous subsurface

It is convenient to begin the description of TDEM responses using the simplest case of an electrically homogeneous ground where the only contrast in electrical properties occurs at the ground surface, i.e. the ground–air interface. This is known as a half-space, it is a useful model to introduce the key concepts of diffusion, smoke ring, diffusion depth and decay rate which describe the electromagnetic diffusion process and are used for the analysis of the measured secondary decay.

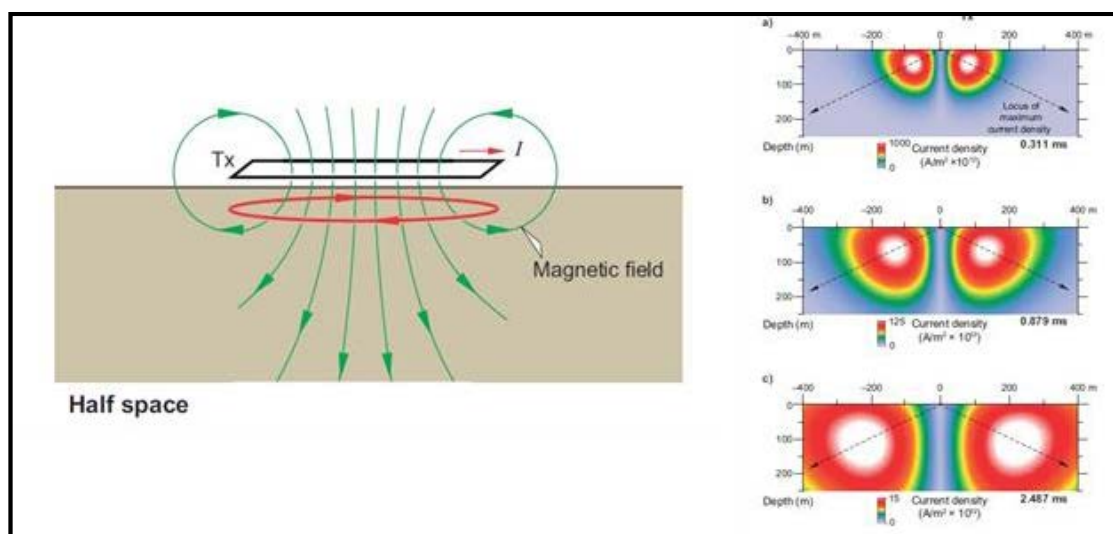


Figure 5.2 Schematic illustration of the diffusion of the eddy current system in a conductive half-space at different delay times (Reid and Macnae, 1998). (a) Early, (b) mid and (c) late delay times.

Figure-5.2 shows a cross-section through a horizontal transmitter loop on the surface of a half-space and the induced migrating eddy current at progressively greater delay times. Immediately upon its creation the eddy current begins to expand and migrate outward and downward, losing energy rapidly and causing the region to experience a changing magnetic field. The result is a doughnut-shaped zone of current flow below the loop referred to as a 'smoke ring'. It is a deformed image of the loop that becomes more blurred with time. As the system continues diffusing into the subsurface, the current and the speed with which it moves decrease. After a very short initial period, the smoke ring expands further and moves downwards at an angle of approximately 30°. The amplitude of the response depends strongly on the conductivity and the velocity with which the current system moves away from the transmitter loop. An important aspect of diffusion in a half-space is that the only boundary confining the expanding current system is the ground–air interface, the system is otherwise unconfined and free to expand in all other directions. The half-space is referred to as an unconfined conductor.

Diffusion depth

The depth to the maximum current density at a particular delay time (t) is known as the diffusion depth (d). It is a measure of skin depth in the time domain and depends on the conductivity (σ) and magnetic properties of the ground, it is given by the expression

$$d = \sqrt{\frac{2t}{\mu\sigma}} \quad (5.2)$$

where t = Time in seconds

d = Depth in metres

σ = Conductivity in Siemens/metre.

For most rocks μ is nearly the same as that of a vacuum ($\mu = \mu_0 = 4\pi \times 10^{-7}$ henry/m) (Zhdanov and Keller, 1994) so the expression can be rewritten as

$$d = 1261.6 \sqrt{\frac{t}{\sigma}} \quad (5.3)$$

For a given half-space conductivity, diffusion depth is a function of the square-root of 't'. Diffusion depth is larger for more resistive ground because the current system diffuses faster into it. A receiver at the surface senses the smoke ring attenuating quickly, i.e. a rapid decay in signal amplitude as the distance to the moving smoke ring rapidly increases. In resistive ground it is necessary to make measurements at early delay times in order to detect the rapidly expanding smoke ring. Its velocity decreases with increasing conductivity, in other words, diffusion is a slow process in conductive ground. As a consequence, measurements made at early delay times pertain to shallower depths in conductive environments than in resistive ones. Note that without the conductivity being known, delay time is an unreliable indicator of the depth to which particular measurements pertain. At late times when it has diffused to a very large distance from the transmitter loop, the current system limits its own expansion and its position changes very slowly, i.e. its velocity decreases to a low value. This creates a large region where the secondary field is vertical and of fairly constant amplitude everywhere. This is known as the late-stage response of the half-space, and the amplitude of the secondary field decays with a power law, i.e. the signal varies with delay time at the rate of ' t^{-k} ' where k is the power-law constant.

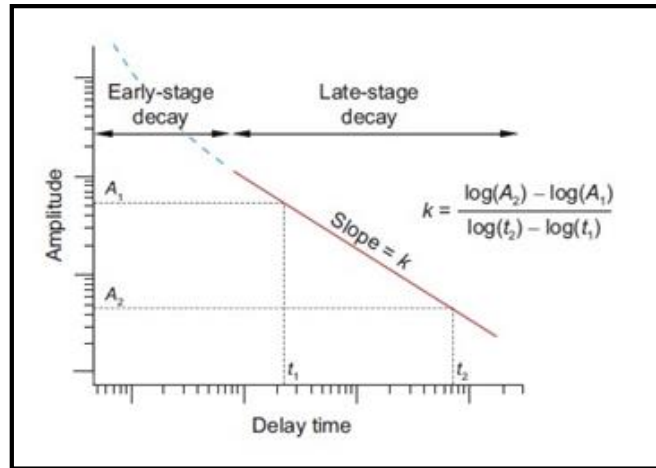


Figure 5.3 TDEM secondary decay for power-law response plotted on log–log axes with decay constant k

A graph of the logarithm of the signal amplitude on the vertical axis versus the logarithm of the delay time on the horizontal axis shows the power-law decay as a straight line with slope equal to the decay constant ($-k$). The value of k depends upon whether an impulse or step response is being measured and on the component of the secondary magnetic field measured, and is independent of the conductivity. Note that the late-stage response of a half-space is the same everywhere, so it does not matter where the receiver is in relation to the transmitter loop.

5.3.2 Confined conductor

When a homogenous subsurface contains a discrete zone of contrasting conductivity, two eddy current systems are created when the primary field is turned off. One current system is induced in the background material, and the other induced in the discrete conductor. Those in the conductor try to reproduce the primary field in the vicinity of the conductor, then immediately begin to diffuse over and through the body with their expansion being confined by its boundaries, which have a significant influence on the nature of the transient decay. It is known as a confined conductor, also referred to as a discrete conductor. When the conductor is in a high-resistivity environment and there is no interaction with its surroundings, the

initial surface eddy current flow is dependent in a complex way on the geometry of the conductor. With time the current system migrates through the body and, for an electrically homogeneous body, the late-stage decay is exponential. The amplitude (A) as a function of delay time t for the step response is then given by

$$A(t) = A_0 e^{-t/\tau} \tag{5.4}$$

where

A_0 = Apparent initial amplitude of the exponential decay which is dependent upon the conductor's shape, size and depth, and

τ = time constant, the time taken for the signal to decay to 1/e or 36.8% of its initial value and has the same units as t, usually milliseconds.

5.3.3 Conductor quality

The time constant τ quantifies the 'quality' of the conductor; a low value is indicative of a poor conductor having low conductivity and/or small size, a high value indicative of a good conductor having high conductivity and/or large size. The value of τ for mineralization ranges typically from about 200 μ s to hundreds of milliseconds, and to several seconds for very high-quality conductors. The time constant τ and the conductor geometry control the amplitude of the secondary field. Good conductors (large τ) maintain the current system for a long time and are referred to as late-time conductors. Poor conductors (small τ) lose the energy faster because of their higher resistivity and are referred to as early-time conductors.

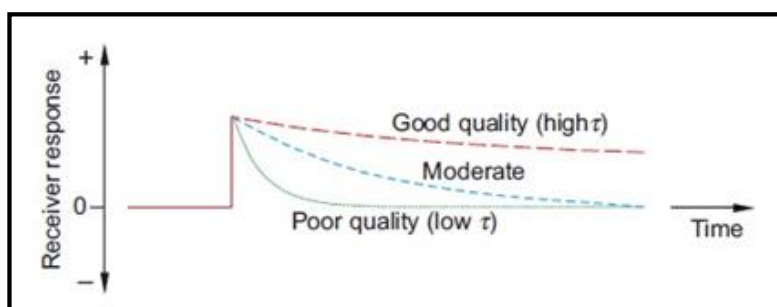


Figure 5.4 Decay curve for different quality conductor.

5.4 Acquisition of Time-Domain Electromagnetic data

Time-Domain Electromagnetic data (TEM) is acquired using In-loop and fixed loop configurations over promising zones identified from magnetic and gravity data sets towards east and north east of Bijepar village as shown in. Data has been acquired in high resolution series mode with 4th gain by using In-loop system geometry of 100 m X 100 m and 400 m X 400 m of loop sizes. Large loop configuration (400 m X400 m) is intended to know basement depth whereas small loop configuration (100 m X100 m) is used in profiling to identify conducting zones. EM soundings also done for every station of 100 m X 100 m loops along with vertical and horizontal components measurements (Figure 5.5).

5.4.1 System parameters

a). Wave form: Current in transmitter loop can be sent in a systematic way called waveform. Wide variety of waveforms is used by TDEM systems, such as square, rectangular and triangular etc. Waveform is the main important parameter and different type of wave forms having their own advantage and disadvantages with respective to objective survey. Here we used “square” wave form in our present study.

b). Base Frequency: Base frequency is the repetition rate of the primary field pulse, called the system base frequency. Reducing the base frequency creates a primary field with more low-frequency energy. It also increases the transmitter off-time so the secondary field can be measured to later delay times, important for resolving good-quality conductors. Increasing the base frequency has the opposite effect of increasing the high-frequency energy. It also produces a faster pulse turn-off allowing the secondary field to be measured closer in time to the pulse turn-off, important for resolving poor-quality conductors and near-surface features. Here we used base frequency of 12.5 Hz in our study.

c). Duty cycle: The waveform duty cycle is the proportion of the cycle occupied by the transmitter on-time and it varies with varying base frequency values. For our study, duty cycle is 50% over 12.5 Hz of base frequency.

d). Ramp time: The ramp time of the pulse turn-off determines the delay time of the earliest measurement. In general, high-powered systems have slower turn-off ramp times and lower-powered systems have faster turnoff and significantly influences the resolution of fast-decaying conductors, whilst the width of the pulse affects the resolution of slower-decaying conductors. The TDEM system used for present study is low powered. Throughout the study 13 ampere of current has been sent in transmitter loop and for this power ramp time was 75 microseconds.

e). System acquisition mode: Data has been acquired in high resolution series mode having 149 time windows over 4th gain with 1024 stacks.

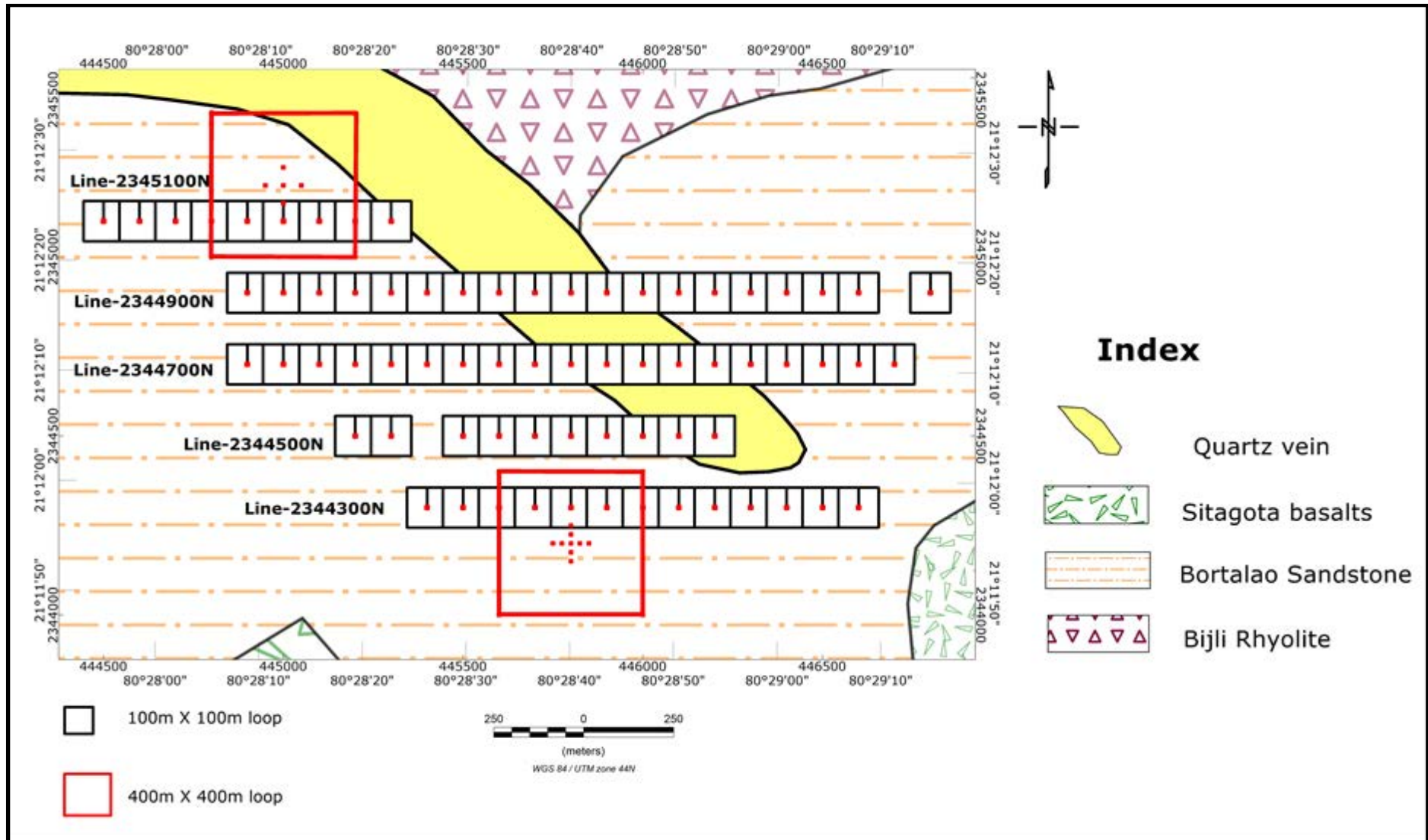


Figure 5.5 TEM survey lay out over imposed on geology map of Bijepar village block.

5.4.2 System geometry

The system geometry is the arrangement, spacing, sizes and orientations of the transmitter and receiver. Whether the survey is for reconnaissance work or for prospect-scale surveying will determine the transmitter–receiver configuration used, which also determines the systems lateral resolution. Transmitter loops for ground surveys are rectangular and generally consist of a single turn of insulated wire laid on the surface. Larger transmitter loops produce a stronger EM field penetrating a larger volume of the ground. Maximum signal-to-noise ratio and vertical resolution are obtained when the size of the loop is of the same order as the depth being investigated. In general, a loop-size to investigation-depth ratio of about 1:3 is suitable in resistive environments, in conductive areas where thick conductive overburden is present, a ratio of say 1:2. Most EM systems simultaneously measure both the vertical (Z) and the along-line (X) components of the secondary field. Sometimes the across-line (Y) component is also measured. In our present study, In-loop survey configuration has been chosen to find conductor presence in the study area.

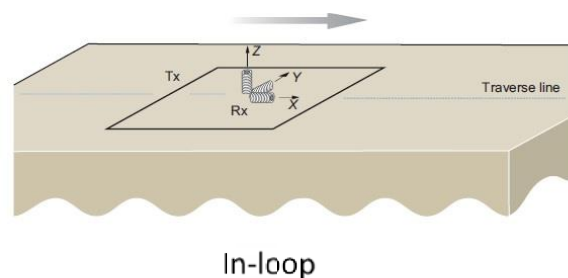


Figure 5.6 Schematic diagram of In-loop configuration

The most common configuration is the In-loop configuration and the receiver located at the center of the transmitter loop. The data are located to the loop center. This is very useful for detecting conductors whose dip and orientations are unknown. A couple of batteries is used in present study to supply current to the transmitter loop, typically up to 15 amperes.

5.5 Data Interpretation

5.5.1 Profile and pseudo-conductivity cross section analysis

The In-loop data is plotted and interpretation has been done. Secondary magnetic fields of both vertical (dBz/dt) and horizontal (dBx/dt) components are plotted. From In-loop sounding data of every station pseudo conductivity depth section maps are prepared for TEM profiles along 2344300N, 2344500N, 2344700N 2344900N and 2345100N (Figure 5.7, Figure 5.8, Figure 5.9 and Figure 5.10). After analysing the data channels of all the lines, earlier channels from 1 to 15 and late channels from 60 and above are removed due to dominance of noise.

Cross over point of dBx/dt associated with two peaks of dBz/dt component is observed for Line-2344300N at two stations (446150E and 445700E). It is due to the response of conductor may be a fracture filled with sulphides. Three conductor locations (445300E, 446200E and 446500E) are picked up for Line-2344700N. These are interpreted in terms of fractures filled with sulphides and or ground water. For Line-2344900N also three conductor locations (445300E, 446200E and 446700E) are identified associated with peak and cross over response of secondary magnetic fields components and could be fracture zones associated with sulphides and or any other conducting materials. Along with Line-2345100N, conductor location is picked up based on the peak responses of vertical component and zero crossover of horizontal component of secondary magnetic fields at 445100E point. This conductor location could be a fracture zone/anomalous conductivity zone either within basement Rhyolite and or Bortalao sandstones.

Peak of vertical (dBz/dt) and crossover of horizontal (dBx/dt) component are offset for the Line-2344300N and Line-2345100N, it could be due to dip of conductor. Inferred conductor locations are falling within the intersection zones of NW-SE and NE-SW structural features identified from gravity and magnetic data sets may be important for exploration activities in the area.

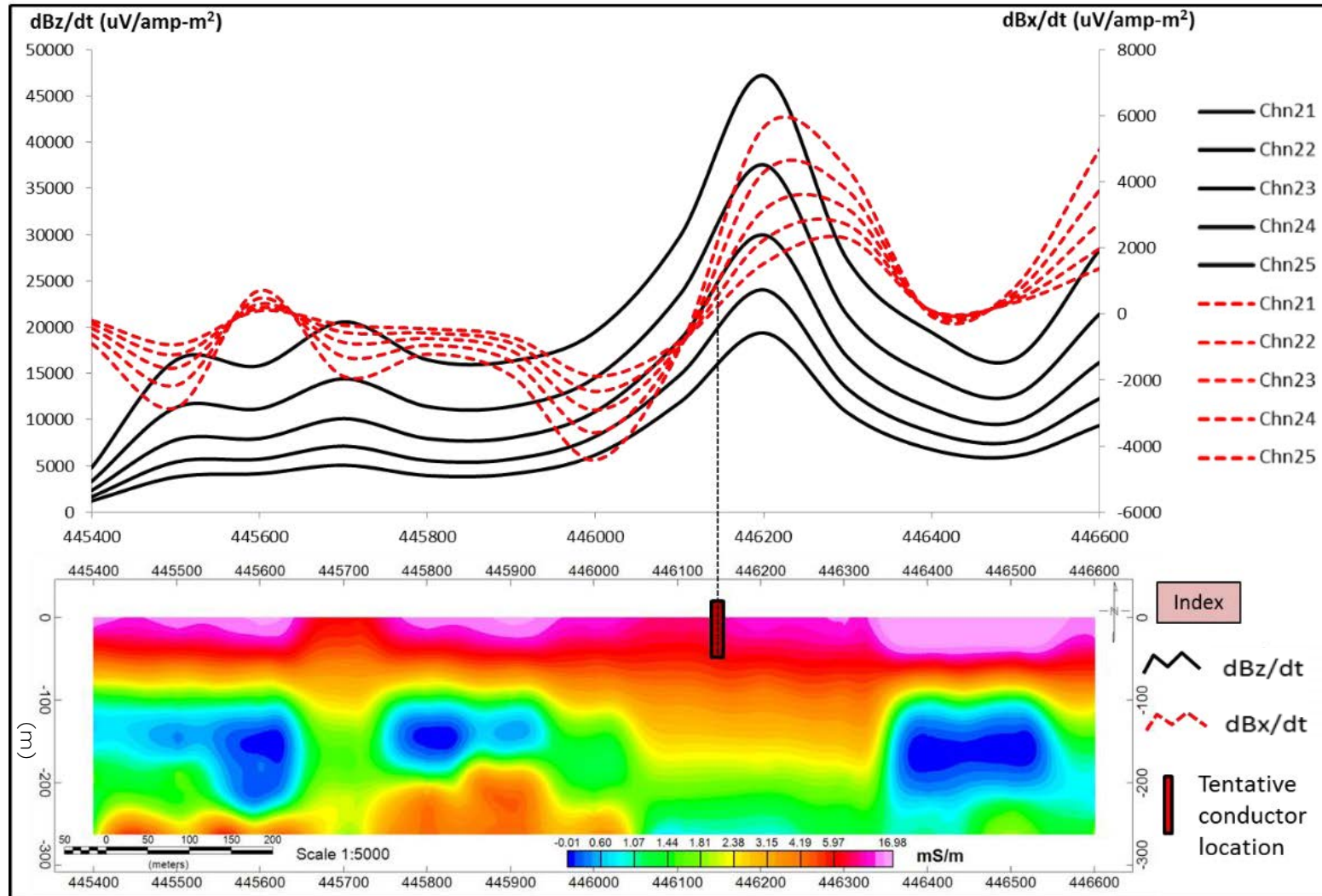


Figure 5.7 1D stitched 2D pseudo conductivity cross section along 2344300N line.

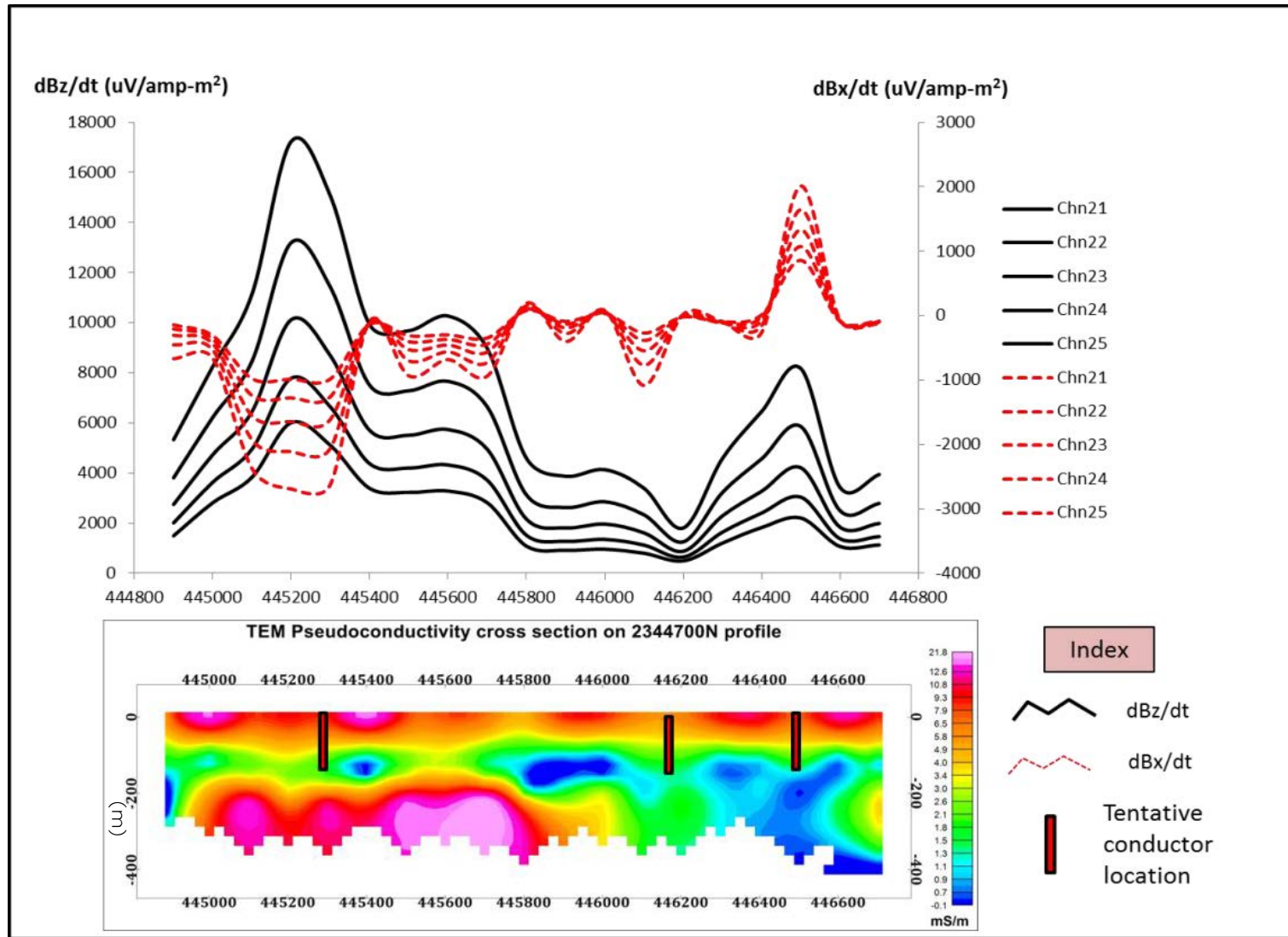


Figure 5.8 1D stitched 2D pseudo conductivity cross section along 2344700N line.

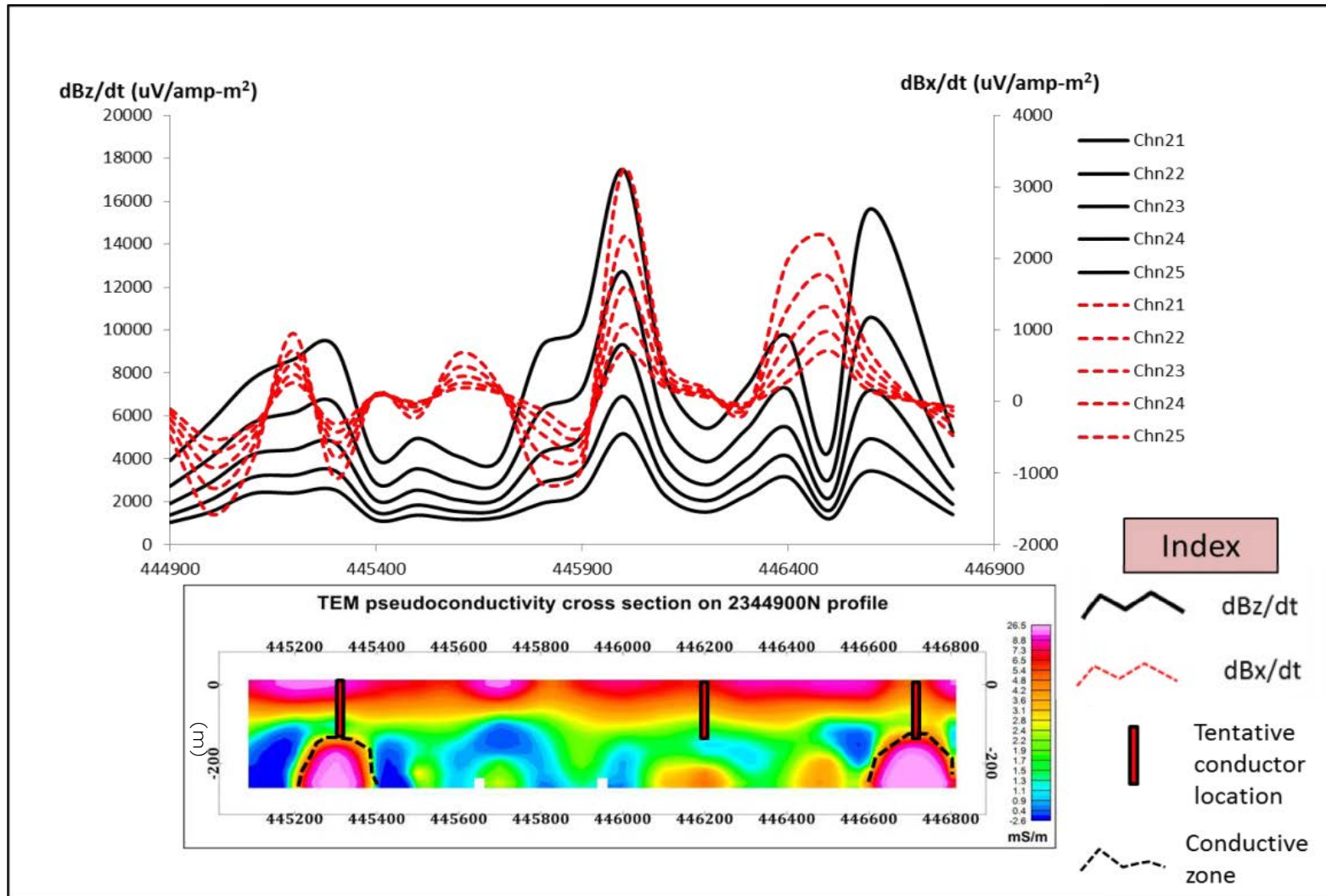


Figure 5.9 1D stitched 2D pseudo conductivity cross section along 2344900N line.

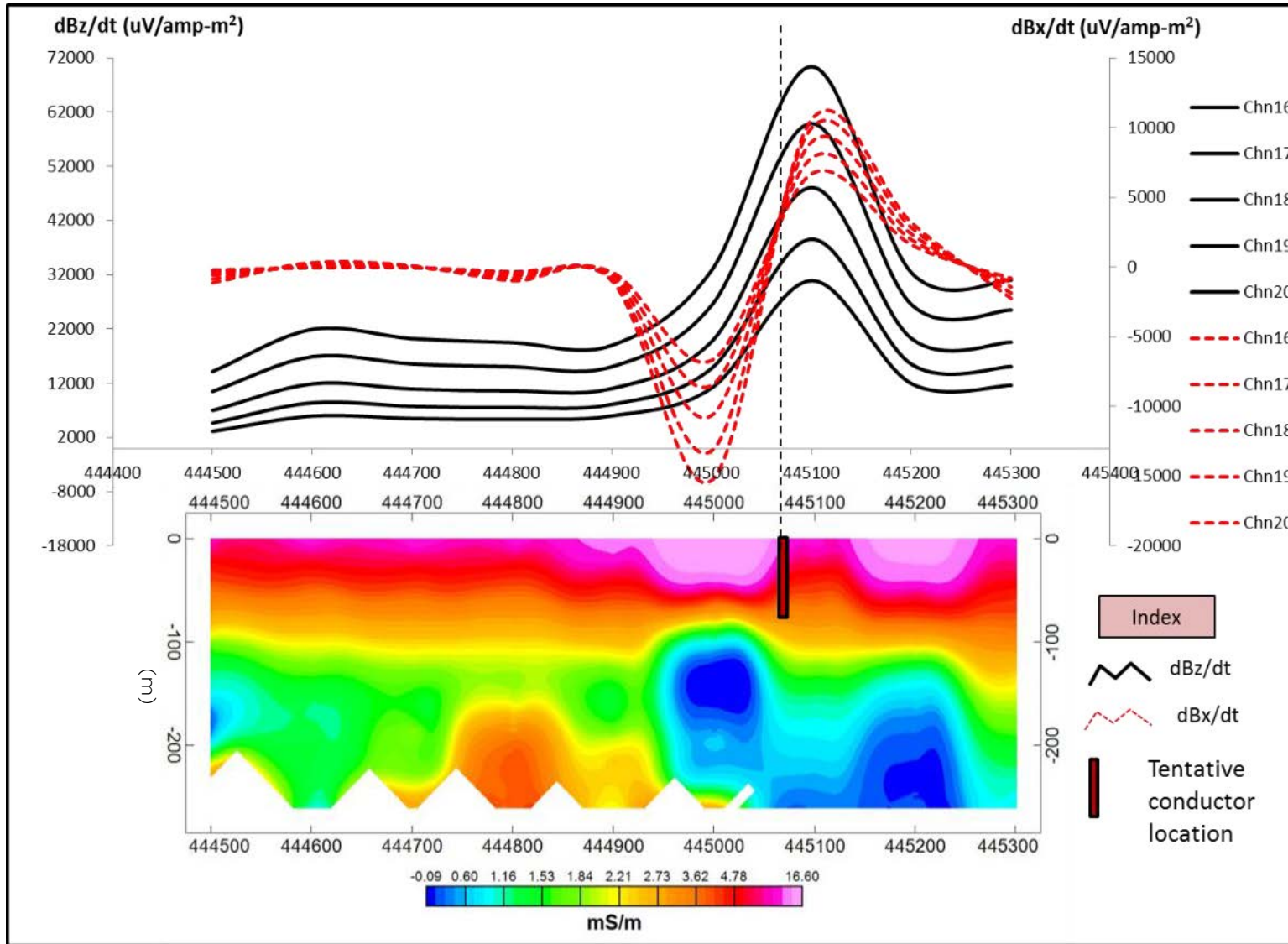


Figure 5.10 1D stitched 2D pseudo conductivity cross section along 2345100N line.

5.5.2 Decay curve analysis over conducting zones

For measurements defining the peak of a target anomaly, plotting the measured decay on log-linear axes allow to reveal the exponential decay of an underlying confined conductor as a straight line if present. The time constant can be determined from the slope of the line and, possibly, estimates made of the quality of the conductor, i.e. its conductivity and thickness.

Curve analysis is attempted on line number 2344300N (Figure 5.11). Locations are chosen from profile analysis of secondary magnetic field and pseudo conductivity cross section for that particular line. In-Loop sounding stations over inferred conducting zones and non-conducting zones are selected for decay curve analysis to know presence of conducting zone based on decay constant (τ). For this line, geological succession is overburden as a top layer followed by Bortalao sandstone (sediment) unconformably overlain by basement Bijli rhyolite. Early channel data belongs to overburden is removed. Due to high resistive shallow basement, signal after 0.90 ms died out for most of the stations and considered as a noise data. Data remained after considerable neglected data, which is falling mainly between 0.50-0.80 ms time bound channels. This data has plotted on log-linear scale and calculated time constant (τ) manually as shown in Figure 6.12. Three (3) successive stations of identified conducting zone are showing higher value time constant (0.3251ms, 0.3632ms and 0.3733ms) compare to other stations of non-conducting zone. These time constant(τ) values are indicating presence of conductor.

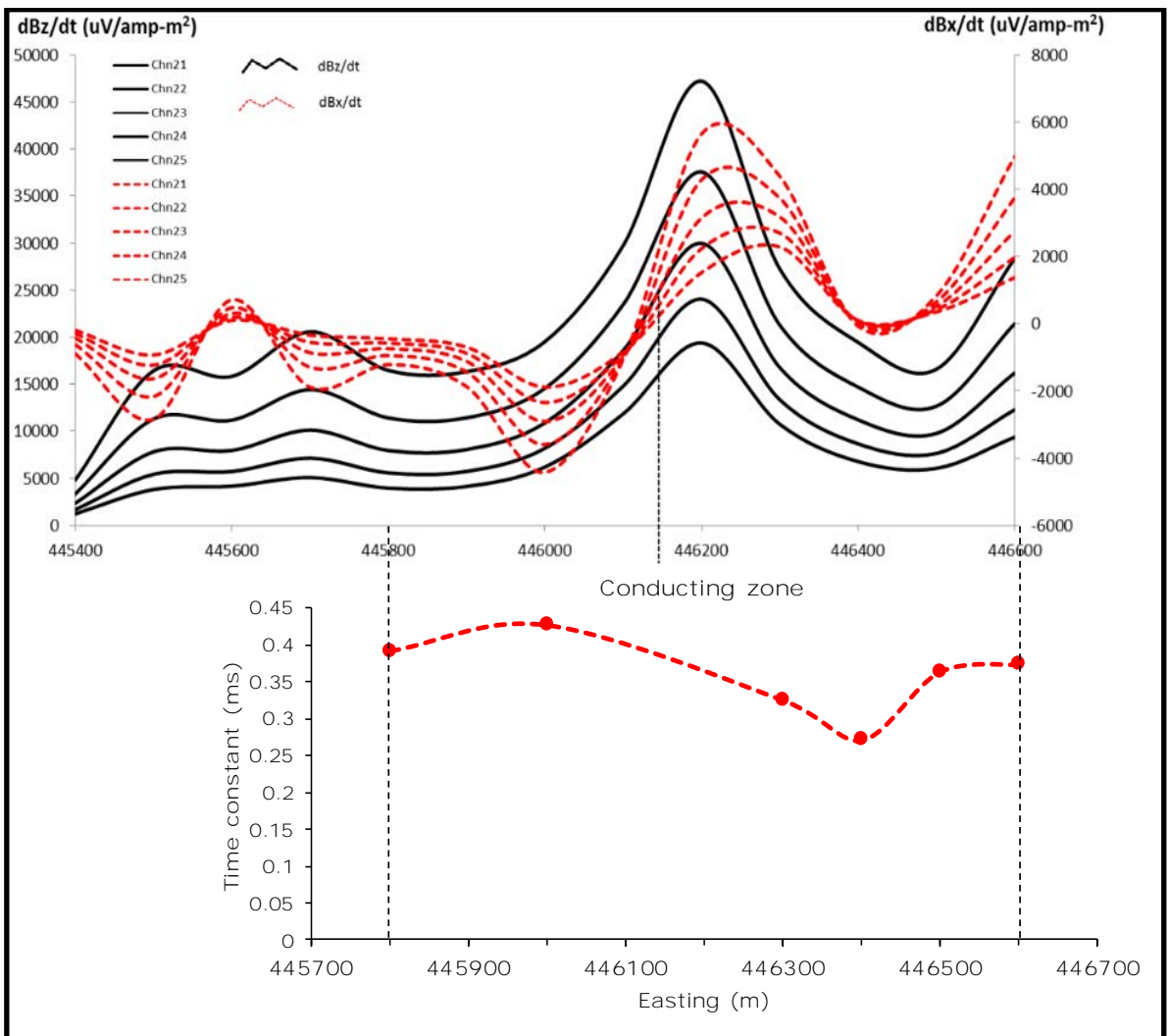


Figure 5.11 TEM profile response showing conducting zone on Line No-23443000N.

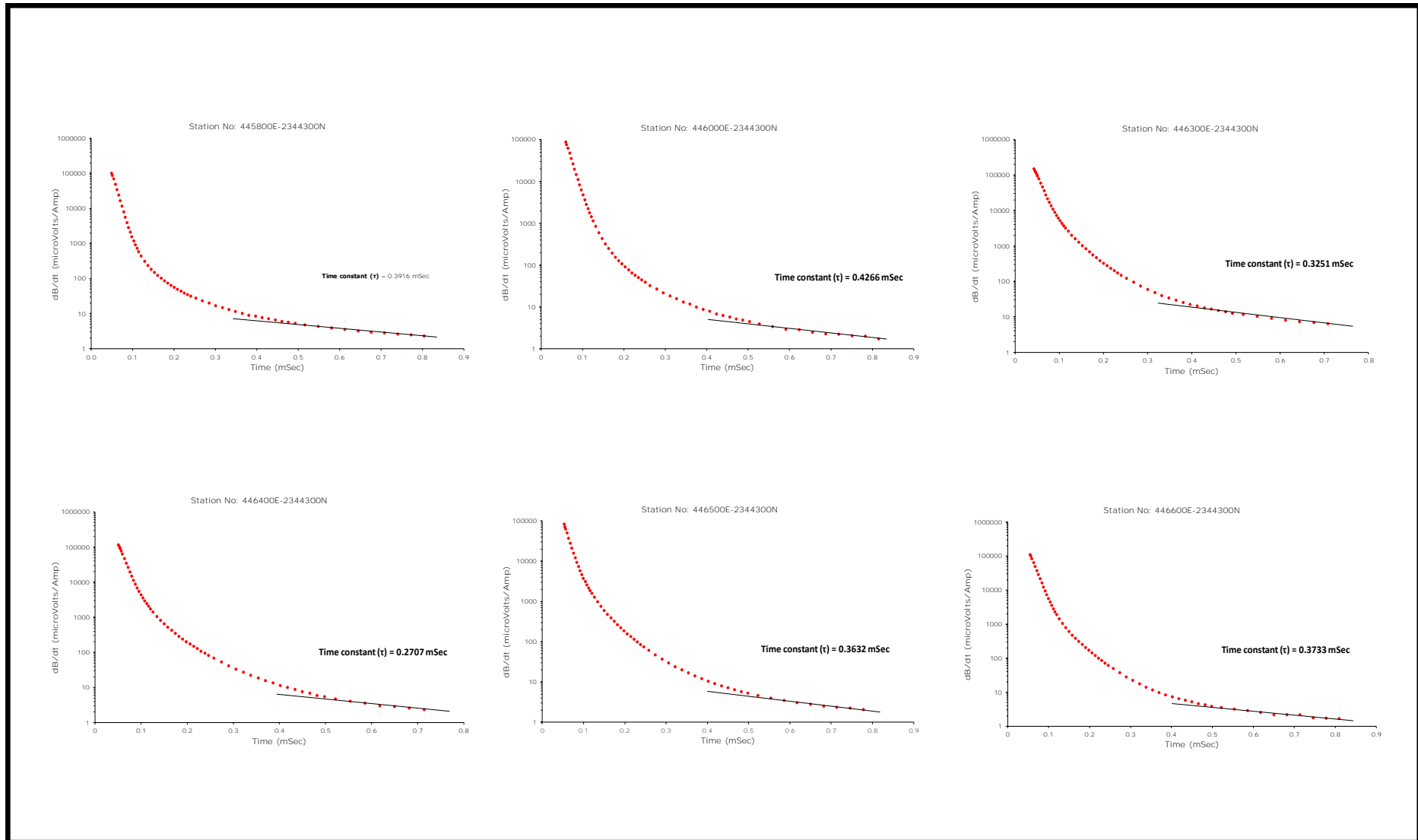


Figure 5.12 Decay curve and their respective time constant (τ) of stations for Line No-2344300N.

5.5.3 1D Inversion of In-loop soundings

1D Inversion technique attempted over sounding data for a loop sizes of 400m x 400m and 100m x 100m, which are falling at NE and NEE of Bijepar village respectively and. Based on the known lithological setup in this area and their respective resistivity values in geological environments, inversion has attempted with multiple iterations and editing of model data with as possible as minimum fitting error, depth and resistivity sections are prepared.

For each station of line number 2344300N (Figure 5.13), three-layer resistivity model has been obtained from resistivity curves. These three (3) inferred layers are attributed as high resistivity sandstone, followed by unconformity contact and/or weathered basement of low resistivity overlain very high resistive basement Bijli rhyolite an order 6559 Ohm-m. In order to understand the continuity of lithological succession over this line, 1D stitched 2D section is generated. It is observed that the conducting/unconformity layer thickness is varying 10 to 30 m towards basin (west to east for this line). For loop size 400 m X 400 m, 0.1 to 1 ms data of TEM is provided good result in basement depth estimation and this sounding data also inverted with a minimum fitting error and drawn lithological correlation between different stations (Figure 5.14).

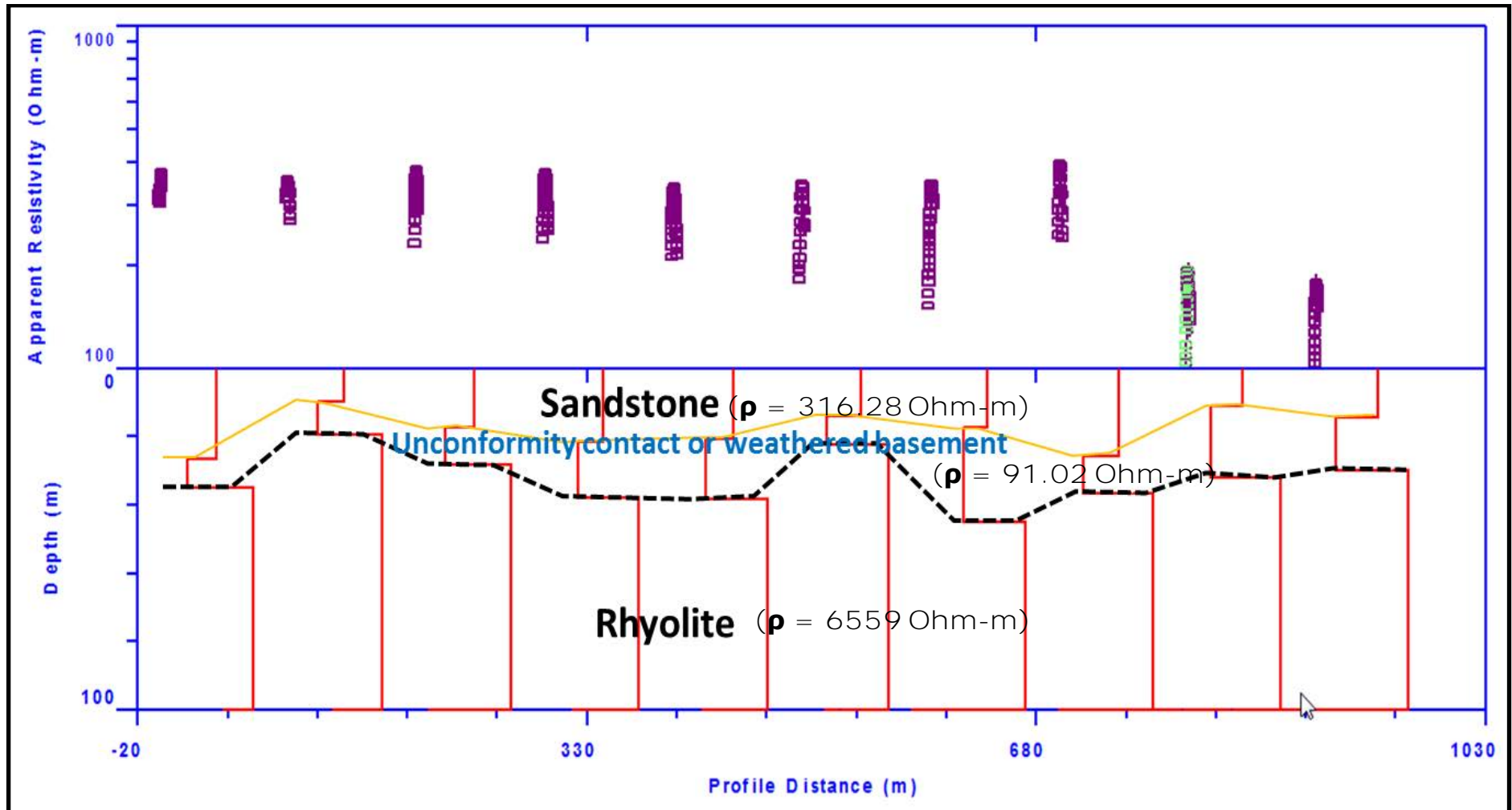


Figure 5.13 1D stitched 2D cross section of Line No-2344300N.

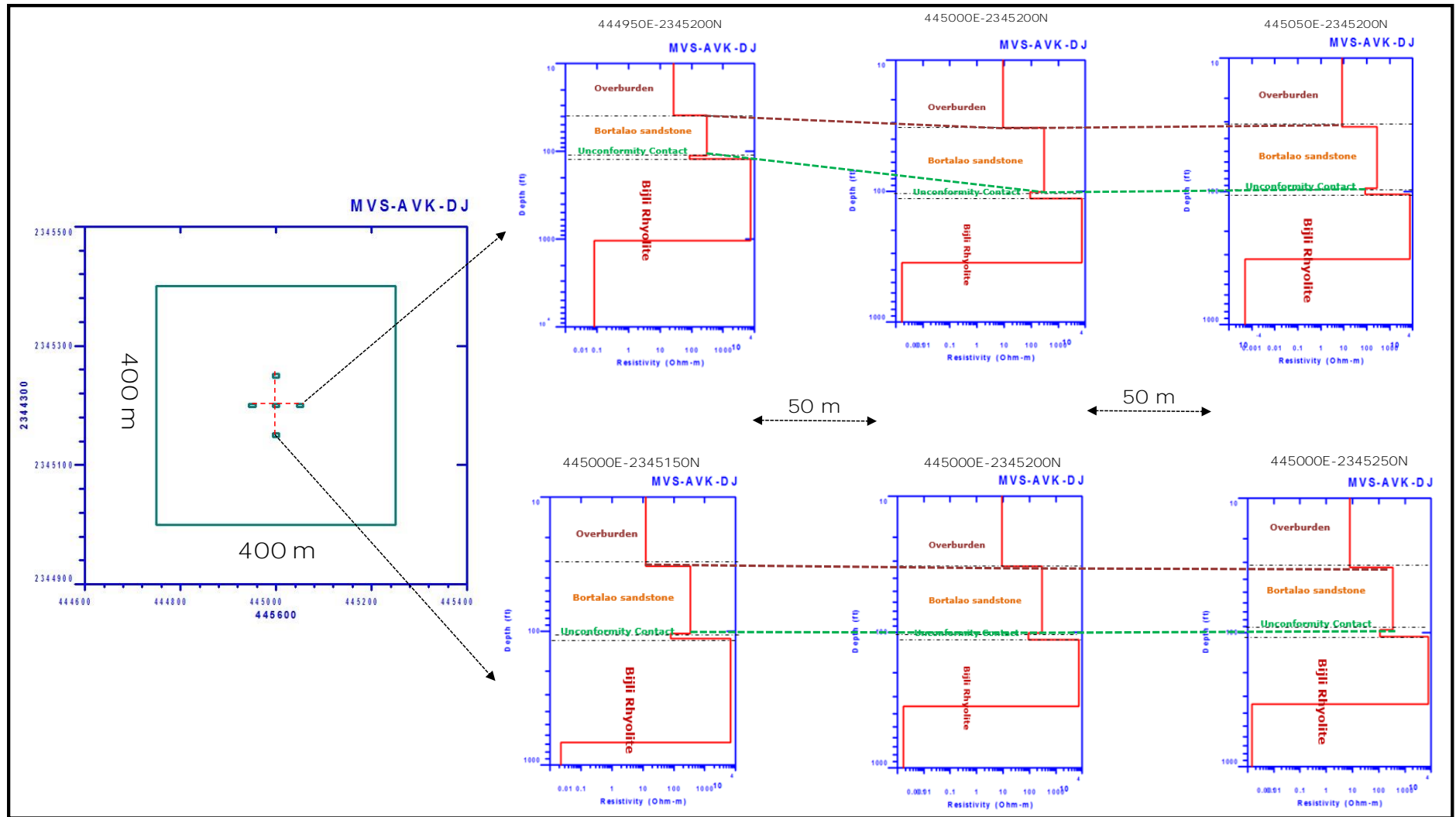


Figure 5.14 1D Inversion of loop size 400 m X 400 m at station number 445000E-2345200N.

5.5.4 Demarcation of conducting zones

After applying all data processing and refinement techniques, TEM survey has brought two major conducting zones which are trending in NW-SE and NE-SW directions. These zones are also inferred as structurally disturbed from magnetic and gravity surveys. This conducting zones attributed as fracture zones/anomalous zones (alterations) either within the basement Rhyolite and or Bortalao sandstones (Figure 5.15).

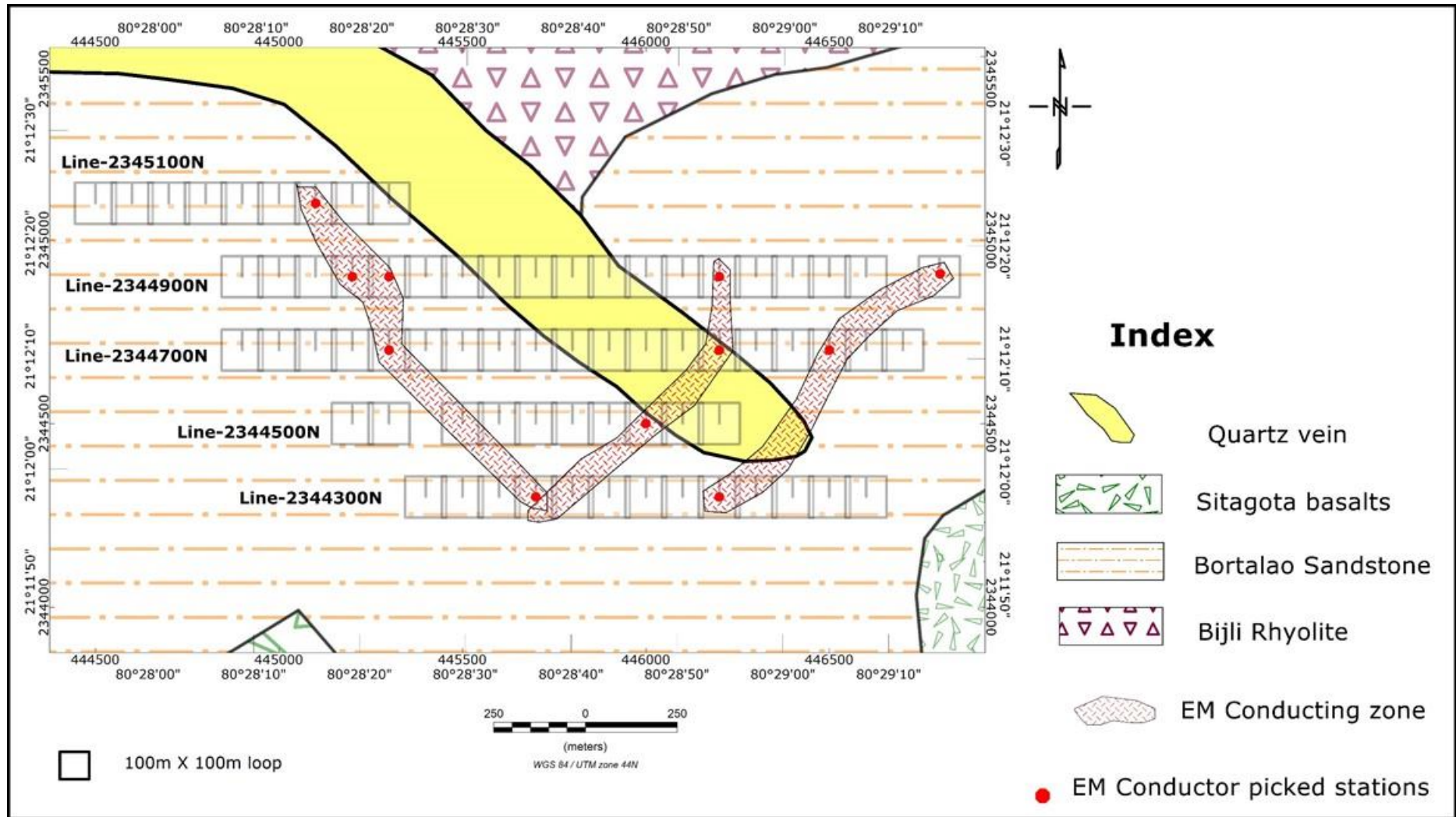


Figure 5.15 Inferred EM conducting zones super imposed on geology map.

CHAPTER 6

INTEGRATED INTERPRETATION, RESULTS AND DISCUSSIONS

6.1 Gravity method

Unconformity contact between basement Bijli rhyolites and Bortalao sandstone, litho-contact between Bortalao sandstone and Sitagota basalt in the eastern part of the study area is deciphered by a sharp gradient of Bouguer anomaly. Structural features i.e. faults/fractures and lineaments trending in NW-SE, NE-SW and E-W are identified within basement Bijli rhyolites and few of these features are running below the sandstones. Out of all these inferred structural features, NW-SE trending features are dominating in the study area. Two (2) parallel NW-SE faults/fractures intruded by quartz vein are demarcated towards the NE of *Bijepar* village, where surface radioactive anomalies are reported.

6.2 Magnetic method

Interpretation of magnetic data facilitated in identifying structural features trending in NW-SE & NE-SW in the study area. Among the identified magnetic lineaments, NW-SE trending lineaments are dominated which are linked with a major fault zone. Basement faults/fractures showing their depth persistency and majority of which are confined to basement rocks and rest are running into deeper parts of basin. A few NW-SE structural features are coinciding with features inferred from gravity data and found good correlation. One major NW-SE trending fault cross cut by two (2) NE-SW trending fractures at north-east of *Bijepar* village, form a zone where surface radioactive anomalies are reported. Radioactive anomalies reported at *Ramatola* and *Patratola* villages are falling at the intersection zones of fault/fractures and unconformity contact. Magnetic anomaly maps depicted the lithological variations in basement rhyolites. Basement rhyolites are divided into two types i.e., grey and

pink rhyolites based on magnetic susceptibility values and amplitude ranges of anomalies in the study area. Interpretation of magnetic data demarcated the zones dominantly associated with intrusive basic activity within the sediment as well as basement rocks apart from the identification of structural features. One E-W trending ultra-mafic rock at a depth of 70 to 100 m with vertical to sub-vertical nature towards NE of *Bijepar* village is clearly mapped and quantitatively interpreted using 2D and 3D modelling techniques.

6.2.1 Understanding of causative sources of magnetic anomalies from petrology results

A set of grab rock samples from Bijepar-Ramatola-Managad-Surjatola areas were taken up for petromineralogical studies with special reference to know causative sources (presence of Iron-titanium bearing minerals/ magnetite) of magnetic anomalies with in the rhyolite and sulphides. Based on mineralogy and texture the rock types are characterized as ferruginous breccia, rhyolitic tuff, rhyolite, altered rhyolite and rhyolite with flow texture.

Ferruginous breccia: This sample is collected at north-east of Bijepar village falling in NW-SE trending major fault zone. Ferruginous breccia is highly brecciated (Figure. 6.1 a), containing fragments of various sizes constituted mainly by vein quartz, chert and quartzite. The fractures are filled in by goethite and chamosite? Anatase is the minor mineral occurring as fine granular segregations.

Rhyolitic tuff: Rhyolitic tuff is extremely fine grained, displays a kind of lamination, composed of quartz, feldspar, shards of glass/ quartz, sericite and tuffaceous matter of beyond microscopic resolution (Figure 6.1 b). Pyrrhotite, magnetite, chalcopyrite, sphene and anatase constitute minor minerals. The rock is traversed by randomly oriented fractures filled by quartz, epidote and biotite.

Rhyolites: Rhyolites exhibit porphyritic texture with phenocrysts of quartz, K-feldspar and plagioclase set in cryptocrystalline to microcrystalline ground mass composed of quartz and feldspar. Quartz phenocrysts are typical with perlitic cracks and embayed grain margins

(Figure. 6.1 c), whereas plagioclase often shows zoning and are highly sericitised. Subhedral to euhedral disseminated magnetite, titanomagnetite, biotite often altering to chlorite, euhedral, prismatic, zoned zircon (Figure. 6.1 d), granular sphene altering anatase and apatite constitute accessory minerals. Calcite, sericite and chlorite are found as irregular segregations within the rock mosaic and also along fractures. Albitization of the feldspar phenocrysts is commonly observed. One rock sample is highly infested fine anhedral to euhedral magnetite.

Altered rhyolite: Altered rhyolite is similar mineralogy and texture to that of the rhyolites mentioned above, but for the degree of alterations. Sericitisation and albitisation (Figure.6.1 e) are very prominent in this rock, specially the phenocrysts, whereas patchy chloritisation is prominent in the groundmass.

Rhyolite with flow texture: Rhyolite with flow texture, this rhyolite typically exhibits flow texture wherein both the phenocrysts and groundmass feldspars show alignment in the flow direction (Figure. 6.1 f). The phenocrysts are constituted by quartz, plagioclase and K-feldspar. The ground mass contains microcrystalline feldspars, quartz, patchy chlorite and granular anatase segregations. The rock is traversed by more than one generation of fractures filled by chlorite, quartz and calcite. The rock is pigmented by fine dust of iron imposing pink color to the rock

Magnetite, is the main mineral responsible for high magnetic susceptibility of the rocks and pyrrhotite is observed in one sample. High susceptibility pink rhyolites in northern portion is separated from grey rhyolites at west of *Ramatola-Kolarbhatti* villages by a E-W trending faulting at south of *Managad* village. Two volcanic tuff zones are also identified with low and medium range amplitudes anomalies at north of *Ramatola-Managad* villages. Ferruginous breccia fallig in NW-SE major fault zone at NE of *Bijepar* village.

Petrological results have immensely helped in identifying different lithological and structural zones over total magnetic intensity (TMI) map.

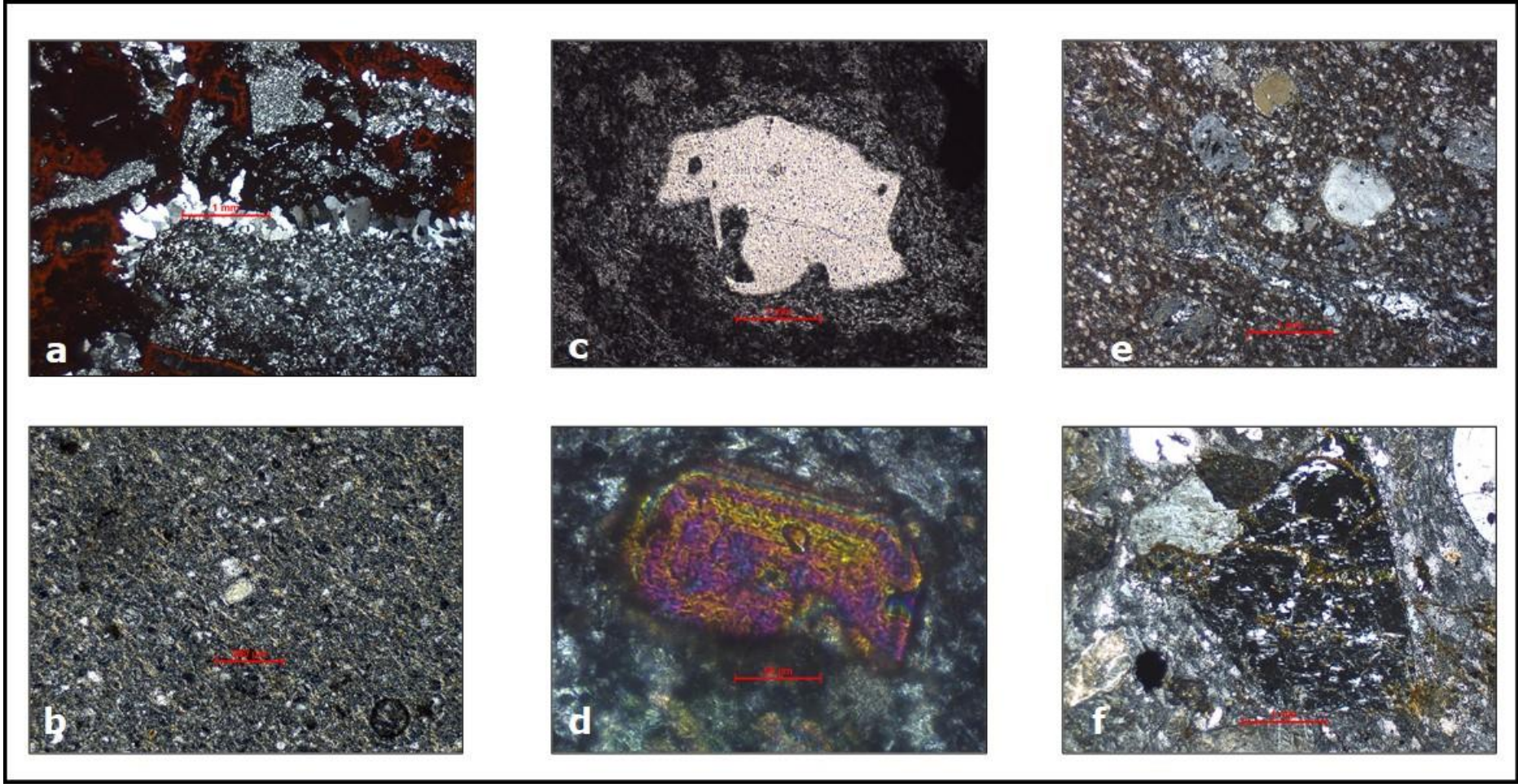


Figure 6.1 Thin sections under microscope for different type of rhyolites collected from study area.

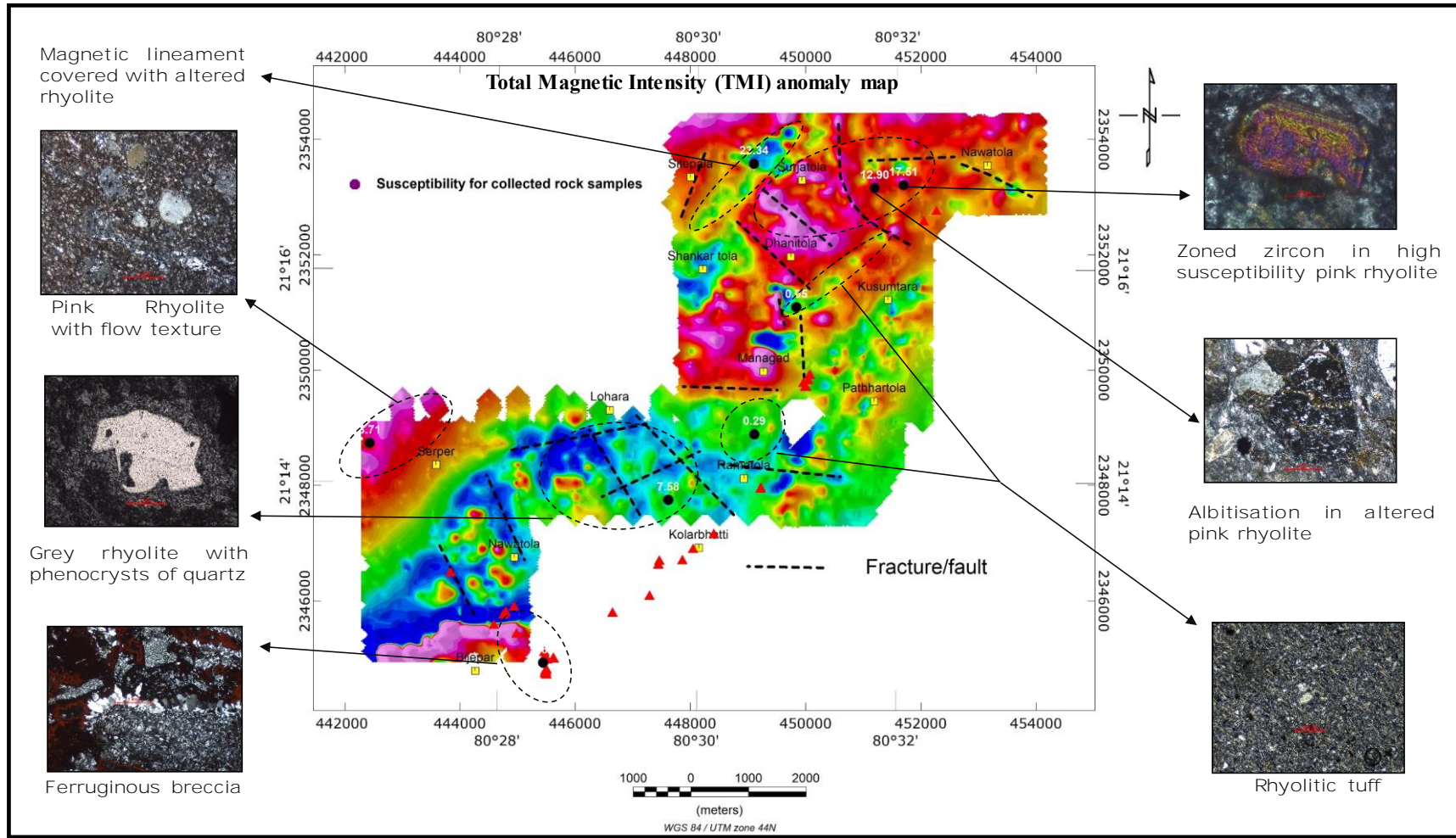


Figure 6.2 Total magnetic Intensity (TMI) showing petrological results with their respective geophysical anomalous zones.

6.3 Time-Domain Electromagnetic (TEM) method

Interested Zones of interest are demarcated from potential methods are covered by TEM survey and data have helped in identifying conducting zones at north-east of *Bijepar* village. These inferred conducting zones could be fractures filled with conducting minerals i.e. sulphides within the Bortalao sandstone and/or at unconformity contact important for mineralization. Near and around *Bijepar* village EM soundings data offered lithological succession.

Integrated map of inferred structural features from all geophysical methods along with geology has been prepared. Integrated interpretation of Gravity, Magnetic and TDEM data along with other exploration data sets i.e. Geology and borehole data successfully mapped potential target areas for planning boreholes in the part of subsurface exploration phase (Figure. 6.3).

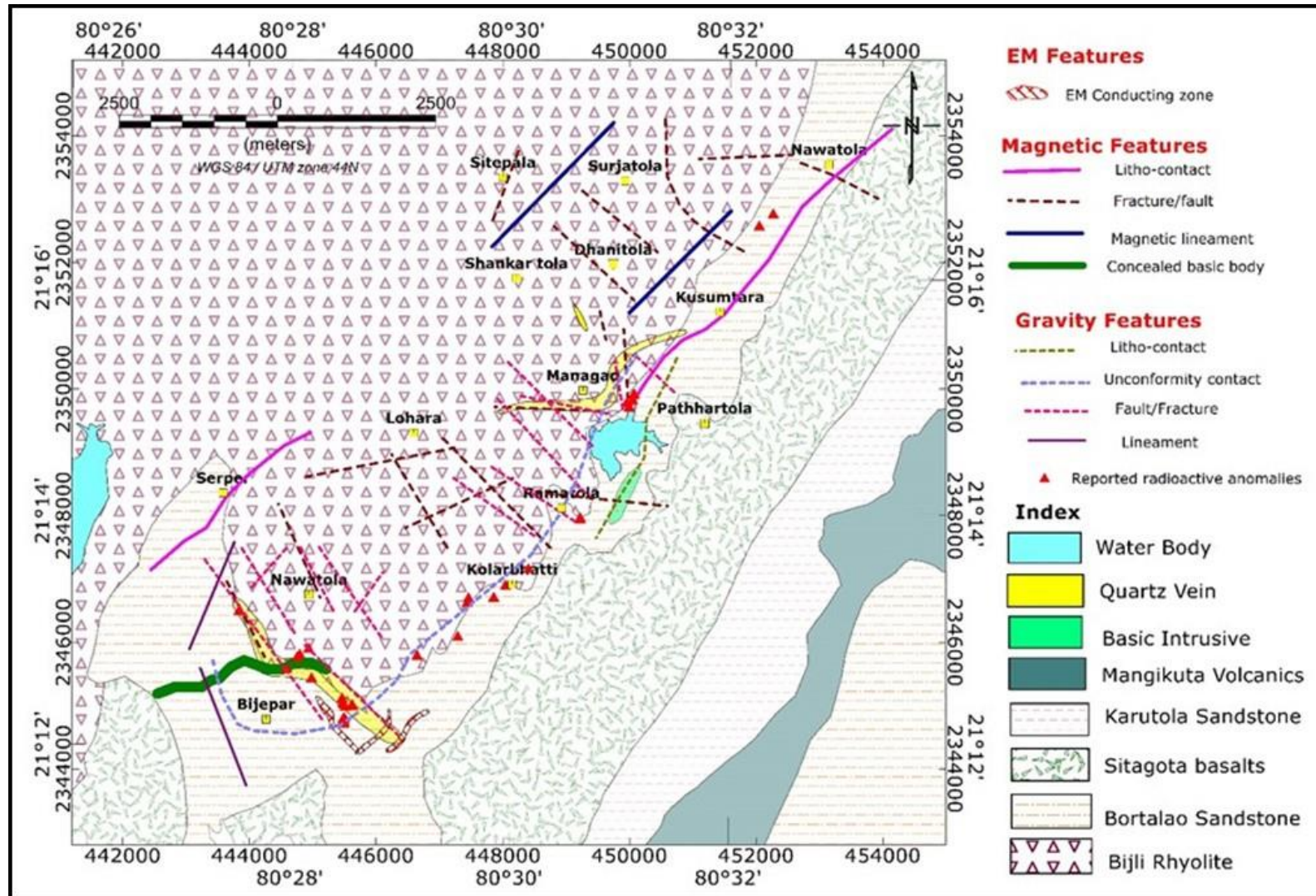


Figure 6.3 Inferred structural features superimposed over geology map.

CHAPTER 7

CONCLUSIONS

- Interpretation of Gravity and Magnetic data facilitated in mapping litho-units of Bijli Rhyolites, Bortalao sandstones and Sitagota basalts in study area.
- Gravity data have effectively helped in depicting the unconformity contact between Bijli Rhyolites and Bortalao sandstones, as well as litho contact between Bortalao sandstones and Sitagota basalt.
- Structural features trending in NW-SE and NE-SW are well demarcated. Among these features, NW-SE is dominating and looks to be basement fractures/faults.
- Inferred structural features (NW-SE to NNW-SSE and NE-SW) at *Bijepar* block are well corroborating with reported surface radioactive occurrences whereas at *Ramatola* and *Pathratola* villages reported anomalies are associated with intersection zone of unconformity and NW-SE to E-W fault/fracture.
- A few structural features (NW-SE and E-W) identified within the rhyolite terrain away from unconformity contact, at the north of *Ramatola*, *Pathratola* and *Kusumtara*, are dominantly associated with quartz veins and are devoid of radioactivity. Therefore, it is worth mentioning that the intersection zones of structural features with unconformity contact are more important for subsurface exploration.
- An ultra-mafic body (picked up by high magnetic signature) has been demarcated in the study area. Modelling and inversion of magnetic data revealed the orientation (E-W strike and dipping towards north) and the depth to the top of the body is in between 70m to 100m (Euler solutions). This information is useful while planning the boreholes to avoid the basic unit in *Bijepar* exploration block.

- TEM surveys successfully delineated the conductors indicating the presence of sulphides associated with NW-SE trending fault zones deciphered from the interpretation of magnetic and gravity data.
- Integrated interpretation of magnetic, gravity and TEM data has revealed the basement fracture zone associated with sulphides favourable for uranium mineralisation towards north and NE of Bijepar for further subsurface exploration.

PUBLICATION TITLE:

“Role of geophysical surveys in delineating concealed geological structures and zones favourable for Uranium Exploration using Magnetic and Time-Domain Electromagnetic methods: A Case study from Bijepar area, Gondia district, Maharashtra.”

***The above titled paper would be prepared for publication**

FUTURE SCOPE OF THE STUDY

Presence of potential zones for uranium mineralization in and around *Bijepar* and *Ramotola* villages are identified by utilizing Gravity, Magnetic and Time-Domain Electromagnetic (TEM) methods effectively. The potential zone for uranium mineralization near *Bijepar* village is a conducting zone of basement fractures could be associated with sulphides and or any other conducting materials i.e., alterations where surface radioactive occurrences are reported.

Time-Domain Electromagnetic (TEM) method delivered ideal signatures about presence of conductor. In the part of further study, these zones can be cover with close line and station spacing by using in-loop layouts of TEM survey and these results will give us clear cut picture about conductor zone and its trend precisely. After delineating its trend precisely, fixed-loop layouts can be help us in delineating dip direction and dip amount of conductor zone. So, these detailed TEM studies in future will give an idea about planning bore hole locations to strike conductor zone in subsurface precisely. In further, IP/Resistivity surveys can be done to confirm the identified structures, conductor zones and their association with sulfide mineralization and conductive alterations. Geophysical well logging also preferable in available bore holes in this area to validate geophysical signatures.

References

- Chaturvedi, A.K. (1986). An unpublished annual report on Balaghat- Rajanadagoan-Bhandara area, Atomic Minerals Division.
- Chapin, D. (1998). Gravity instruments: past, present, future. *The Leading Edge*, vol. 17, pp. 100–112.
- Clark, D.A., (1997). Magnetic petrophysics and magnetic petrology: aids to geological interpretation of magnetic surveys. *AGSO Journal of Australian Geology & Geophysics*, vol. 17(2), pp. 83–103.
- Cooper, G. and Cowan, D. (2003). The application of fractional calculus to potential field data. *Exploration Geophysics*, vol. 34, pp. 51–56.
- Dahlkamp, F.J. (2010). *Uranium Deposits of the World*, Springer Science & Business Media, p.520.
- Deshpande, G.G., Mohabey, N.K. and Deshpande, M.S. (1990). Petrography and tectonic setting of Dongargarh volcanics. *Geol. Surv. India Spl. Publ. No. 28*, pp. 260-286.
- Dean, W.C., (1957). Frequency analysis for gravity and magnetic interpretation. *Geophysics*, 23, 97–127.
- Dunlop, D.J. and Ozdemir, O., (1997). *Rock Magnetism: Fundamentals and Frontiers*. Cambridge University Press, New York, pp. 95-123.
- Dentith, M. and Mudge, S. T., (2014). *Geophysics for the Mineral Exploration Geoscientist*. Cambridge University Press, New York, pp. 85-190.
- Dobrin, M. B. and Savit, C.H., (1976). “Introduction to Geophysical Prospecting”, McGraw-Hill International editions, New York, pp. 499-504.
- Harrison, R.J. and Freiburg, J.M. (2009). Mineral magnetism: Providing new insights into geoscience processes. *Elements*, vol. 5, pp. 209–215.

- Hsu, S.K., Sibuet, J.C. and Shyu, C.T. (1996). High-resolution detection of geologic boundaries from potential field anomalies: An enhanced analytic signal technique. *Geophysics*, 61, 373–386.
- International Atomic Energy Agency, World Distribution of Uranium Deposits (UDEPO) with Uranium Deposit Classification, IAEA-TECDOC-1629, IAEA, Vienna (2009).
- Kearey, P., Brooks, M., and Hill, I. (2002) “An introduction to geophysical exploration”, Blackwell Science Ltd, UK, pp. 125-182.
- Longman, I.M., (1959). Computing the tidal accelerations due to the sun and the moon. *Journal of Geophysical Research*, vol. 64, pp. 2351–2355.
- Leaman, D.E., (1998). The gravity terrain correction – practical considerations. *Exploration Geophysics*, vol. 29, pp. 467–471.
- Lowrie, W. (2007) *Fundamentals of Geophysics*, Second edition, Cambridge University Press, pp. 393-410.
- Li, X. (2008). Magnetic reduction-to-the-pole at low latitudes: Observations and considerations. *The Leading Edge*, vol. 27, pp. 990–1002.
- MacLeod, I.N., Jones, K. and Dai, T.F. (1993). 3-D analytic signal in the interpretation of total magnetic field data in low magnetic latitudes. *Exploration Geophysics*, vol. 24, pp. 679–688.
- McNeil, J.D., (1980). Applications of transient electromagnetic techniques. Technical Note TN-7, Geonics Ltd.
- McNeill, J.D., (1990). Use of electromagnetic methods for groundwater studies. In: Ward, S.H. (Ed.), *Geotechnical and Environmental Geophysics*, Vol. 1: Review and Tutorial, Society of Exploration Geophysics Investigations No. 5, pp. 107–112.

- Nabighian, M.N., (1974). Additional comments on the analytic signal of two-dimensional magnetic bodies with polygonal cross section, *Geophysics*, vol. 39, pp.85-92.
- Nabighian, M.N. (1984). Toward a three-dimensional automatic interpretation of potential field data via generalized Hilbert transforms Fundamental relations. *Geophysics*, vol. 49, pp. 780–786.
- Nabighian, M.N., (1972) The analytic signal of two-dimensional magnetic bodies with polygonal cross-section: Its properties and use for automated anomaly interpretation: *Geophysics*, vol. 37, pp. 507-517.
- Pawlowski, R.S., (1995). Preferential continuation potential-field anomaly enhancement. *Geophysics*, vol. 60, pp. 390–398.
- Pilkington, M., and Keating, P. (2004). Contact mapping from gridded magnetic data A comparison of techniques. *Explor. Geophys.*, vol. 35, pp. 306–311.
- Rama rao, B.S and Murthy, I.V.R (1978). Gravity and magnetic methods of prospecting
- Rao, R.L.N., Srinivas, R., Sethuram, S., and Rao, J.R.S. (1994). Gravity and magnetic studies over parts of Khairagarh Basin, central India. 43. pp. 139-148.
- Reid, A.B., Allop, J.M., Granser, H., Millett, A.J., and Somerton, W. (1990). Magnetic interpretation in three dimensions using Euler deconvolution. *Geophysics*, vol. 55, pp. 80-91.
- Reid, J.E. and Macnae, J.C., (1998). Comments of the electromagnetic “smoke ring” concept. *Geophysics*, 63, 1908–1913.
- Sinha, D.K. (1986). An unpublished annual report on Reconnaissance Radiometric survey in Rajanadagoan and Balaghat dist., Atomic Minerals Division.
- Sinha, D.K. (1991). An unpublished annual report on Darekasa-Lanji-Sitapala area, Atomic Minerals Division

- Sarkar, S.N., Sarkar, S.S. and Ray, S.L. (1994). Geochemistry and genesis of the Dongargarh Supergroup Precambrian rocks in Bhandara - Durg Region, Central India. *Indian Jour. Earth Sci.*, vol. 21, pp. 117- 126.
- Satyanarayana, M.V., Rajesh, K., and Satish, CH. (2019). An unpublished annual report on Geophysical Surveys in Kolarbhatti-Magardhokra area, Atomic Minerals Directorate for Exploration and Research, Central Region Nagpur.
- Sensarma, S. and Mukhopadhyay, D. (2003). New Insight on the stratigraphy and volcanic history of the Dongargarh Belt, Central India. *Gond. Geol. Magz. Spl. Vol. No.7*, pp.129-136.
- Sharma, P.V. (1987) Magnetic methods applied to mineral exploration. *Ore Geol. Rev.*, v.2, pp. 323-357.
- Telford, W.M., Geldart, L.P. and Sheriff, R.E. (1990) *Applied Geophysics*, 2nd edition. Cambridge University Press, Cambridge, pp. 6-135.
- Thompson, D. T. (1982). EULDEP: A new technique for making computer-assisted depth estimates from magnetic data. *Geophysics*, v.47, pp. 31-37.
- Ramesh Babu, V., Ram, Subhash and Sundararajan, N. (2007). Modeling and inversion of magnetic and VLF-EM data with an application to basement fractures: A case study from Raigarh, India. *Geophysics*. 72. 10.1190/1.2759921.
- Vivek bist, Shukla, S. and Hansari, M.H. (2018). An unpublished annual report on Dongargarh –Kotri investigation, Atomic Minerals Directorate for Exploration and Research, Central Region Nagpur.
- Zhdanov, M.S. and Keller, G.V. (1994). The geoelectrical methods in geophysical exploration. *Methods in Geochemistry and Geophysics*, vol. 31, Elsevier.